2016

The Role of SOD1 Acetylation in Neurodegeneration

Michael Kaliszewski
University of Central Florida

THE ROLE OF SOD1 ACETYLATION IN NEURODEGENERATION

by

MICHAEL KALISZEWSKI
B.A. Johns Hopkins University, 2000
M.S. George Washington University, 2010

A dissertation submitted in partial fulfillment of the requirements
for the degree of Doctor of Philosophy
in the Burnett School of Biomedical Sciences
in the College of Medicine
at the University of Central Florida
Orlando, Florida

Fall Term
2016

Major Professor: Ella Bossy-Wetzel

ABSTRACT

Amyotrophic lateral sclerosis (ALS) is a fatal neurodegenerative disorder affecting motor neurons. Cu, Zn superoxide dismutase (SOD1), a cytoplasmic free radical scavenging enzyme, is mutated in familial ALS (fALS) and post-translational modification of the wild-type protein has been associated with sporadic ALS (sALS). Proteomic studies indicate that SOD1 is acetylated at Lys123; however, the role of this modification remains unknown. To investigate its function, we generated antibodies for Lys123-acetylated SOD1 (Ac-K123 SOD1). Sod1 deletion in Sod1-/- mice, K123 mutation, or preabsorption with Ac-K123 peptide suppressed immunoreactivity, confirming antibody specificity. In the normal central nervous system, Ac-K123 SOD1 maps to glutamatergic neurons of the cerebellar cortex, dentate gyrus, hippocampus, olfactory bulb, and retina. In cultured neurons, Ac-K123 SOD1 localized to defined regions of axons and dendrites. Previous studies have suggested a role for SOD1 in cell cycle regulation. Therefore, we tested the distribution of Ac-K123 SOD1 during the cell cycle of astrocytes. In G1 Ac-K123 SOD1 localized to the nucleus, in G0 to the primary cilium, in metaphase and anaphase to chromosomes, and in telophase to the midbody. The deacetylase HDAC6 and acetyl-transferase α-TAT1 are associated with the primary cilium. Therefore, we tested whether they regulate reversible acetylation of SOD1. HDAC6 knockdown or pharmacological inhibition markedly increased, while HDAC6 overexpression decreased, SOD1 Lys123 acetylation. By contrast, SOD1 Lys123 acetylation was decreased by α-TAT1 knockdown and increased by α-TAT1 overexpression. These results suggest that HDAC6 and α-TAT1 regulate SOD1 Lys123 acetylation. Next, we examined Lys123 acetylation in fALS SOD1 mutants. Remarkably, Lys123

acetylation was dramatically increased in fALS mutants including SOD1 A4V. The acetyl-Lys123 mimetic of wild-type SOD1 caused axonal transport deficits similar to those observed in SOD1 pathogenic mutants such as A4V. Interestingly, HDAC6 deacetylation or acetylation resistance by Lys123 mutation, abolished A4V protein misfolding, axonal transport defects, and neuronal cell death. These results suggest that Lys123 acetylation plays a key role in the neurotoxicity of fALS mutants and may have implications in sALS. Because Ac-K123 SOD1 maps to the primary cilium, we examined whether ciliogenesis is altered in fALS mutant SOD1 astrocytes. Strikingly, fALS mutants caused centriole and primary cilia proliferation with ciliary ectosome secretion. Notably, multiciliated ependymal cells in the brain ventricles and spinal cord central canal, which are critical for cerebral spinal fluid circulation, stained strongly for Ac-K123 SOD1. Thus, we speculate that ciliary ectosome shedding from ependymal cells accounts for the presence of misfolded SOD1 in the CSF in fALS and perhaps sALS. In summary, we identified SOD1 Lys123 acetylation as a novel mechanism underlying protein misfolding and neurodegeneration in ALS. Ac-K123 SOD1 may emerge as novel target for the diagnosis and treatment of ALS.

To my parents Michael and Barbara, for igniting the sparks of curiosity.

To my wife Tosin, for stoking the flames of perseverance.

And to my children Iggy and Funlola, for fueling the fire of hope and lighting the future.

Olọrun jẹ ti o dara gbogbo awọn akoko.

ACKNOWLEDGMENTS

First and foremost I would like to thank my mentor, Dr. Ella Bossy-Wetzel, for all of her support and guidance over the years. I would also like to thank Dr. Blaise Bossy for experimental advice and analysis, Mr. Austin Kennedy for microscopy and image processing assistance, Mr. Andrew Knott for manuscript editing, Dr. Wenjun Song for project insight and technical expertise, and all other members of the Bossy-Wetzel laboratory, past and present, for the invaluably constructive criticism and friendly advice during the project work.

I am also grateful to the members of my dissertation advisory committee, Dr. Alvaro Estevez, Dr. Yoon-Seong Kim, and Dr. Suren Tatulian, for all of their feedback and advice during the course of this research. Finally, I would like to acknowledge the funding support for this project (NIH R01 N5055193 and UCF COM SharkTank Pilot Grant to EBW).

TABLE OF CONTENTS

LIST OF FIGURES xiv

LIST OF TABLES xvii

LIST OF ABBREVIATIONS xviii

CHAPTER ONE: GENERAL REVIEW 1

1.1 Overview of SOD1 1

1.1.1 SOD1 structure 1

1.1.2 SOD1 function 3

1.1.3 SOD1 subcellular localization 4

1.1.4 SOD1 post-translational modifications 4

1.2 Protein Acetylation 7

1.2.1 Overview of lysine acetylation 7

1.2.2 Functional effects of lysine acetylation 9

CHAPTER TWO: SOD1 ACETYLATION IN THE NORMAL CNS 11

2.1 SOD1 in the CNS 11

2.1.1 SOD1 knockout mice 11

2.2 Materials and Methods 13

2.2.1 Reagents 13

2.2.2 Antibodies 14

2.2.3 Mice and rats 16

2.2.4 Site-directed mutagenesis 16

2.2.5 Transfection of human cells 17

2.2.6 Deacetylase inhibitor treatment of human cells 18

2.2.7 Cell lysate and western blot 18

2.2.8 Tissue Preparation 19

2.2.9 Immunohistochemistry of mouse tissue cryosections 21

2.2.10 $Sod1^{-/-}$ transgenic mice and protein extractions 22

2.2.11 Cortical neuron isolation and transfection 22

2.2.12 Microscopy and image analysis 23

2.3 Results 24

2.3.1 Antibodies demonstrate specificity towards SOD1 24

2.3.2 Antibodies are specific to Lys123 acetylation 27

2.3.3 Ac-K123 SOD1 localizes to hippocampal pyramidal neurons and granule cells of the dentate gyrus 32

2.3.4 Ac-K123 SOD1 is found in granular cell bodies and molecular layer axons of cerebellum 37

2.3.5 Ac-K123 SOD1 in ependymal cells of ventricle and choroid plexus 40

2.3.6 Ac-K123 SOD1 localizes to interneuron cell bodies and the major afferent and efferent neuronal processes of the olfactory bulb 43

2.3.7 Ac-K123 SOD1 is found with specific layers of the retina 47

2.3.8 Ac-K123 SOD1 localizes to neurites and the nucleus in cortical neurons 52

2.4 Discussion 55

CHAPTER THREE: SOD1 ACETYLATION AND THE CELL CYCLE 58

3.1 Protein acetylation and the cell cycle 58

3.1.1 SOD1 and the cell cycle 58

3.1.2 Structure and function of primary cilia 59

3.1.3 Primary cilia in the nervous system 61

3.1.4 Primary cilia and the cell cycle 62

3.1.5 Histone deacetylase 6 66

3.1.6 α-Tubulin acetyltransferase 1 66

3.2 Materials and Methods 67

3.2.1 Reagents 67

3.2.2 Antibodies 68

3.2.3 Mouse embryonic fibroblasts 69

3.2.4 Rats 69

3.2.5 Isolation and transfection of spinal astrocytes 69

3.2.6 Nutrient depletion and recovery of astrocytes 70

3.2.7 Immunocytochemistry 70

3.2.8 Microscopy 72

3.2.9 Expi293 cells 73

3.2.10 Pharmacologic inhibitor treatment against HDAC6 73

3.2.11 HDAC6/α-TAT1 siRNA mediated knockdown 73

3.2.12 SOD1 and HDAC6/α-TAT1 overexpression 74

3.2.13 Immunoprecipitation 74

3.3 Results 75

3.3.1 Antibodies are specific for K123-acetylated SOD1 by immunocytochemistry 75

3.3.2 Ac-K123 SOD1 localizes to nucleus and primary cilium in spinal astrocytes 78

3.3.3 Ac-K123 SOD1 localization is dependent on cell cycle phase 80

3.3.5 SOD1 interacts with HDAC6 in cells 89

3.3.6 HDAC6 inhibition or knockdown increases SOD1 K123 acetylation 90

3.3.7 Deacetylation of SOD1 by HDAC6 in vivo 94

3.3.8 SOD1 interacts with α-TAT1 in cells 95

3.3.9 α-TAT1 knockdown decreases SOD1 K123 acetylation 96

3.3.10 α-TAT1 acetylates SOD1 K123 97

3.4 Discussion..... 98

CHAPTER FOUR: SOD1 LYS123 ACETYLATION PROMOTES MISFOLDING AND CILIARY TARGETING 103

4.1 SOD1 and ALS..... 103

4.1.1 Overview of ALS 103

4.1.2 SOD1 toxic gain of function 104

4.1.3 Misfolding of modified wild-type SOD1..... 108

4.1.4 Conformation specific misfolded SOD1 (C4F6) antibody 108

4.1.5 ALS and non-cell autonomous toxicity 109

4.1.6 Prion-like spreading of SOD1 in ALS 109

4.1.7 Evidence of vesicle secretion from primary cilia 112

4.1.8 Genes linking primary cilia to ALS..... 114

4.2 Materials and Methods..... 116

4.2.1 Reagents..... 116

4.2.2 Antibodies 116

4.2.3 Rats..... 117

4.2.4 Site directed mutagenesis 117

4.2.5 Expi293 cells 118

4.2.6 Immunoprecipitation and western blotting 119

4.2.7 Primary cortical neurons and transfection 119

4.2.8 Primary spinal astrocytes and transfection 120

4.2.9 Confocal microscopy 121

4.2.10 Live-cell imaging and quantification 121

4.3 Results 123

4.3.1 ALS-linked SOD1 mutants demonstrate increased K123 acetylation 123

4.3.2 Lys123 acetylation promotes mutant SOD1 misfolding 124

4.3.3 Ciliary Ac-K123 SOD1 is misfolded 126

4.3.4 Mutant SOD1 promotes primary cilia secretion 126

4.3.5 Ac-K123 SOD1 is found in primary cilia derived vesicles 129

4.3.6 Ac-K123 SOD1 in choroid plexus and ependymal cells of ventricle and central canal 132

4.3.7 Acetyl mimetic SOD1 K123Q impairs axonal transport 133

4.3.8 K123R mutation rescues SOD1 A4V from axonal transport defects 135

4.4 Discussion 137

CHAPTER FIVE: DISCUSSION 143

APPENDIX: PERMISSION FOR REPRINT 149

LIST OF REFERENCES 152

LIST OF FIGURES

Figure 1. SOD1 and the superoxide dismutase reaction. 3

Figure 2. SOD1 is acetylated at conserved Lysine 123 6

Figure 3. Schematic overview of protein acetylation. 8

Figure 4. Customized antibodies demonstrate specificity for SOD1. 26

Figure 5. Antibodies are specific for K123-acetylated SOD1. 28

Figure 6. Distribution of Ac-K123 SOD1 within dentate gyrus granule cells and CA1 field hippocampal neurons. 36

Figure 7. Ac-K123 SOD1 localization within granule, basket, and stellate cell somata and molecular layer neurites of the cerebellum. 40

Figure 8. Ac-K123 SOD1 localization in choroid plexus and ependymal cells. 42

Figure 9. Ac-K123 SOD1 within the olfactory bulb and lateral olfactory tract. 47

Figure 10. Ac-K123 SOD1 localization to retinal ganglion cells, outer and inner nuclear layer cell bodies, and inner plexiform layer neurites..... 51

Figure 11. Lys123 acetylated SOD1 is localized within somata and neurites of cortical neurons. 52

Figure 12. Lys123 acetylated SOD1 is localized within dendrites and axons of cortical neurons. 54

Figure 13. The primary cilium is a specialized signaling organelle. 61

Figure 14. The functional relationship between primary cilia and autophagy. 65

Figure 15. Ac-K123 SOD1 antibodies demonstrate specificity for use in immunohistochemistry 77

Figure 16. Ac-K123 SOD1 is localized to the primary cilium and nucleus. 79

Figure 17. Cell cycle withdrawal decreases nuclear Ac-K123 SOD1 while promoting ciliary localization in mouse embryonic fibroblasts. 82

Figure 18. Cell cycle arrest promotes Ac-K123 SOD1 ciliary localization in primary astrocytes. . 84

Figure 19. Ac-K123 SOD1 localization to primary cilium correlates to decreased nuclear signal. 85

Figure 20. Lys123 acetylated SOD1 is associated with chromosomes during mitosis. 86

Figure 21. Lys123 acetylated SOD1 is concentrated within the transient midbody structure during the end stage of telophase. 87

Figure 22. Ac-K123 SOD1 localization in astrocytes during specific stages of interphase and mitosis. 88

Figure 23. HDAC6 and SOD1 interact in cells. 90

Figure 24. HDAC6 inhibitor treatment increases immunodetection of Ac-K123 SOD1. 92

Figure 25. HDAC6 knockdown increases SOD1 K123 acetylation. 93

Figure 26. HDAC6 deacetylates Ac-K123 SOD1. 95

Figure 27. α-TAT1 and SOD1 interact in cells. 96

Figure 28. α-TAT1 siRNA mediated knockdown decreases SOD1 K123 acetylation. 97

Figure 29. α-TAT1 acetylates SOD1 K123. 98

Figure 30. Model of the prion-like transfer of misfolded SOD1. 112

Figure 31. ALS-linked SOD1 mutants demonstrate increased K123 acetylation. 124

Figure 32. Lys123 acetylation promotes mutant SOD1 misfolding. 125

Figure 33. Ac-K123 SOD1 and misfolded SOD1 co-localize of within the primary cilium. 126

Figure 34. Mutant SOD1 promotes the release of ciliary vesicles from astrocytes. 129

Figure 35. Ac-K123 SOD1 is found in primary cilia derived vesicles. 131

Figure 36. Ac-K123 SOD1 localization in choroid plexus and ependymal cells. 133

Figure 37. Lys123 acetylated SOD1 impairs axonal transport of mitochondria in cortical neurons. 135

Figure 38. Mutant SOD1 Lys123 deacetylation rescues neurons from mitochondrial trafficking defects..... 137

Figure 39. Current model for promotion of SOD1 misfolding and cell-to-cell transfer by K123 acetylation. 147

LIST OF TABLES

Table 1. Primers used for mutagenesis of GFP-tagged SOD1 K123..... 16

Table 2. The primers used for mutagenesis of SOD1 K123. 117

LIST OF ABBREVIATIONS

Aβ	amyloid beta
Ac-K123 SOD1	lysine 123-acetylated SOD1
AD	Alzheimer's disease
ALS	amyotrophic lateral sclerosis
AMPA	α-amino-3-hydroxy-5-methyl-4-isoxazole propionic acid
BBSome	complex of Bardet-Biedl syndrome proteins
BSA	bovine serum albumin
CA1	cornus ammonis field 1
CA3	cornus ammonis field 3
CFP	cyan fluorescent protein
CHAPS	3-[(3-cholamidopropyl)dimethylammonio]-1-propanesulfonate
CNS	central nervous system
Co-IP	co-immunoprecipitation
CSF	cerebrospinal fluid

DIV	days *in vitro*
DMEM	Dulbecco's Modified Eagle Medium
DMSO	dimethyl sulfoxide
DsRed	*Discosoma* sp. red fluorescent protein
EBSS	Earle's Balanced Salt Solution
ELISA	enzyme-linked immunosorbent assay
ER	endoplasmic reticulum
FALS	familial amyotrophic lateral sclerosis
FBS	fetal bovine serum
GCL	granular cell layer
GFAP	glial fibrillary acidic protein
GFP	green fluorescent protein
HBSS	Hank's balanced salt solution
HDAC	histone deacetylase
HEK	human embryonic kidney
IFT	intraflagellar transport
INL	inner nuclear layer

IP	immunoprecipitation
IPTG	isopropyl β-D-1-thiogalactopyranoside
K123	lysine 123
LB	Luria Bertani broth
MAP2	microtubule-associated protein 2
MEFs	mouse embryonic fibroblast cells
ML	molecular layer
NA	numeric aperture
NAD^+	nicotinamide adenine dinucleotide
NAM	nicotinamide
NMDA	*N*-methyl-D-aspartate
OCT	optimal cutting temperature
ONL	outer nuclear layer
PBS	phosphate buffered saline
PCL	Purkinje cell layer
PTM	post-translational modification
RGCL	retinal ganglion cell layer

ROS	reactive oxygen species
SALS	sporadic amyotrophic lateral sclerosis
SDS	sodium dodecyl sulfate
Shh	Sonic hedgehog
SOB	super optimal broth
SOD1	superoxide dismutase 1
SOD1 K123Q	acetylated mimetic of SOD1
SOD1 K123R	unacetylated mimetic of SOD1
SSTR3	somatostatin receptor type III
TSA	trichostatin A
WT	wild type

CHAPTER ONE: GENERAL REVIEW

1.1 Overview of SOD1

Cu,Zn superoxide dismutase, or superoxide dismutase 1 (SOD1), is a highly conserved and ubiquitously expressed protein best known for its role in defense against oxidative stress (Fridovich, 1995). SOD1 is abundant, particularly in the central nervous system where it comprises 1–2% of the total soluble protein (Pardo et al., 1995). In 1993 a large collaborative group demonstrated that some inherited forms of amyotrophic lateral sclerosis (ALS), a rapidly progressive and lethal neurodegenerative disease affecting motor neurons, are caused by mutations of the human *SOD1* gene (Rosen et al., 1993). To date, more than 180 point mutations in the *SOD1* gene have been identified (http://alsod.iop.kcl.ac.uk/).

1.1.1 SOD1 structure

The active SOD1 enzyme is a 32 kDa homodimeric enzyme, consisting of 153 amino acids per monomer subunit. Each monomer subunit consists of eight anti-parallel strands connected by three external loops, which after proper folding forms a Greek key β-barrel structural motif (Getzoff et al., 1989).

Three post-translational modifications are required for SOD1 maturation: intramolecular disulfide bond formation, dimerization, and copper and zinc acquisition (Kawamata and Manfredi, 2010). Within each subunit, the intramolecular disulfide bond between C57 and C146 facilitates correct folding and stabilizes the active homodimer (Arnesano et al., 2004). The

dimer is held together at the dimer interface, a region consisting of the hydrophobic contacts between subunits (Tainer et al., 1982). Dimerization reduces the solvent accessible surface area, greatly increasing the stability of SOD1 (Goodsell and Olson, 2000). SOD1 is unstable in its metal-free and disulfide-reduced forms, but when mature, the protein is highly stable (Khare et al., 2004). Fully metallated SOD1 has a melting point between 85–95°C, depending on the buffer, and remains enzymatically active in 8 M urea or 4 M guanidine-HCl (Forman and Fridovich, 1973; Lepock et al., 1985). This stability is also demonstrated by an extremely long half-life. A recent *in vivo* kinetic approach revealed a slow turnover of SOD1 within the CNS, with the average half-life of SOD1 in the CSF measured at approximately 25 days (Crisp et al., 2015).

The electrostatic and zinc-binding loops are of great importance to the superoxide scavenging ability of SOD1. Together these loops form a compact and highly ordered structure around the active site. Both are coordinated by zinc, an ion essential for overall monomer structure and dimer stability. The zinc-binding loop supports the dimer interface at the outer surface and contains the conserved disulfide bond important for dimer stability. The highly specific dismutase catalysis occurs at the redox-active $Cu^{1+/2+}$ and depends on electronic guidance of the superoxide substrate to the active site via charged residues contained within the electrostatic loop. Dissociation of zinc results in disorganization of the active-site loops, making the loops more dynamic and increasing non-specific substrate access to the copper ion (Sahawneh et al., 2010).

1.1.2 SOD1 function

Superoxide dismutase 1 (SOD1) is an enzyme whose canonical role is to protect the cell against oxidative damage by reactive oxygen species (ROS). These highly reactive, free radical-harboring molecules, produced by mitochondria as a byproduct of cellular respiration (Muller et al., 2004), result in cumulative damage that includes DNA mutations and deletions, lipid peroxidation, oxidation of amino acids in proteins, and inactivation of enzymes by oxidation of co-factors. In its role as an antioxidant, SOD1 metabolizes two superoxide radicals to molecular oxygen and hydrogen peroxide (McCord and Fridovich, 1969). Using copper at its active site, SOD1 catalyzes a disproportionation reaction where one superoxide molecule is oxidized and another molecule is reduced in what can described as a 'ping-pong' mechanism (Figure 1).

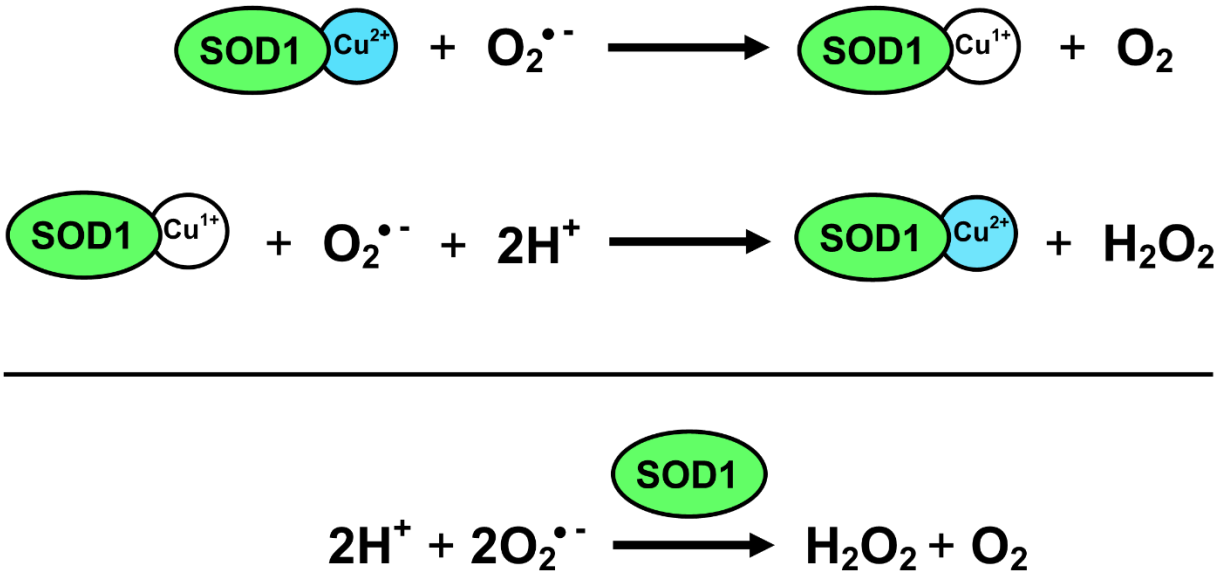

Figure 1. SOD1 and the superoxide dismutase reaction.

Other SOD1 functions include copper buffering, zinc homeostasis, phosphate activation, and protein nitration (Beckman et al., 1993; Culotta et al., 1997; Wang et al., 1996; Wei et al., 2001). A more recently described role involves metabolic state signaling, where SOD1 integrates signals from oxygen and glucose in order to modulate respiration within cells through casein kinase signaling (Reddi and Culotta, 2013). Additional cellular functions of SOD1 include RNA binding and transcriptional regulation in response to oxidative stress (Tsang et al., 2014; Volkening et al., 2009). Furthermore, studies have shown that only a small amount of the total SOD1 within cells (less than 1%) is actually required to prevent toxicity from superoxide (Corson et al., 1998). As SOD1 is produced at high levels in many organisms, this hints at other as-of-yet undetermined functions.

1.1.3 SOD1 subcellular localization

SOD1 is primarily a cytosolic protein, but is also found within the nucleus, lysozymes, peroxisomes, and mitochondrial inner membrane space (Chang et al., 1988; Crapo et al., 1992; Keller et al., 1991; Sturtz et al., 2001).

1.1.4 SOD1 post-translational modifications

SOD1 post-translational modification (PTM) by phosphorylation, palmitoylation, sumoylation, succinlyation, and glutathionylation has been described (Antinone et al., 2013; Lin et al., 2013; Redler et al., 2011). Proteomics studies have also identified acetylation at conserved lysine 123 (K123), located within the electrostatic loop, in human, mouse, and rat SOD1 (Choudhary et al.,

2009; Lundby et al., 2012; Weinert et al., 2013; Yang et al., 2011; Zhao et al., 2010) (Figure 2A-B). Sequence alignment demonstrates that Lys123 and surrounding sequences are highly conserved across many species, suggesting an essential (yet uncharacterized) regulatory function (Figure 2C). SOD1 PTM can alter enzymatic efficiency, induce monomer formation, and promote aggregation and cell death (Wilcox et al., 2009). SOD1 K123 is located at the mouth of the electrostatic loop and within close proximity to the copper-containing active site. K123 acetylation may cause slight perturbations of the electrostatic loop that allow non-specific substrates to enter the active site. This can cause aberrant redox chemistry and possibly reverse catalysis which results in the production of superoxide. For these reasons it is important to gain a better understanding of Lys123 acetylation and any impact this PTM may have on SOD1 structure and function.

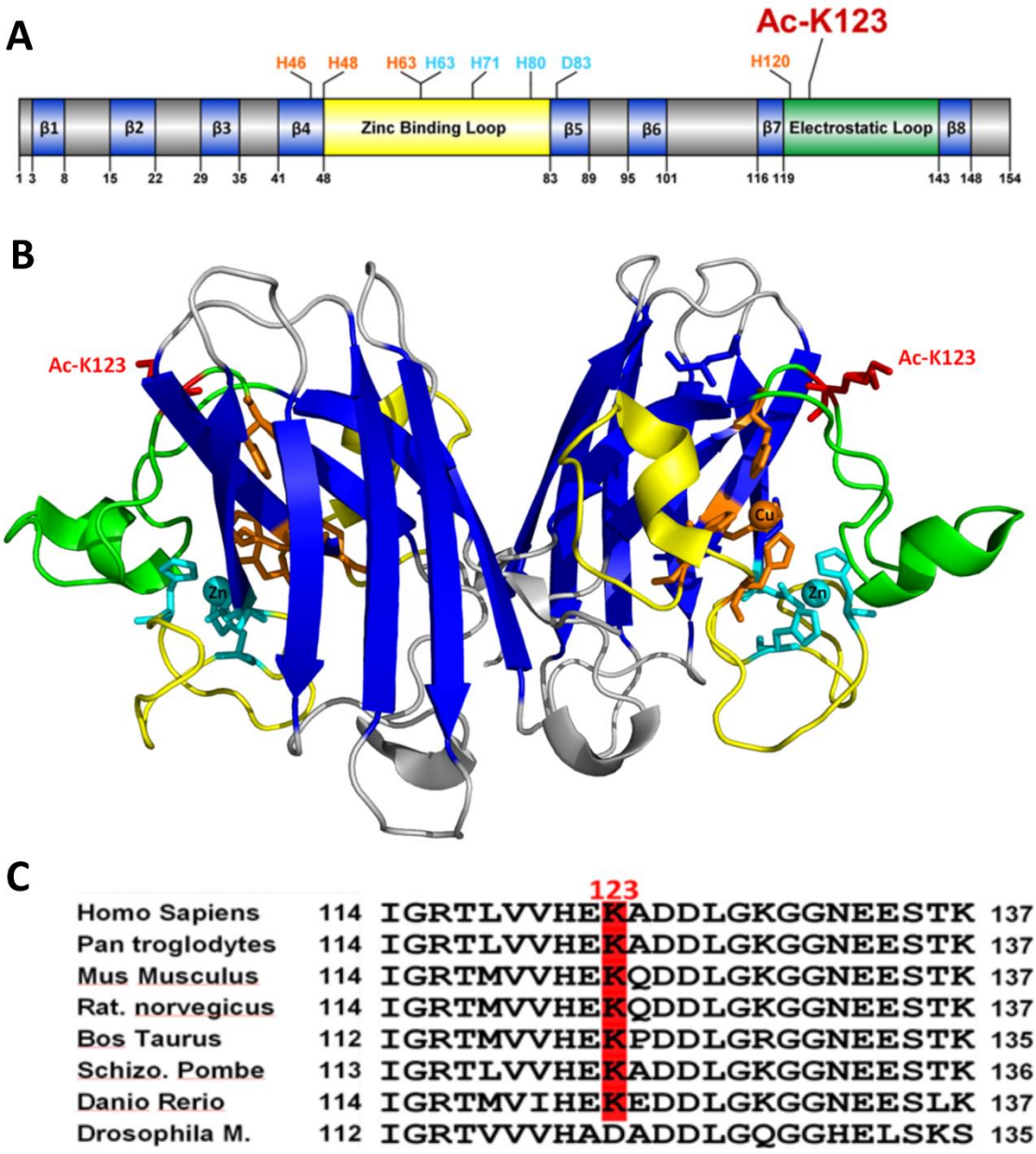

Figure 2. SOD1 is acetylated at conserved Lysine 123

A. Domain graph of SOD1 depicting acetylation at Lys123. Graph was created from the SOD1 amino acid sequence and referenced metal binding sites located on Uniprot (ID**:** P00441**)** using Domain Graph 2.0. B. Lys123 is located within the electrostatic loop, a functional domain important for superoxide substrate recruitment into the active site of SOD1. Modeling was done by A. Kennedy with Pymol 1.3 utilizing a SOD1 structure located on the Research Co-laboratory for Structural Bioinformatics Protein Data Bank (RSCB PDB) using the ID, 2V0A. The

structure is represented in ribbon format while the metal binding sites are represented in stick format. C. Lys123 (highlighted in red) is highly conserved among many species. All sequences are isoform 1 of their respective species and were obtained from Uniport. BLAST sequence alignment by A. Kennedy. Sequences were copied into Cobalt to generate a multiple protein alignment. The sequence was then exported from Cobalt into ClustalX 2.0 using Clustal formatting option.

1.2 Protein Acetylation

1.2.1 Overview of lysine acetylation

PTMs allow cells to rapidly respond to changes in the external and internal microenvironment. Perhaps the most intensively studied PTM is phosphorylation, which occurs at approximately 24,000 known sites on more than 8,000 proteins (Gnad et al., 2011). However, phosphorylation is not the only major protein modification that is under enzymatic regulation. Proteins are also commonly modified by methylation, SUMOylation, ubiquitination, and acetylation.

During acetylation, the functional acetyl group from acetyl coenzyme A (Ac-CoA) is transferred to proteins. Catalyzed by N-terminal acetyltransferases, acetylation occurs co-translationally at the α-amino group of the N-terminus in the vast majority of proteins (Figure 3A) (Arnesen et al., 2009). Acetylation can also occur post-translationally at the ε-amino group of lysine residues (Figure 3B). Unlike acetylation of the N-terminus, lysine acetylation is a reversible and tightly regulated process.

Lysine acetylation is catalyzed by lysine acetyltransferases (KATs), while the deacetylation of lysine is catalyzed by lysine deacetylases (KDACs). It should be noted that KATs and KDACs are also more commonly referred to as histone acetyltransferases (HATs) and histone deacetylases

(HDACs) for historical reasons, as acetylated lysine residues were first discovered in histones, the proteins within eukaryotic cell nuclei that packages DNA into chromatin (Allfrey et al., 1964). However, we now know that numerous other nuclear and non-nuclear proteins are modified by lysine acetylation (Glozak et al., 2005). To date, proteomic studies have identified more than 15,000 lysine acetylation sites on 4,541 proteins (Choudhary et al., 2009; Lundby et al., 2012).

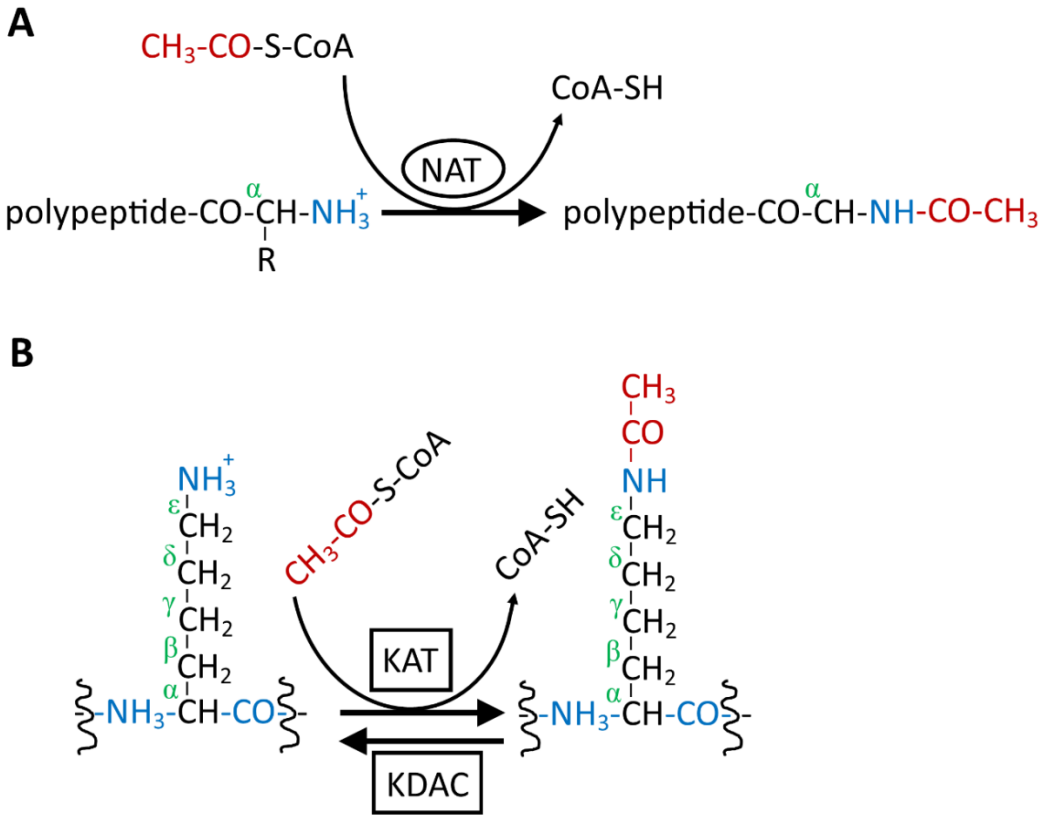

Figure 3. Schematic overview of protein acetylation.

A. The enzymatic transfer of an acetyl group from acetyl-CoA to the N-terminal α-amino group of a polypeptide. The irreversible reaction is catalyzed by N-terminal acetyltransferases (NATs). B. The reversible acetylation of the ε-amino group of a lysine residue is catalyzed by lysine acetyltransferases (KATs), whereas lysine deacetylases (KDACs) catalyze the deacetylation of lysine residues.

The 22 identified KATs are grouped into three major families: the GNAT family, the MYST family, and the p300/CBP (CREB-binding protein) family (Allis et al., 2007). Most KATs form multiprotein complexes with various subunits, with the catalytic activity and substrate specificity of the KAT largely dependent on the context of the other subunits in the complex (Lee and Workman, 2007).

KDACs comprise a family of 18 enzymes that play diverse roles in mammalian cell homeostasis. The 18 KDAC isoforms are grouped into four classes based on sequence homology of the catalytic domain to yeast deacetylases. The isoforms within Class I (HDAC1, 2, 3 and 8), Class II (HDAC4, 5, 6, 7, 9, and 10), and Class IV (HDAC11) are all zinc-dependent amidohydrolases. They possess a zinc-binding domain at the active site, which is required for enzymatic activity. The final seven isoforms belong to Class III and are referred to as silent information regulator 2 (Sir2) proteins, or more commonly the sirtuins (Sirt1–7). They differ from the other HDAC classes in that their enzymatic activity is dependent on the use of NAD^+ as a co-substrate. In addition, some of the sirtuins exhibit localization to mitochondria where they regulate various metabolic processes (Verdin et al., 2010).

1.2.2 Functional effects of lysine acetylation

Reversible acetylation plays an important role in regulating the structure, function, and interaction of proteins. The functional effects of lysine acetylation were first described for histones, where acetylation stimulates transcription by remodeling chromatin, weakening histone-DNA interactions, and providing binding sites for transcription factors (Bannister and

Kouzarides, 1996; Mizzen et al., 1996; Ogryzko et al., 1996; Parthun et al., 1996; Taunton et al., 1996).

Acetylation has also been examined in a growing number of non-histone proteins, where it may induce conformational change and steric hindrance. This can potentially affect the catalytic activity, stability, protein-protein interactions, and subcellular localization and targeting of many proteins (Kouzarides, 2000; Zhao et al., 2010). Consequently, the functional effects of lysine acetylation are wide ranging and encompass diverse biological processes. Cellular processes regulated by acetylation include cell cycle, nucleic acid splicing, subcellular localization and transport, and mitochondrial function and metabolism. At the level of the organism, acetylation plays important roles in immunity, circadian rhythmicity, and memory formation (Haberland et al., 2009). Dysregulation of lysine acetylation has been reported in numerous disorders including neurodegeneration, cancer, and cardiovascular disorders, making protein acetylation a favorable target in drug design (Drazic et al., 2016).

CHAPTER TWO: SOD1 ACETYLATION IN THE NORMAL CNS

2.1 SOD1 in the CNS

The central nervous system is highly prone to toxicity from ROS. This susceptibility stems from high oxygen consumption and a relatively poor antioxidant defense (Aksenov et al., 1998; Slivka et al., 1987). SOD1 is an abundant protein that is ubiquitously expressed in the central nervous system (Pardo et al., 1995). The development of age-related neuromuscular and neuronal abnormalities in *Sod1* knockout (*Sod1* -/-) mice underscores the importance of SOD1 protein in the central nervous system.

2.1.1 SOD1 knockout mice

SOD1 deficiency renders mice more sensitive to oxidative stress and results in many different phenotypes that resemble accelerated aging. *Sod1* -/- mice do not exhibit abnormalities during development and early adulthood, but they have reduced lifespan and evidence of various oxidative stress markers, including a markedly increased incidence of liver cancer (Elchuri et al., 2004).

Within the nervous system, SOD1 deficiency results in a wide range of phenotypes (Saccon et al., 2013). *Sod1* -/- mice are prone to early vision loss due to the development of progressive retinal cell degeneration and age-related macular degeneration (Hashizume et al., 2008;

This chapter includes material from the article "SOD1 Lysine 123 Acetylation in the Adult Central Nervous System" accepted for publication in *Frontiers in Cellular Neuroscience* by Frontiers Media SA

Imamura et al., 2006). Within the cochleae of the inner ear, the absence of SOD1 causes hair cell degeneration and decreased spiral ganglion cell density, resulting in a progressive hearing loss (Keithley et al., 2005). Adult-onset progressive motor axonopathy is observed in *Sod1* -/- mice, demonstrated by a slowly progressive motor deficit and decreased repair after axonal injury (Fischer et al., 2012; Flood et al., 1999; Larkin et al., 2011). *Sod1* -/- mice are more susceptible to brain damage following cerebral ischemia, in part due to increased disruption of the blood-brain-barrier (Kim et al., 2003; Kondo et al., 1997). Following traumatic brain injury, *Sod1*-/- mice exhibit increased damage (Lewén et al., 2000), further signifying a protective role of SOD1 in the CNS. SOD1 deficiency results in increased susceptibility to neurodegeneration, demonstrated by exacerbated memory loss, tau phosphorylation, amyloid beta (Aβ) oligomerization, and plaque deposition in the double mutant progeny of *Sod1* -/- mice crossed to a mouse model of Alzheimer's disease (Murakami et al., 2011, 2012). Furthermore, there is a link between SOD1 deficiency and Fragile X syndrome, the most frequent form of inherited mental retardation. Interestingly, the RNA-binding protein Fragile X Mental Retardation Protein (FMRP), whose absence is the cause of Fragile X syndrome, has been shown to increase SOD1 translation through the binding of *Sod1* mRNA (Bechara et al., 2009). This suggests that the reduced level of SOD1 protein observed in *Fmrp1* -/- mice plays a role in the physiopathology of Fragile X syndrome. Taken together, these phenotypes highlight a critical role for SOD1 in the nervous system.

Here, we report the generation of new polyclonal rabbit antibodies against the K123-acetylated form of SOD1 and characterize the distribution of Ac-K123 SOD1 in the normal mouse nervous system.

2.2 Materials and Methods

2.2.1 Reagents

Kanamycin A monosulfate, phosphate buffered saline, pH 7.4 (PBS), EDTA, Tubastatin A hydrochloride, gelatin from cold water fish skin 45% in H2O, Ponceau S solution 0.1% w/v and 5% acetic acid, and sodium orthovanadate were obtained from Sigma. Trichostatin A (TSA) was obtained from Cayman Chemicals. Nicotinamide (NAM) was obtained was from Fluka Chemical. Fetal bovine serum (FBS), 100x penicillin-streptomycin solution, and Dulbecco's Modified Eagle Medium (DMEM) containing 4500 mg/L D-glucose, GlutaMax-1, and 110 mg/L sodium pyruvate were obtained from Gibco by Life Technologies. Neutralized bacteriological peptone was obtained from Oxoid. HEPES-free acid, NaCl, and KCl were obtained from OmniPur/Calbiochem. Sucrose-ultrapure was obtained from J.T. Baker. Tris-proteomic grade, and β-Mercaptoethanol-proteomic grade were obtained from AMRESCO. 3-[(3-Cholamidopropyl)dimethylammonio]-1-propanesulfonate (CHAPS) was obtained from G-Biosciences. Paraformaldehyde-EM grade, Prill purified was obtained from Ted Pella, Inc. Optimal Cutting Temperature (OCT) compound, Tissue-Tek Cryomolds, and Accu-Edge low profile microtome blades were obtained from Sakura. Isoflurane, USP was obtained from Abbott Laboratories. Tissue Protein Extraction Reagent (T-PER), 10% Tween-20 Surfact-Amps detergent solution, HALT protease inhibitor

cocktail, HALT phosphatase inhibitor cocktail, Gene Jet Plasmid Maxiprep kit, TurboFect transfection reagent, Bolt LDS sample buffer, Bolt Bis-Tris Plus 4-12% gradient polyacrylamide gels, Bolt MES sodium dodecyl sulfate (SDS) running buffer, Pierce Coomassie Plus Bradford assay kit, iBlot Gel transfer stacks, iBolt Dry Blotting System, Pierce Western Blotting Substrate, 20 mM Hoechst 33342 solution, Cytoseal 60, and premium cover glass were all obtained from Thermo Fisher Scientific. The QuikChange Lightning site-directed mutagenesis kit and XL10-Gold Ultracompetent cells were obtained from Agilent Technologies. PCR primers for site-directed mutagenesis were obtained from Integrated DNA Technologies. QIAprep Spin Miniprep Kit was obtained from Qiagen. Difco Luria Bertani broth (LB), Lennox, was obtained from BD. Agar, yeast extract, and tryptone were obtained from EMD Millipore. Tissue culture dishes (100 and 145 mm) were obtained from Greiner Bio. Costar cell scrapers were obtained from Corning. cOmplete Mini, EDTA-free protease inhibitors were obtained from Roche. Amersham Hyperfilm ECL high performance chemiluminescence films were obtained from GE Healthcare Limited. Histochoice MB Tissue Fixative was obtained from AMRESCO. VECTAShield fluorescent mounting medium was obtained from Vector Laboratories, Inc. Superfrost Plus slides were obtained from VWR.

2.2.2 Antibodies

Custom polyclonal rabbit antibodies for Ac-K123 SOD1 were generated by YenZym Antibodies, LLC, by immunization of two rabbits (R25 and R26) with the peptide VVHE-acK-ADDLGKGGC (Ac-K123 peptide) of human $SOD1_{119\text{-}131}$ conjugated to the carrier protein THY. Pre-immune serum,

test serum, and final anti-serum were collected and antibody titers were confirmed by enzyme-linked immunosorbent assay (ELISA). Acetylation-specific antibodies were purified from anti-sera using an affinity matrix conjugated with the acetylated peptide. To eliminate any cross-reactive material, the antibody fraction was then further purified using a matrix conjugated with the unacetylated peptide VVHEKADDLGKGGC (K123 peptide). Purification of the acetylation-specific antibodies was confirmed using ELISA with the acetylated and unacetylated peptide.

Commercial mouse monoclonal SOD1 (G-11), rabbit polyclonal SOD1 (FL-154), goat polyclonal calbindin D28K (N-18), and goat polyclonal doublecortin (C18) antibodies were obtained from Santa Cruz Biotechnology, Inc. Chicken polyclonal glial fibrillary acidic protein (GFAP) (ab4674) antibody and rabbit polyclonal beta-III tubulin (ab18207) antibody were obtained from Abcam. Mouse monoclonal α-tubulin (DM1A) antibody was obtained from Cell Signaling Technology. Mouse monoclonal NeuN (A60) monoclonal antibody was obtained from EMD Millipore. Mouse monoclonal acetylated-α-tubulin (6-11B-1) antibody was obtained from Sigma. Rabbit polyconal SOD1 (rat) (10011387) was obtained from Cayman Chemical.

Secondary peroxidase-conjugated AffiniPure donkey anti-rabbit IgG (H+L), peroxidase-conjugated AffiniPure donkey anti-mouse IgG (H+L), and Alexa Fluor 594 AffiniPure Fab fragment donkey anti-rabbit IgG (H+L) antibodies were obtained from Jackson ImmunoResearch Laboratories, Inc. Goat anti-rabbit IRDye 800CW and goat anti-mouse IRDye 680LT antibodies were obtained from LI-COR. Alexa Fluor 488 goat-anti-rabbit IgG (H+L), highly

cross-absorbed, Alexa Fluor 594 goat anti-mouse IgG (H+L), Alexa Fluor 594-donkey anti-goat IgG (H+L), and Alexa Fluor 647 donkey-anti-chicken IgG (H+L) were obtained from Molecular Probes.

2.2.3 Mice and rats

B6;129S-Sod1tm1Leb/J (Sod1 -/+), B6126F1/J, (Sod1+/+), DBA/2J, and129S1/SvlmJ mice (Jackson Laboratories) were used for immunohistochemical analysis of brains and eyes. Sod1-/- mice were generated as previously described (Kondo et al., 1997). Spinal cords were isolated from CFW mice (Charles River). Timed-pregnant Sprague Dawley rats (Charles River) were used for the isolation of primary neurons. All experiments were approved by the Institutional Animal Care and Use Committee of University of Central Florida College of Medicine.

2.2.4 Site-directed mutagenesis

SOD1 K123 nonacetylated mimetic (K123R) was created by site-directed mutagenesis of pEGFP-C1 WT SOD1 (gift from Dr. Kurt J. DeVos, University of Sheffield) using the QuikChange Lightning kit and the following primers:

Table 1. Primers used for mutagenesis of GFP-tagged SOD1 K123.

Primer	Sequence
K123R Forward	5’-GCACACTGGTGGTCCATGAAAGAGCAGATGACTTGGGC-3’
K123R Reverse	5’-GCCCAAGTCATCTGCTCTTTCATGGACCACCAGTGTGC-3’

Briefly, mutation-containing primers were designed and synthesized (Integrated DNA Technologies, Coralville, IA) for incorporation into the respective plasmids using linear amplification followed by digestion of parental DNA with the methylated DNA specific restriction endonuclease DpnI. XL10-Gold Ultracompetent cells were then transformed with DpnI-treated DNA via the heat shock method, recovered with Super Optimal Broth (SOB) (0.5% yeast extract, 2% tryptone, 10 mM NaCl, 2.5 mM KCl, 20 mM MgSO4), and plated onto LB agar plates containing 100 µg/mL kanamycin A. After 37°C overnight incubation, colonies were selected from plates and used for inoculation of LB medium containing kanamycin A. Cultures were grown and used for DNA plasmid extraction via the QIAprep Spin Miniprep Kit per manufacturer's instructions. Plasmid sizes were verified by agarose gel electrophoresis, mutations were confirmed by DNA sequencing (Eurofins Scientific), and larger cultures were inoculated and grown for large scale endotoxin-free plasmid purification using the Gene Jet Plasmid Maxiprep kit.

2.2.5 Transfection of human cells

For expression of GFP-tagged recombinant SOD1 WT or K123R in human cells, Turbofect transfection reagent was added to 10 µg DNA diluted in serum-free DMEM medium. After incubation at room temperature for 20 minutes, the DNA mix was added to HEK293 cells seeded on 100 mm tissue culture plates growing at approximately 70% confluency at time of transfection. Cells were harvested and lysed 72 hours post-transfection for analysis by western blot.

2.2.6 Deacetylase inhibitor treatment of human cells

To enhance detection of Ac-K123 SOD1, HEK293 cells were treated for 6 hours with both class I/II histone deacetylase inhibitor trichostatin A and class III histone deacetylase inhibitor nicotinamide, or vehicle control. Treated cells were harvested and lysed for analysis by western blot.

2.2.7 Cell lysate and western blot

Briefly, the cells were placed on ice and the growth medium was aspirated and replaced with 5 mL ice-cold PBS. Cells were removed from the plate using a cell scraper and pelleted by centrifugation at 100x g for 10 minutes at 4°C in an Eppendorf 5810R table centrifuge. The cell pellets resuspended in ~500 µL of ice-cold lysis buffer (50 mM HEPES-Na pH 7.4, 150 mM NaCl, 1mM EDTA, 2% CHAPS, 2 mM DTT, 1 mM MgCl2, 1 mM NAM, 1 µM TSA, 2 mM Sodium Orthovanadate, and cOmplete EDTA-free protease inhibitors). After a 30 minutes incubation on ice and occasional vortexing, soluble proteins were obtained by centrifugation at 18,200x g for 20 minutes at 4°C in an Eppendorf 5417R microcentrifuge. Supernatants were removed and protein concentrations were determined using a Pierce BCA protein assay kit. Cell extracts were mixed with LDS sample buffer and β-mercaptoethanol, boiled for five minutes, and applied to a Bolt Bis-Tris 4-12% gradient precast polyacrylamide gel for gel electrophoresis using Bolt MES sodium dodecyl sulfate running buffer. Proteins were next transferred to a nitrocellulose membrane via the iBlot Dry Blotting System. Transfer efficiency was evaluated by Ponceau S

staining of transferred membrane, followed by washes with ddH2O and blocking with 5% bacteriological peptone /1% fish gelatin in Tris-buffered saline containing 0.1% Tween-20 (TBST) overnight at 4°C. Membranes were then washed with TBST followed by 4°C overnight incubation with anti-Ac-K123 SOD1 antibody (1 μg/mL) and anti-SOD1 clone G11 monoclonal antibody (1:5,000). Incubation with anti-α-Tubulin clone DM1A monoclonal antibody (1:2,500) was performed as a loading control. Following primary antibody incubations, membranes were washed with TBST and incubated with donkey anti-rabbit or donkey anti-mouse horseradish peroxidase-conjugated secondary antibodies (1:20,000) for 1 hour at room temperature. Membranes were then washed with TBST, rinsed once in TBS, and visualized with enhanced chemiluminescence after application of Pierce ECL Western Blotting Substrate.

2.2.8 Tissue Preparation

Brains and eyes were collected from 5-month-old male mice, with at least 3 separate mice from both DBA/2J and 129S1/SvlmJ strains (Jackson Laboratory, Bar Harbor, ME). Spinal cords were isolated from three CFW mice, aged 4 months (Charles River Laboratories, Wilmington, MA). All mouse experiments were performed in accordance with guidelines set by the Institutional Animal Care and Use Committee of the University of Central Florida. To isolate retinas, 129S1/SvlmJ mice were sacrificed by a lethal dose of isoflurane. Eyes were removed and radial cuts were made in the cornea to remove the lens. The isolated eye cups were then fixed in 4% paraformaldehyde, 5% sucrose, in PBS, for 15 minutes at room temperature. Retinas were then isolated and fixed for an additional 45 minutes in 4% paraformaldehyde, 5% sucrose, in PBS.

After fixation, the retinas were rinsed 3x for 10 minutes with 5% sucrose in PBS. For cryoprotection, the retinas were incubated for 30 minutes with 5% and then 10% sucrose in PBS. Finally, the retinas were kept in 20% sucrose in PBS overnight at 4^{o} C. For embedding, retinas were incubated for 30 minutes in 100% OCT, followed by 30 minutes in one part 20% sucrose in PBS to two parts OCT, and then 30 minutes in two parts 20% sucrose in PBS to one part OCT. Finally, the retinas were embedded in two parts 20% sucrose in PBS to one part OCT in Tissue-Tek Cryomolds (25 mm x 20 mm x 5 mm) using a dry ice/2-methyl butane bath after the boiling stopped. Brains from 129S1/SvlmJ or DBA2/J mice were processed in the same manner, except that final embedding was in 100% OCT. CFW mice were anesthetized by administration of isofluorane gas (~10%) and transcardially perfused with 0.1 M PBS followed by freshly prepared 2% paraformaldehyde/2% Histochoice MB Tissue Fixative in PBS. Following fixation, spinal cords were removed and placed in the same fixative solution for a 6 hour incubation at 4°C. After fixation, tissues were rinsed in PBS and cryoprotected by 30 minute incubations in 10% sucrose–PBS solution, 20% sucrose–PBS solution, and finally 30% sucrose–PBS solution. Following sucrose infusion, spinal cords were frozen in OCT matrix by embedding within a cryomold in a dry ice/2-methyl butane bath, and stored at -80°C. Unfixed brains of *Sod1*$^{+/+}$ and *Sod*$^{-/-}$ mice were stored at -70°C and directly embedded in 100% OCT as described above. Prior to cryosectioning, tissue blocks were placed in the chamber of a Microm HM 560 Cryostat (ThermoFisher Scientific) and allowed to equilibrate to the cutting temperature in the chamber of a Leica CM 1850 cryostat. Coronal and sagittal cryosections (10–12 µm thick) were obtained using a low profile microtome blade at -20°C to -22°C and thaw-mounted onto

silanized Superfrost Plus slides. Sections were dried using a desiccator for 1 hour, and stored at -70°C under desiccant until used for immunohistochemistry.

2.2.9 Immunohistochemistry of mouse tissue cryosections

For immunostaining, sections were rehydrated in PBS, permeabilized with 0.1% Triton X-100 in PBS, and blocked for 1 hour in 5% cold fish skin gelatin in PBS. Incubation with primary antibody solution (dilutions in 1% fish gelatin in PBS) was performed overnight at 4°C. Sections were then rinsed three times in PBS, incubated for 1 hour at room temperature in the dark with a fluorescent secondary antibody, washed 3 times in PBS, and mounted in Vectashield mounting media (Vector Labs). Nuclei were counterstained with 1 µg/mL Hoechst 33342. Tissue immunostaining controls included omission of the primary antibodies, incubation with pre-immune serum, and incubation with antibody neutralized by immunizing peptide. None of these immunohistochemistry controls revealed significant immunostaining beyond background. The Zeiss LSM 710 confocal microscope and inverse Axio Observer (Carl Zeiss, Thornwood, NY) were used for imaging tissue sections immunostained for Ac-K123 SOD1, rat SOD1, acetylated-α-tubulin, GFAP, doublecortin, NeuN, and calbindin D28K. Goat-anti-rabbit Alexa Fluor 488, goat-anti-mouse Alexa Fluor 594, goat-anti-chicken Alexa Fluor 647, and donkey-anti-goat 594 conjugated secondary antibodies (1:250) were used for detection of primary antibodies. Images were acquired and processed using Zen 2012 imaging software (Carl Zeiss, Thornwood, NY). Composite images of acetyl-Lys123 SOD1 immunostained sagittal brain sections were created

using the stitching function in MetaMorph Image Analysis Software Version 7.1.3.0 (Molecular Devices, Sunnyvale, CA).

2.2.10 $Sod1^{-/-}$ transgenic mice and protein extractions

Isolated brains from $Sod1^{-/-}$ or $Sod1^{+/+}$ mice were frozen and stored at -70°C. Prior to tissue lysate preparation, brains were equilibrated to -20°C for 30 minutes, minced into small pieces, and 1 g tissue was resuspended in 10 mL ice-cold T-PER Tissue Protein Extraction Reagent with 200 µM NAM, 10 µM TSA, 10 µM Tubastatin A, Halt protease inhibitors, and Halt phosphatase inhibitors. Following a 30 minute incubation on ice, tissues underwent five cycles of sonication on ice (20 seconds at output 5 and 50% duty cycle) using a Branson Sonifer 450. Tissue lysates were then passed through a syringe fitted with a 25½ gauge needle until no longer viscous. Cellular debris was removed by centrifugation at 18,200 x g for 30 minutes at 4°C in an Eppendorf 5417R microcentrifuge. Supernatants were collected and protein concentrations were determined using a Pierce Bradford assay kit.

2.2.11 Cortical neuron isolation and transfection

Primary cortical neurons were isolated from fetal rat cortices dissected and prepared from one litter of E18 Sprague Dawley rat embryos. Isolated neurons were seeded at a density of 1 x 10^5 cells/cm^2 alone or upon an astrocyte feeder layer on poly-L-lysine pre-coated 12 mm diameter #1 glass coverslips (Chemglass Life Sciences) for subsequent immunostaining analysis. For expression of GFP-tagged recombinant Tau, isolated embryonic (E18) cortical neurons were

transfected by electroporation. For transfections, $5x10^6$ cells were mixed with 100 µL of Primary Rat Neuron Nucleofector Solution (Amaxa, Lonza, Switzerland) and 2 µg pRK5-EGFP-Tau plasmid DNA (Addgene, Cambridge, MA) and then electroporated using an Amaxa Nucleofector I device (Lonza, Switzerland) following an optimized protocol for primary rat neurons provided by the manufacturer.

2.2.12 Microscopy and image analysis

Imaging was carried out with a Zeiss LSM 710 Inverted Axio Observer confocal laser scanning microscope with six laser excitation lines (405, 458, 488, 514, 543, and 633 nm), a 34 channel QUASAR detector for spectral analysis, and several objectives including a EC Plan-Neofluar 10x 0.3 numeric aperture (NA) air objective, Plan-Apochromat 20x 0.8 NA air objective, EC Plan-Neofluar 40x 1.3 NA oil objective, and a Plan-Apochromat 63x 1.4 NA oil objective. Image acquisition and processing were performed using Zen 2012 software from Zeiss. To visualize Hoechst 33342, the excitation/emission wavelength was 405/495 nm using the diode laser. For Alexa Fluor 488, the excitation/emission wavelength was 488/540 nm using the multiline argon laser. For Alexa Fluor 594, the excitation/emission wavelength was 543/660 nm using a diode pumped solid state laser plus a QUASAR detector for all emission wavelengths. On average 25 z-stacks of 0.5 µm step-size were acquired for 354 µm x 354 µm scaled image size. The z-stacks were maximally projected and the gamma value adjusted to 0.70–0.85 using the ZEN 2012 software.

Montage images were acquired using a Zeiss Axiovert Zeiss 100M fluorescence microscope with a Plan-Neofluar 10 × 0.3 NA or Plan-Neofluar 20 × 0.5 NA air objective (Zeiss), a DG-4/ Xe-arc illumination unit (Sutter Instruments), a BioPrecision 2 linear encoded XY-motorized stage operated by a MAC 5000 modular control system (Ludl), and a Sensicam QE CCD camera (PCO AG) controlled by MetaMorph 7.1 software (Molecular Devices). To visualize Ac-K123 SOD1-Alexa 488, the excitation filter was S490/20x (Chroma) and the emission filter was S528/38m (Chroma). To generate the montage, the "scan slide" function in Metamorph 7.1 was used. At each z position in the scan slide area, a three dimensional image was acquired using the "stream Z" module, generating an average of 100−400 image tiles (1x1 binning, 4 µm step size, 11 z-planes). The z-stacks were processed in MetaMorph 7.5 using the "remove haze" function and maximally projected. Finally, the montage was stitched with a 10% image overlay using the "make montage" function.

2.3 Results

2.3.1 Antibodies demonstrate specificity towards SOD1

To investigate the role of SOD1 K123 acetylation in the central nervous system, we generated affinity purified polyclonal rabbit antibodies. Two independent rabbits (R25 and R26) were immunized with an acetylated peptide (VVHE-AcK-ADDLGKGGC), representing $SOD1_{119-131}$, conjugated to the carrier protein thyroglobulin (Figure 4A). To test whether the antibodies recognized SOD1, protein extracts were isolated from brains of *Sod1*+/+ or *Sod1*-/- mice, separated by SDS-PAGE, and subjected to western blotting using Ac-K123 SOD1, total SOD1, or

α-tubulin primary antibodies. Protein bands were detected by enhanced chemiluminescence through the use of peroxidase-conjugated secondary antibodies. The Ac-K123 SOD1 antibodies detected a single protein band corresponding to SOD1 in *Sod1*+/+ mice (Figure 4B). By contrast, *Sod1* gene deletion in *Sod1*-/- mice abolished Ac-K123 SOD1 antibody binding. Probing with total SOD1 antibodies confirmed *Sod1* gene deletion, and α-tubulin bands demonstrated equal sample loading. The results indicate that our new Ac-K123 antibody is specific to SOD1.

Next, we tested specificity of the Ac-K123 SOD1 antibodies using immunohistochemistry. Frozen brains of *Sod1*-/- or *Sod1*+/+ mice were embedded in OCT and post-fixed sagittal cryosections were incubated with primary Ac-K123 SOD1 antibodies followed by detection with fluorescently labeled secondary antibodies. Nuclei were visualized by counterstaining with Hoechst 33342 fluorescent dye. Specificity of the immunolabeling was evaluated using confocal scanning microscopy. Figure 4C shows representative confocal micrographs of the cerebellum of *Sod1*-/- or *Sod1*+/+ mice. In *Sod1*+/+ mice (Figure 4C, upper panels) the Ac-K123 SOD1 antibodies stained cell bodies within the granular cell layer and molecular layer. By contrast, in *Sod1*-/- mice no discernible immunostaining could be detected (Figure 4C, lower panels). These results suggest that our custom antibodies are specific to SOD1 and can be used for immunohistochemistry.

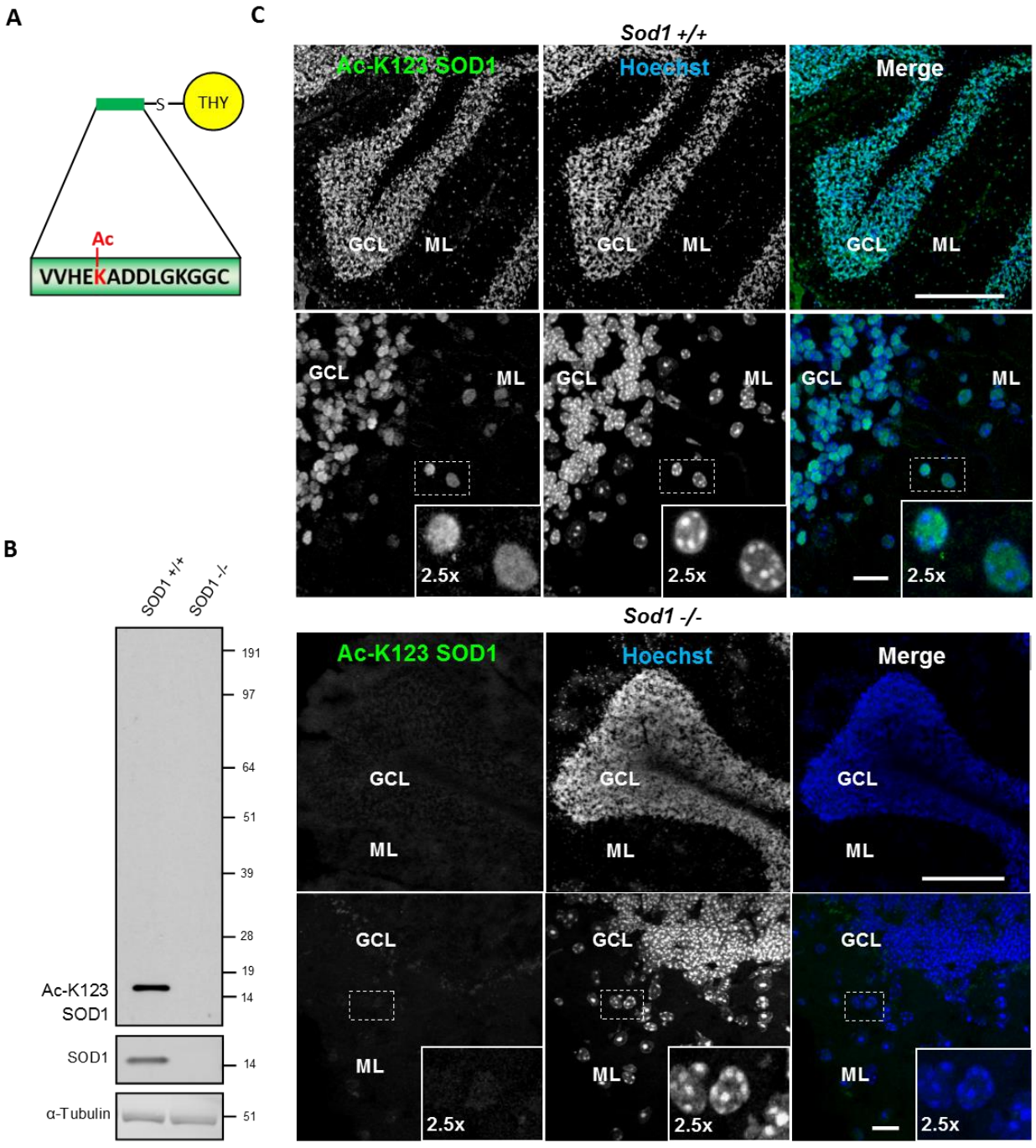

Figure 4. Customized antibodies demonstrate specificity for SOD1.

A. Model of immunogenic peptide used for generation of Ac-K123 SOD1 antibodies. B. Western blot of *Sod1*+/+ and *Sod1*-/- mouse brain lysates probed with Ac-K123 SOD1 (R25), SOD1, and α-Tubulin antibodies. C. Confocal micrographs (scale bar, 200 µm) of *Sod1*+/+ and *Sod1*-/-

mouse cerebellum sagittal sections showing Ac-K123 SOD1 (R26) immunostaining, nuclear Hoechst 33342 labeling, or merged image. The granular cell layer (GCL) and molecular layer (ML) of the cerebellar cortex are identified. Below each image is a higher magnification confocal micrograph (scale bar, 10 μm) of the GCL and ML. Insets show a 2.5x zoom of the boxed region.

2.3.2 Antibodies are specific to Lys123 acetylation

To examine antibody specificity to the K123 acetylated form of SOD1, we transfected HEK293 cells with expression vectors encoding SOD1 WT or the K123R mutant (where lysine was replaced by an arginine making it resistant to acetylation). To differentiate from the endogenous protein, SOD1 was tagged with EGFP. After 48 hours of expression, protein lysates were generated, separated by SDS-PAGE, and processed by infrared fluorescence western blotting. Transiently expressed SOD1 bands were easily distinguishable because endogenous SOD1 has a molecular weight of approximately 16 kDa while EGFP-tagged SOD1 has a molecular weight of 43 kDa. Infrared images indicate EGFP-SOD1 WT was recognized by both Ac-K123 SOD1 and SOD1 antibodies, as demonstrated by the overlapping bands in the merged image (Figure 5A, left lane). By contrast, the acetyl-resistant EGFP-SOD1 K123R mutant was recognized by SOD1 antibodies but not Ac-K123 SOD1 antibodies (Figure 5A, right lane). Thus, the inability to recognize deacetylated mimetic SOD1 K123R, where lysine has been substituted with arginine, suggests that the antibody is specific to the K123 acetylated form of SOD1.

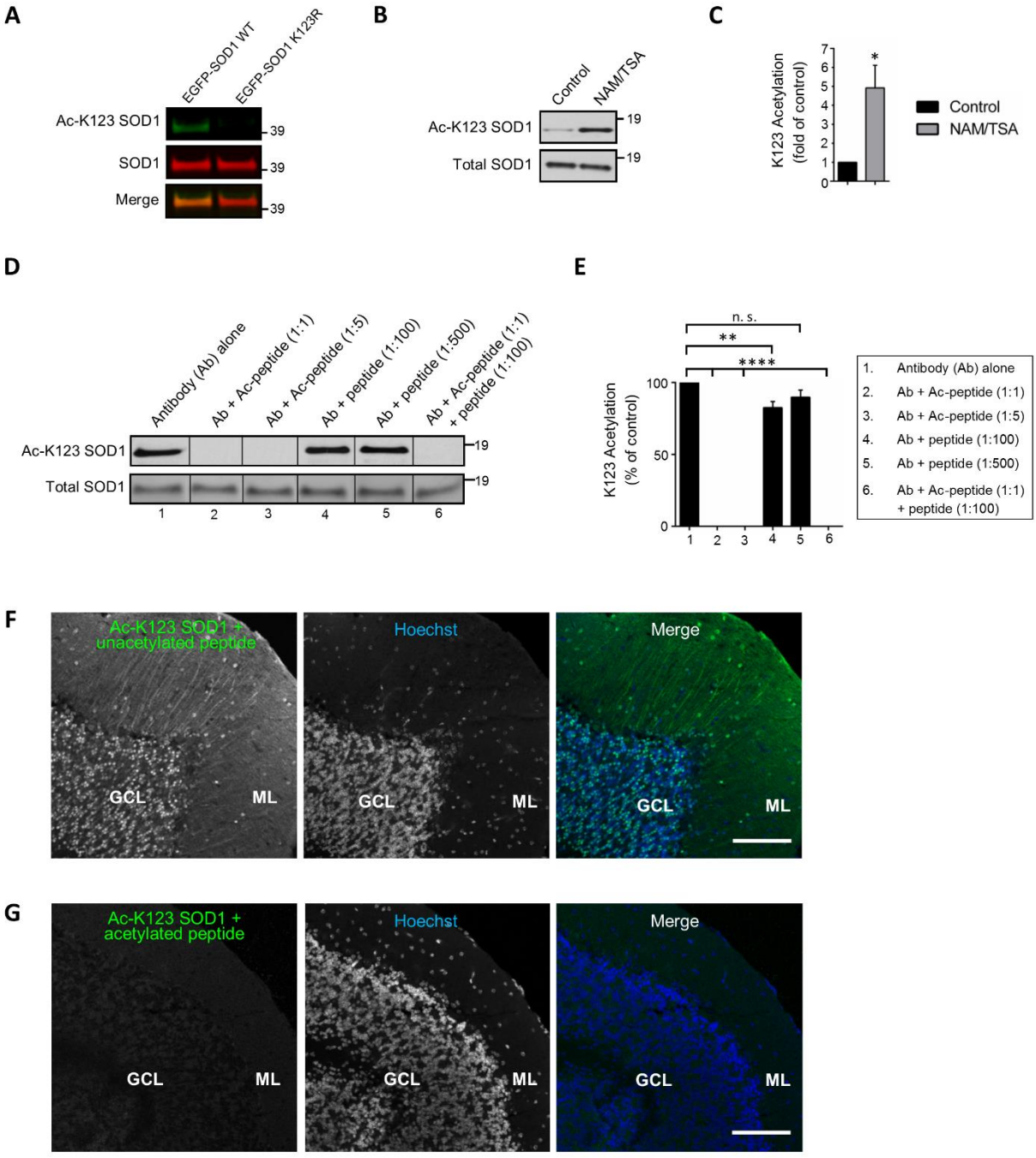

Figure 5. Antibodies are specific for K123-acetylated SOD1.

A. Western blot analysis of transfected HEK293 cells expressing SOD1 WT-EGFP or SOD1 K123R-EGFP. Ac-K123 SOD1 (R26) polyclonal and SOD1 mouse monoclonal antibodies were fluorescently detected by infrared dye conjugated secondary antibodies. B. Western blot

analysis of endogenous Ac-K123 SOD1 (R26) and total SOD1 levels in cell lysates from HEK293 cells that were treated with 10 mM nicotinamide and 1 µM trichostatin A (NAM/TSA) or vehicle control for six hours. Bands were detected by chemiluminescence. C. Quantification of the deacetylase treatment western blot results. Ac-K123 SOD1 band intensities from the blots in (5B) were normalized to those of SOD1, and acetylation level of NAM/TSA treated cells were plotted relative to those in control cells (n = 3, *significance at P<0.05 by Student's *t*-test). D. Western blot analysis of whole cell extracts from deacetylase inhibitor treated HEK293 cells using Ac-K123 SOD1 (R26) antibody that was pre-incubated with no peptide, immunogenic acetylated K123 peptide at a 1:1 or 1:5 (antibody: peptide) molar ratio, unmodified K123 peptide at a 1:100 or 1:500 molar excess, or a mixture of acetylated (1:1) and unacetylated (1:100) K123 peptide. E. Quantification of the antibody preabsorption western blot results. Ac-K123 SOD1 band intensities from the blots in (5D) were normalized to those of SOD1 and plotted as percentage of K123 acetylation relative to the antibody alone (n = 3, ** and **** significance at P<0.01 and P<0.0001 by ANOVA, respectively). F. Confocal micrograph (scale bar, 100 µm) of cerebellum immunostained with Ac-K123 SOD1 (R26) antibody pre-incubated with unacetylated peptide at 1:5 molar ratio prior to immunohistochemistry. S. Blaes performed tissue embedding and cryosectioning. G. Confocal micrograph (scale bar, 100 µm) of cerebellum immunostained with Ac-K123 SOD1 (R26) antibody preabsorbed with acetylated peptide at 1:5 molar ratio prior to immunohistochemistry. S. Blaes performed tissue embedding and cryosectioning. GCL, granular cell layer; ML, molecular layer.

Next, because SOD1 is also succinylated at K123 (Lin et al., 2013) we needed to confirm that our antibody recognized K123 acetylation and not another PTM. To do this, we assessed the detection of endogenous SOD1 K123 acetylation in HEK293 cells treated with either broad-spectrum deacetylase inhibitors (NAM/TSA) or a vehicle control. After a six-hour treatment, cells were lysed and resolved by SDS-PAGE for western blot analysis. Vehicle-control treated cells exhibited a weak signal for Ac-K123 SOD1 (Figure 5B, left lane). By contrast, deacetylase inhibition dramatically increased Ac-K123 SOD1 signal (Figure 5B, right lane). Reprobing the blot with antibodies for total SOD1 indicated that the amount of total SOD1 was similar in both samples (Figure 5B). To quantify the results, we performed densitometric analysis of three independent western blots and observed a four-fold increase in Ac-K123 SOD1 in deacetylase

inhibited cells (Figure 5C). Taken together, these data support that the increased signal detected in deacetylase inhibitor treated cells is due to increased Ac-K123 SOD1 levels, and that the antibody is indeed recognizing acetylation of K123.

Similar to other proteins modified by lysine acetylation, only a small fraction of total SOD1 is predicted to be acetylated (Choudhary et al., 2014). Therefore, despite the use of an affinity matrix during purification (Section 2.2.2), it was important to verify the absence of antibody cross-reactivity with unacetylated SOD1. To assess any cross-reactivity, we performed western blots of deacetylase inhibitor treated lysate using antibody that was pre-incubated with no peptide, acetylated K123 peptide, unacetylated K123 peptide, or a mixture of acetylated and unacetylated peptide. Pre-incubation of the antibody alone resulted in a strong signal for Ac-K123 SOD1 (Figure 5D, lane 1). As expected, preabsorption with acetylated peptide at 1:1 and 1:5 (antibody:peptide) molar ratios totally eliminated antibody binding to Ac-K123 SOD1 (Figure 5D, lanes 2 and 3). By contrast, preabsorption with unacetylated peptide even at 100 and 500 molar excess failed to eliminate binding (Figure 5D, lanes 4 and 5). Finally, pre-incubation with a mixture of both acetylated peptide (1:1) and unacetylated peptide (1:100) also resulted in loss of signal by western blot (Figure 5D, lane 6). Densitometric analysis of three independent western blots is shown in Figure 5E, with the quantification confirming that preabsorption with acetylated peptide at low molar ratios totally eliminated antibody binding to Ac-K123 SOD1. Conversely, unacetylated peptide did not abolish antibody recognition of Ac-K123 SOD1. In fact, even a 500 fold molar excess of unacetylated peptide failed to cause any significant reduction in

detection of Ac-K123 SOD1. Combined, these western blot results confirm antibody specificity to Ac-K123 SOD1 and demonstrate an absence of cross-reactivity to unmodified SOD1.

Finally, to confirm antibody specificity by immunohistochemistry, we probed cerebellar tissue sections with Ac-K123 SOD1 antibodies pre-incubated with the unacetylated or acetylated peptides. In tissue stained with Ac-K123 antibodies pre-incubated with unacetylated peptide, staining was evident in cell bodies of the granular cell layer (GCL) and molecular layer (ML) and processes extending through the molecular layer (Figure 5F). By contrast, in tissue stained with Ac-K123 antibodies preabsorbed with acetylated peptide the staining pattern was abolished (Figure 5G). In addition to preabsorption of the Ac-K123 SOD1 antibody, we performed other negative controls including Ac-K123 SOD1 primary antibody omission and incubation with pre-immune serum. The lack of discernible immunostaining from the *Sod1*$^{-/-}$ tissue and within the negative controls validates antibody specificity for Ac-K123 SOD1.

In summary, these findings strongly indicate that our antibody is specific for Ac-K123 SOD1. The antibody showed increased detection of Ac-K123 SOD1 in lysate derived from cells treated with deacetylase inhibitors, while failing to recognize acetylation-resistant SOD1 expressed in transfected cells. Preabsorption of antibodies to acetylated peptide prevented binding to Ac-K123 SOD1 in western blots, fixed cells, and tissue sections, further demonstrating specificity to acetylated K123.

2.3.3 Ac-K123 SOD1 localizes to hippocampal pyramidal neurons and granule cells of the dentate gyrus

SOD1 carries out important neuromodulatory functions within the hippocampus. Secreted SOD1 modulates synaptic transmission and inhibits long-term potentiation, the long-lasting form of synaptic enhancement linked to learning and memory, within the dentate gyrus and cornus ammonis region 1 (CA1) of the hippocampus (Knapp and Klann, 2002; Viggiano et al., 2012). SOD1 deficiency exacerbates memory loss and amyloid deposition in a mouse model of AD, and SOD1 levels are significantly decreased in human AD patients (Murakami et al., 2011). Based on these important functions and previous findings, we sought to analyze Ac-K123 distribution within the hippocampus and dentate gyrus by immunostaining sagittal brain sections with Ac-K123 SOD1 antibodies.

A micrograph montage of the hippocampal region showed Ac-K123 SOD1 immunostaining was most prominent in the fimbria, the principle hippocampal pathway that connects to subcortical regions, and subiculum, the major hippocampal output structure adjacent to CA1 (Figure 6A). Within the hippocampus labeling of CA1 was observed, while region CA3 stained less strongly (Figure 6A). Staining was also observed in the dentate gyrus, the major target of cortical input to the hippocampus. Cells lining the lateral ventricle wall and from the surrounding cortex were also labeled, and diffuse staining was observed in the corpus callosum (Figure 6A).

Closer examination of the hippocampus indicated Ac-K123 SOD1 localization to CA1 stratum pyramidale cell bodies and processes within the CA1 stratum radiatum (Figure 6B). The CA1 stratum pyramidale mostly consists of pyramidal neurons, which receive input from Schaffer

collaterals and send axons to the subiculum and entorhinal cortex. Also present within this layer, at a much lower density, are the soma and processes of local circuit inhibitory interneurons that include axo-axonic, basket, bistratified, and radial trilaminar cells. The CA1 stratum lacunosum-moleculare, an important layer where performant pathway fibers from the entorhinal cortex synapse onto apical dendrites of CA1 pyramidal cells, also exhibited strong labeling (Figure 6B). Staining was also observed in the dentate gyrus within granule cells, the principal excitatory neurons of the dentate gyrus, and in cell bodies of the molecular layer and polymorphic layer (Figure 6B).

We used a higher magnification view of the CA1 stratum pyramidale to better assess labeling of pyramidal neuron cell bodies and processes of the stratum radiatum. Co-labeling with antibodies against NeuN, neuron-specific marker of the nucleus and cytoplasm, confirmed Ac-K123 SOD1 localization to neuronal cell bodies within the stratum pyramidale (Figure 6C). These labeled cell bodies are tightly packed and layered in a characteristic pattern for pyramidal neurons of the hippocampus. A characteristic of CA1 pyramidal cells is the presence of a single apical dendrite that branches into secondary oblique dendrites farther away from the soma. Immunostaining results demonstrated Ac-K123 SOD1 distribution to the apical dendrites extending from pyramidal neurons into the CA1 stratum radiatum (Figure 6C). Interestingly, labeling was not observed in any dendritic branches emanating from the apical dendrites of pyramidal neurons. Based on the closely arranged soma in the stratum pryamidale and the homogenous morphology of processes that extend into the stratum radiatum, the observed Ac-

K123 labeling within these layers can mostly, if not exclusively, be attributed to pyramidal neurons.

Next, we assessed immunostaining of the dentate gyrus granule layer cell bodies at higher magnification. Interestingly, Ac-K123 SOD1 labeling did not appear to be uniform (Figure 6D). Because of this uneven Ac-K123 SOD1 staining pattern of granule cells and the important role of this region in adult neurogenesis (the dentate gyrus is one of two neurogenic zones in the adult brain) (Ming and Song, 2011), we sought to explore any possible relationship between Ac-K123 SOD1 and neuronal development. Adult hippocampal neurogenesis originates from radial glia-like precursor cells in the subgranular zone of the dentate gyrus and culminates with generation of mature granule cell neurons. To examine Ac-K123 SOD1 in cells undergoing this process, brain tissue was co-labeled with antibodies against doublecortin, a microtubule-associated protein involved in neuronal migration and a marker for adult neurogenesis. Doublecortin expression is transient and tapers off in mature neurons (Brown et al., 2003). Ac-K123 SOD1 immunostaining was strongest in the nuclei of doublecortin-positive immature granule cells of the dentate gyrus (Figure 6D), demonstrating that acetylation of K123 in SOD1 might decrease once granule cells reach maturity.

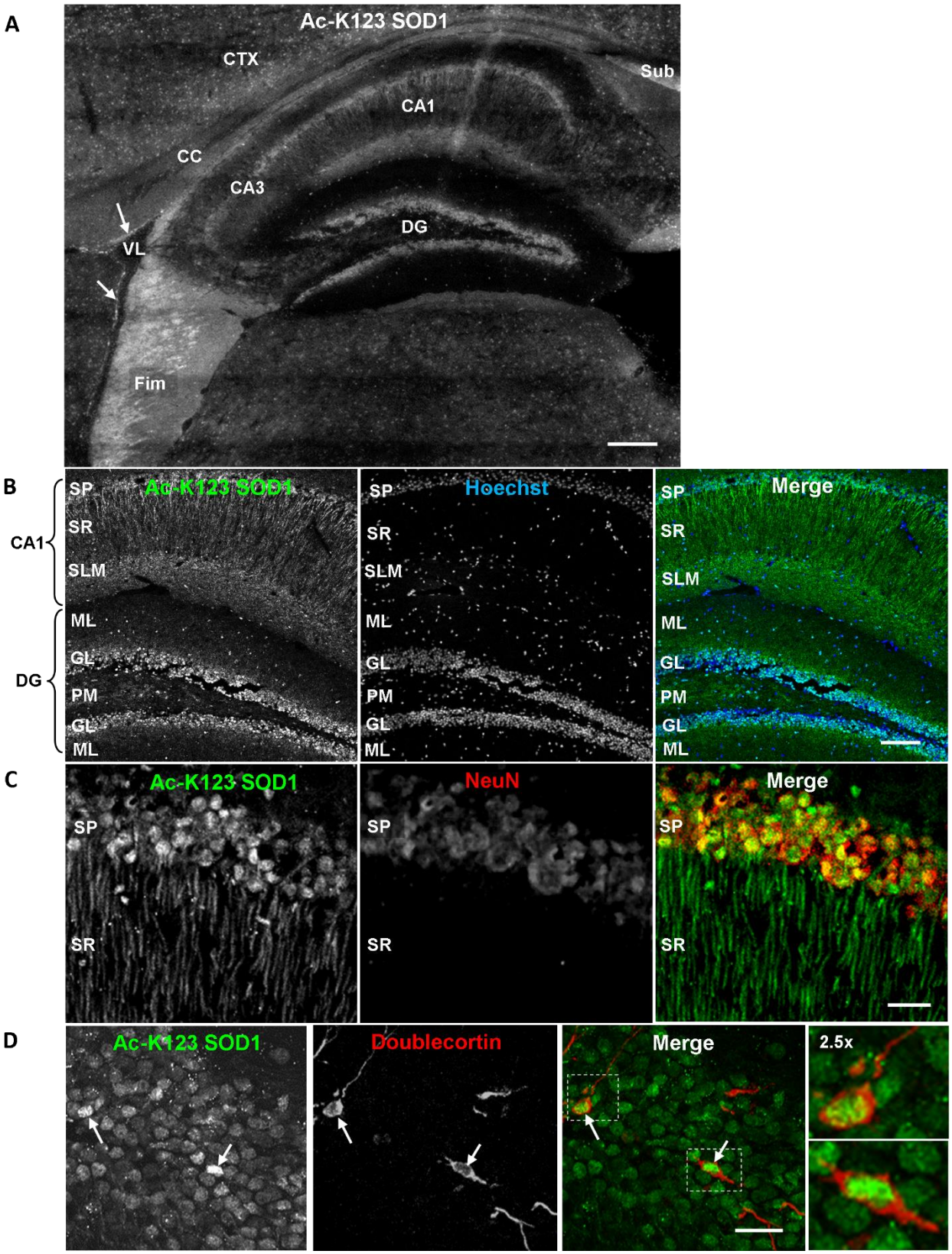
A
Ac-K123 SOD1
CTX
Sub
CA1
CC
CA3
DG
VL
Fim
B
CA1
DG
SP
SR
SLM
ML
GL
PM
GL
ML
Ac-K123 SOD1
Hoechst
Merge
C
Ac-K123 SOD1
NeuN
Merge
D
Ac-K123 SOD1
Doublecortin
Merge
2.5x

Figure 6. Distribution of Ac-K123 SOD1 within dentate gyrus granule cells and CA1 field hippocampal neurons.

A. Sagittal view micrograph montage (scale bar, 200 µm) of the hippocampal region immunostained with Ac-K123 SOD1 (R26) antibodies. Areas of interest include the subiculum (Sub), fimbria (Fim), corpus callosum (CC), cortex (CTX), lateral ventricle (VL), dentate gyrus (DG), hippocampus CA1 field (CA1), and hippocampus CA3 field (CA3). Ac-K123 SOD1 labeling within cells lining the ventricle wall is also shown (arrows). S. Blaes performed tissue embedding and cryosectioning and A. Kennedy performed wide-field fluorescence microscopy and image montage stitching. B. Confocal micrograph (scale bar, 100 µm) of the dentate gyrus and CA1 field of the hippocampus proper labeled with Ac-K123 SOD1 (R26) antibodies and Hoechst 33342. Dentate gyrus regions include the granule layer (GL), polymorph layer (PM), and molecular layer (ML). The CA1 layers shown are the stratum pyramidale (SP), stratum radiatum (SR), and stratum lacunosum-moleculare (SLM). S. Blaes performed tissue embedding and cryosectioning. C. Confocal micrograph (scale bar, 20 µm) of hippocampus CA1 field pyramidal neurons immunostained with antibodies against Ac-K123 (R26) SOD1 and the adult neuron specific marker NeuN. D. Confocal micrograph (scale bar, 20 µm) showing the GL of the dentate gyrus immunostained with antibodies against Ac-K123 SOD1 (R26) and doublecortin. Immature adult granule neurons are noted (arrows). Insets show a 2.5x zoom of the boxed regions of merged image.

In summary, immunostaining of the hippocampus region resulted in strong Ac-K123 SOD1 labeling of neuronal tracts, including the subiculum and fimbria. The principal neurons within the hippocampus and dentate gyrus, the pyramidal and granule cells, also stained for Ac-K123 SOD1. CA1 pyramidal cells of the hippocampus exhibited Ac-K123 SOD1 localization to soma and along apical dendrites. Ac-K123 SOD1 was also found in the soma of dentate gyrus granule cell layer and appeared to be highest in immature granule cells. Interestingly, SOD1 K123 acetylation may be at its highest in cells undergoing neuronal maturation. If this is indeed the case, Ac-K123 SOD1 represents a novel biomarker for assessing adult neurogenesis within the dentate gyrus.

2.3.4 Ac-K123 SOD1 is found in granular cell bodies and molecular layer axons of cerebellum

The cerebellum is a dorsal structure important for control and coordination of movement. In order to investigate the distribution of Ac-K123 SOD1 within the cerebellum, we performed immunostaining of sagittal brain sections. A low magnification micrograph montage of the cerebellum showed strong Ac-K123 SOD1 labeling of the granular cell layer within the highly convoluted cerebellar cortex (Figure 7A). The molecular layer of the cortex exhibited less intense labeling, while the central core of white matter known as the arbor vitae was mostly void of Ac-K123 SOD1 staining.

A higher magnification view allowed better evaluation of Ac-K123 SOD1 distribution within the three layers of the cerebellar cortex: the granular cell layer, Purkinje cell layer, and molecular layer. The most intense immunostaining was observed in the somata of small, densely packed glutamatergic neurons of the granular cell layer, the only excitatory neurons of the cerebellar cortex (Figure 7B). Staining was also observed in cell bodies and processes extending through the molecular layer (Figure 7B, inset). Weak staining was observed in the Purkinje cell layer, where the somata of Purkinje cells reside.

To further examine Purkinje cell staining, tissue was co-stained with antibodies against calbindin D28K, a calcium-binding protein and Purkinje cell marker. The GABAergic Purkinje cells are the sole source of output from the cerebellar cortex, making inhibitory connections onto the cerebellar nuclei. Previous immunohistological examination demonstrated that SOD1 was present throughout all cortical layers of the cerebellum, including cell bodies, dendrites,

and axons of Purkinje cells (Yokoyama et al., 2014). Interestingly, we observed weak Ac-K123 SOD1 labeling within the soma of Purkinje cells compared to cells of other cortical layers (Figure 7C).

We next focused on the distribution of Ac-K123 SOD1 within the molecular layer. This outermost layer of the cerebellar cortex comprises granule cell axons, Purkinje cell dendritic arbors, basket and stellate cell interneurons, and glial cells. In order to identify neurons, sections were co-stained with antibodies against the neuron-specific class III β-tubulin (Tuj1). We found that Ac-K123 SOD1 localized to the soma of molecular layer interneurons (Figure 7D). The cerebellar stellate cells, which are located in outer molecular layer regions and synapse onto the dendritic arbors of Purkinje cells, and basket cells, located immediately above the Purkinje cell layer and forming elaborate branches around Purkinje cell bodies, were identified by both location and positive labeling for Tuj1 (Figure 7D). Labeling was also observed within neuronal processes extending into the molecular layer, demonstrating Ac-K123 SOD1 distribution to Purkinje cell dendritic arbors and possibly the axons of granule cells (Figure 7D).

Cerebellar immunostaining demonstrated strong Ac-K123 SOD1 labeling in the soma of granule cells and molecular layer interneurons. Purkinje cell bodies exhibited less pronounced Ac-K123 SOD1 staining, as did neuronal processes extending into the molecular layer.

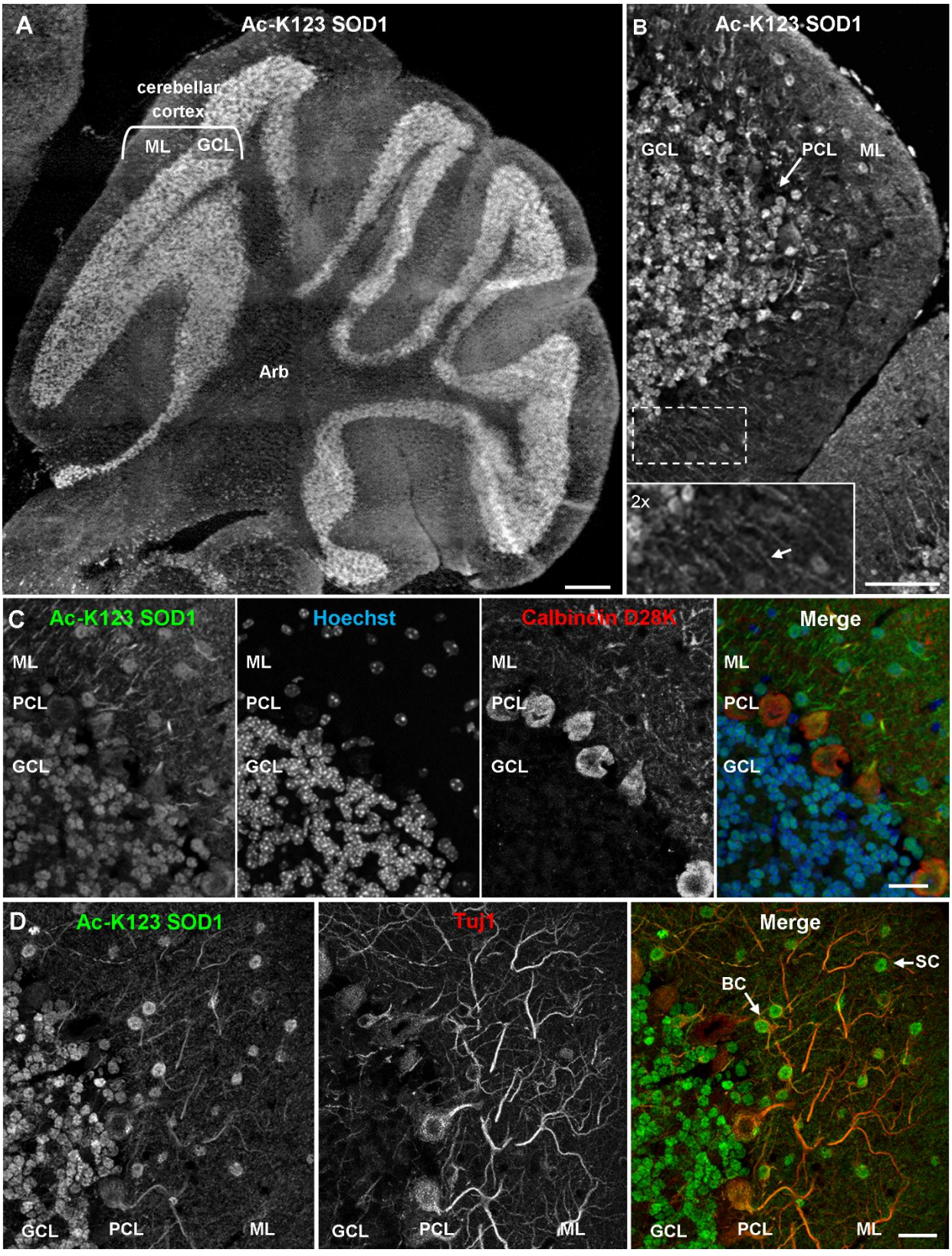
A
Ac-K123 SOD1
cerebellar cortex
ML
GCL
Arb
B
Ac-K123 SOD1
GCL
PCL
ML
2x
C
Ac-K123 SOD1
Hoechst
Calbindin D28K
Merge
ML
PCL
GCL
D
Ac-K123 SOD1
Tuj1
Merge
SC
BC
GCL
PCL
ML

Figure 7. Ac-K123 SOD1 localization within granule, basket, and stellate cell somata and molecular layer neurites of the cerebellum.

A. Sagittal view micrograph montage (scale bar, 500 µm) of cerebellum showing Ac-K123 SOD1 (R26) immunostaining within the cerebellar cortex and underlying arbor vitae (Arb). The cerebellar cortex granule cell layer (GCL) and molecular layer (ML) are noted. S. Blaes performed tissue embedding and cryosectioning and A. Kennedy performed wide-field fluorescence microscopy and image montage stitching. B. Confocal micrograph (scale bar, 50 µm) demonstrating Ac-K123 SOD1 (R26) immunostaining in the cerebellum. Shown is the cerebellar cortex layers, consisting of the GCL, Purkinje cell layer (PCL), and ML. Inset shows a 2x zoom of the boxed region demonstrating Ac-K123 SOD1 labeled processes within the ML (arrow). S. Blaes performed tissue embedding and cryosectioning. C. Higher magnification confocal micrograph (scale bar, 20 µm) of GCL, PCL, and ML immunostained for Ac-K123 SOD1 (R26) and Calbindin D28K with nuclear counterstaining by Hoechst 33342. S. Blaes performed tissue embedding and cryosectioning. D. Confocal micrograph (scale bar, 20 µm) of GCL, PCL, and ML immunostained for Ac-K123 SOD1 (R26) and Tuj1. Examples of stellate cells (SC) and basket cells (BC) are marked by arrows.

2.3.5 Ac-K123 SOD1 in ependymal cells of ventricle and choroid plexus

Recent findings have identified SOD1 in human cerebral spinal fluid (CSF) samples (Winer L et al., 2013). The CSF bathes the central nervous system exterior and is vital for normal brain function, acting as a mechanical cushion and creating an optimal environment for neuronal cells (Speake et al., 2001). Because the mechanism of entry and role of SOD1 in the CSF has yet to be determined, we sought to explore whether Ac-K123 SOD1 is present in specific regions of the brain in contact with CSF.

Analysis of immunostained sagittal sections demonstrated Ac-K123 SOD1 labeling of choroid plexus cells within the 4th ventricle of the brain (Figure 8A). CSF is produced by the four choroid plexuses, branched epithelial structures found within each ventricle of the brain (Speake et al., 2001). Ac-K123 SOD1 labeling was also observed in ependymal cells lining the ventricle wall

(Figure 8A). These multi-ciliated cells are specialized glia involved in the directional movement of CSF.

A higher magnification view confirmed strong SOD1 K123 acetylation within cuboidal epithelial cells of the choroid plexus and ependymal cells, the ciliated cells lining the ventricle wall involved in the directional movement of CSF (Figure 8B). Ac-K123 SOD1 is primarily distributed to the nucleus and cytoplasm of choroid plexus epithelial cells and ependymal cells.

These findings, demonstrating Ac-K123 SOD1 distribution within choroid plexus and ependymal cells, merit further investigation into the role of SOD1 K123 acetylation during the production and circulation of CSF.

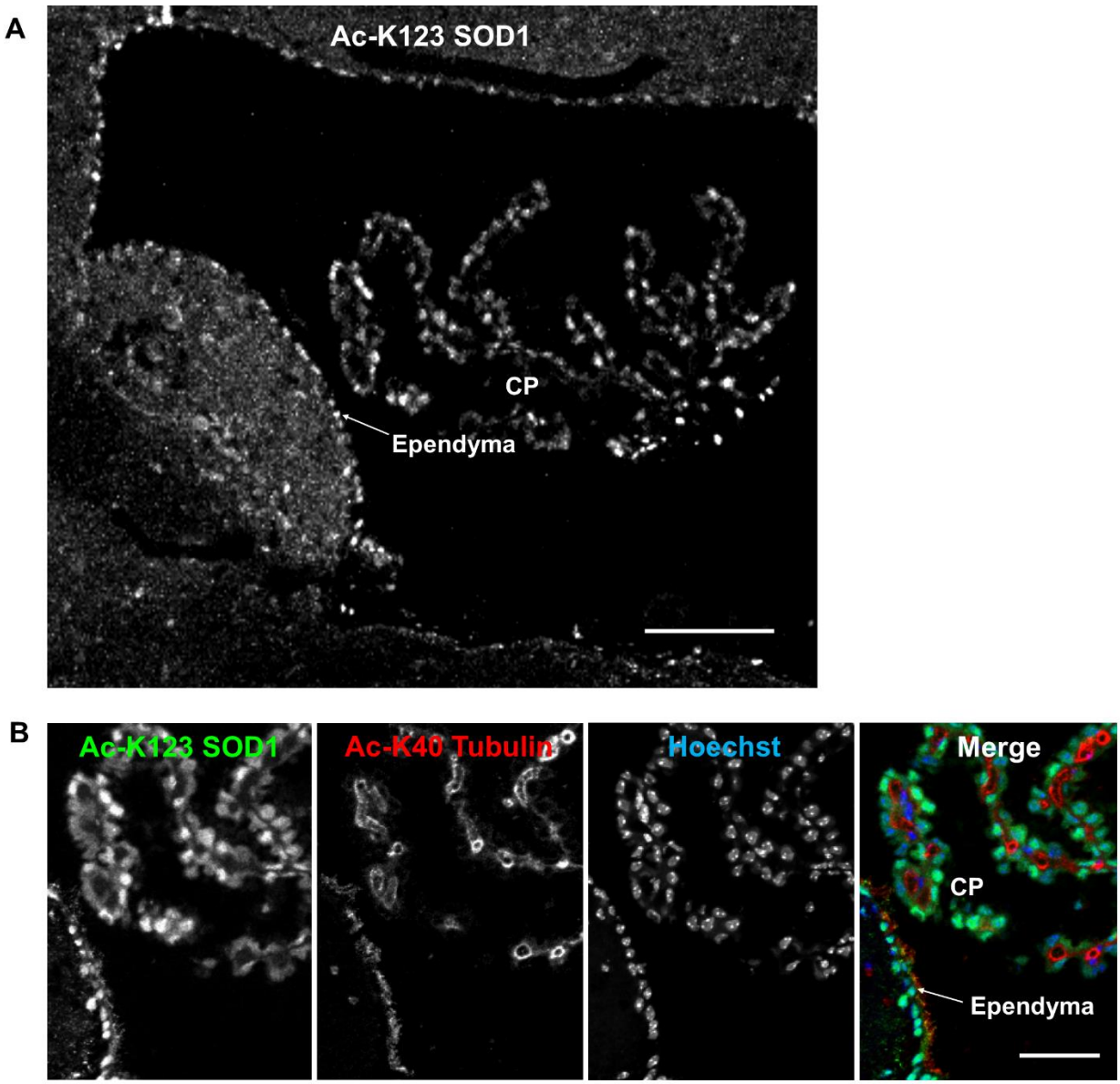

Figure 8. Ac-K123 SOD1 localization in choroid plexus and ependymal cells.

A. Sagittal view confocal micrograph (scale bar, 100 µm) of 4th ventricle immunostained for Ac-K123 SOD1 (R26). Identified are the choroid plexus (CP) and ventricle wall ependymal cells (Ependyma). S. Blaes performed tissue embedding and cryosectioning. **B.** Higher magnification confocal micrograph (scale bar, 50 µm) of CP and Ependyma immunostained for Ac-K123 SOD1 (R26) and Ac-K40 α-Tubulin. Nuclei were counterstained with Hoechst 33342. S. Blaes performed tissue embedding and cryosectioning.

2.3.6 Ac-K123 SOD1 localizes to interneuron cell bodies and the major afferent and efferent neuronal processes of the olfactory bulb

SOD1 is ubiquitously expressed throughout the nervous system of developing and adult mice, including within areas important for olfaction. The oval-shaped olfactory bulb, located in the rostral portion of the forebrain, is the main center in the mouse olfactory system. Olfactory bulb alterations, including vacuolar lesions, have been observed in mutant SOD1 transgenic mice (Dal Canto and Gurney, 1995; Wong et al., 1995). Loss of smell has been observed in ALS patients and excessive lipofuscin deposition has been noted in the mitral and tufted cells of their olfactory bulbs (Elian, 1991; Hawkes et al., 1998). To better understand the pattern of SOD1 Lys123 acetylation within the adult mouse olfactory system, we examined Ac-K123 SOD1 immunostaining within the olfactory bulb.

Examination of main olfactory bulb coronal sections indicated strong Ac-K123 SOD1 antibody staining of the olfactory nerve layer, the surface of the olfactory bulb formed by afferent projections of the olfactory sensory neurons (Figure 9A)**.** Previous immunohistochemical analysis identified high SOD1 immunoreactivity in olfactory sensory neurons (Yon et al., 2008), which are responsible for detection of odorants through their odorant receptors. Axons from olfactory sensory neurons project toward the main olfactory bulb, where they synapse with second-order neurons, the mitral and tufted cells, in specialized compartments called glomeruli.

When viewed at lower magnification, the glomerular layer was for the most part void of staining with the exception of weak labeling in the cell bodies surrounding glomeruli (Figure

9A). Beyond the glomerular layer, Ac-K123 SOD1 staining was observed in processes running through the outer plexiform layer, internal plexiform layer, and granule cell layer (Figure 9A). Cell bodies of the granule cell layer also exhibited Ac-K123 SOD1 labeling (Figure 9A).

To better assess Ac-K123 SOD1 staining of the glomerular layer, we examined this region at higher magnification. Staining results clearly demonstrated Ac-K123 SOD1 distribution within the soma of periglomerular cells, the small interneurons adjacent to the glomeruli, and processes within the olfactory glomeruli core (Figure 9B). These processes are neuronal, as they did not co-label with antibodies against GFAP, an intermediate filament protein specific to astrocytes (Figure 9C). These Ac-K123 SOD1 positive neurites within the glomeruli core could be either olfactory sensory neuron axons or primary dendrites of mitral and tufted cells.

A higher magnification view also showed Ac-K123 SOD1 staining of processes in the outer plexiform layer (Figure 9D). This layer contains the soma of tufted cells, basal dendrites of tufted and mitral cells, and apical dendrites of granule cells. Within the mitral cell layer, crossing processes showed strong Ac-K123 SOD1 labeling while large mitral cell bodies were weakly stained (Figure 9D). In the internal plexiform layer, through which axons of mitral and tufted cells course, staining was observed within processes (Figure 9D). Similar to the periglomerular interneurons, cells within the granule cell layer exhibited Ac-K123 SOD1 distribution within their soma (Figure 9D). These GABAergic granule cells, the principal interneurons of the olfactory bulb, modulate mitral and tufted cell activity by inhibitory feedback. In addition to the granule cell soma, Ac-K123 SOD1 was observed within processes of

the granule cell layer (Figure 9D). Mitral and tufted cells project axons through this layer, eventually emerging from the caudal portion of the olfactory bulb to form the lateral olfactory tract. These efferent fibers of the lateral olfactory tract connect the olfactory bulb to several central brain regions via collateral branching (Schwob and Price, 1984).

A sagittal view of the posterior olfactory bulb identified Ac-K123 SOD1 within axonal tracts extending through the lateral olfactory tract in the area of the olfactory peduncle, the region that connects the olfactory bulb with the basal forebrain. From this view, Ac-K123 SOD1 was also observed in cell bodies of the olfactory bulb granule cell layer (Figure 9E).

In summary, olfactory bulb immunostaining demonstrated Ac-K123 SOD1 localization to cell bodies of interneurons and along processes of the major afferent neurons (olfactory sensory neurons) and efferent neurons (mitral and tufted cells).

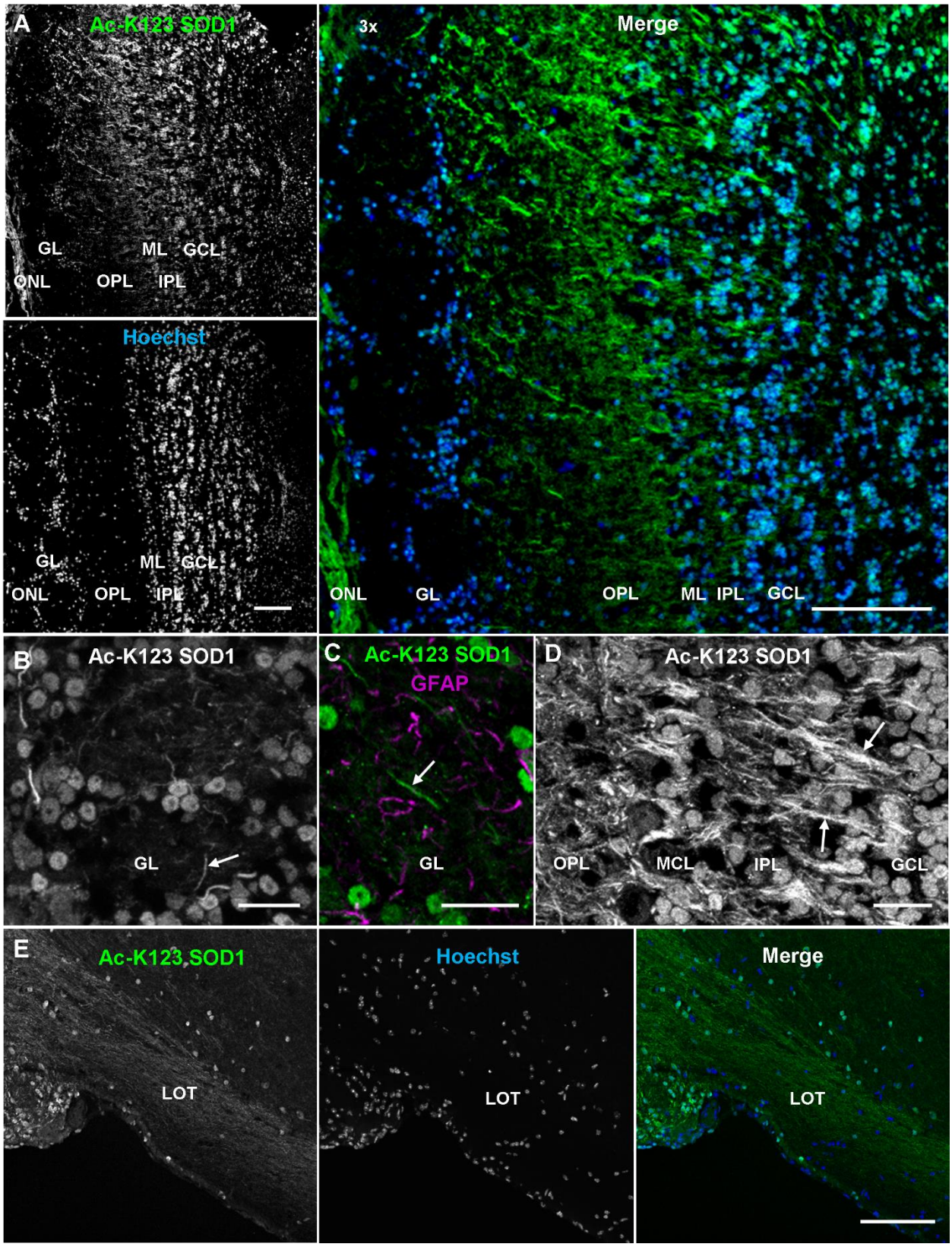
A
Ac-K123 SOD1
GL
ML
GCL
ONL
OPL
IPL
Hoechst
GL
ML
GCL
ONL
OPL
IPL
3x
Merge
ONL
GL
OPL
ML
IPL
GCL
B
Ac-K123 SOD1
GL
C
Ac-K123 SOD1
GFAP
GL
D
Ac-K123 SOD1
OPL
MCL
IPL
GCL
E
Ac-K123,SOD1
LOT
Hoechst
LOT
Merge
LOT

Figure 9. Ac-K123 SOD1 within the olfactory bulb and lateral olfactory tract.

A. Confocal micrograph (scale bar, 100 µm) showing Ac-K123 SOD1 (R26) immunostaining, Hoechst nuclear counterstaining, and 3x merged image of the posterior main olfactory bulb in the coronal plane. Identified regions include olfactory nerve layer (ONL), glomerular layer (GL), outer plexiform layer (OPL), mitral cell layer (MCL), inner plexiform layer (IPL), and granule cell layer (GCL). B. Confocal micrograph (scale bar, 20 µm) of GL immunostained for Ac-K123 SOD1 (R26). An example of a neurite extending into the glomerulus is also labeled (arrow). C. Confocal micrograph (scale bar, 20 µm) of an olfactory glomerulus core within the GL labeled for Ac-K123 SOD1 (R26) and GFAP. An example of a neurite labeled with Ac-K123 SOD1 and not GFAP is shown (arrow). D. Confocal micrograph of the OPL, ML, IPL, and GCL immunostained for Ac-K123 SOD1 (R26) (scale bar, 20 µm). Granule cell processes and tufted or mitral cell primary axons are labeled (arrows). E. Sagittal view confocal micrograph (scale bar, 100 µm) of posterior olfactory bulb showing axonal tracts extending through the lateral olfactory tract (LOT) in the area of the olfactory peduncle. Immunostaining of olfactory bulb was performed with antibodies against Ac-K123 SOD1 (R26) and nuclei were counterstained with Hoechst 33342. S. Blaes performed tissue embedding and cryosectioning (Figure 6E).

2.3.7 Ac-K123 SOD1 is found with specific layers of the retina

SOD1 plays an important protective role in the retina, an area particularly susceptible to oxidative stress. Decreased SOD1 function has been shown to be detrimental to retinal health. SOD1-deficient mice develop age-related retinal degenerative disorders, including macular degeneration (Hashizume et al., 2008; Imamura et al., 2006), and the lens from SOD1-deficient mice has been shown to have increased superoxide levels with accelerated cataract development compared to control mice (Behndig et al., 2001). Age-dependent dry eye also develops in SOD1-deficient mice due to lacrimal gland dysfunction (Kojima et al., 2012). Therefore, we performed immunohistochemistry on vertical sections of mouse retina with Ac-K123 SOD1 antibodies and Hoechst nuclear counterstaining.

Ac-K123 SOD1 staining was detected in cell bodies within the retinal ganglion cell layer, inner nuclear layer, and outer nuclear layer (Figure 10A). Strong labeling was observed within the retinal ganglion cell layer, the site where light first enters before penetrating all other retinal layers. This retinal layer contains cell bodies of retinal ganglion cells, the output neurons of the retina whose axons merge to form optic nerve fibers that transmit visual information to the brain.

Labeling was also observed within soma of the inner nuclear layer (Figure 10A), which contains the cell bodies of bipolar, horizontal, amacrine, and Müller cells. Bipolar cells transmit signals from the photoreceptors to the ganglion cells, amacrine cells form an alternative route between bipolar and ganglion cells, and horizontal cells modulate visual signals through lateral inhibition of neighboring photoreceptor cells. Müller cells, the principal glial cell of the retina, are radial glia that span the entire retina and provide architectural support.

The staining of cell bodies within the outer nuclear layer was strong but less uniform than that of the retinal ganglion cell layer and inner nuclear layer (Figure 10A). The outer nuclear layer contains the cell bodies of rods and cones, the photoreceptor cells responsible for photon detection and transduction into electrochemical signals. Based on the anatomical distribution of rods and cones, namely that the density of rods is much greater than cones throughout most of the retina, we surmise that the relatively sparse number of Ac-K123 SOD1 positive outer nuclear layer cell bodies are those of cone cells. Because it has been shown that SOD1 is an

important component of the antioxidant defense system of cones (Usui et al., 2011), our finding of Ac-K123 SOD1 within the cones of the outer nuclear layer is of high interest.

Ac-K123 SOD1 staining was evident within the neurites of the inner plexiform layer, the area of synaptic contact between the bipolar cell axons and the dendrites of the ganglion and amacrine cells (Figure 10A). Not surprisingly, weaker Ac-K123 SOD1 labeling was observed in the outer plexiform layer, the much thinner layer of processes where projections of rods and cones terminate and synapse with dendrites of bipolar and horizontal cells (Figure 10A). Ac-K123 SOD1 exhibited strong localization to retinal ganglion cell neurites (Figure 10A). The strongest Ac-K123 SOD1 staining of retinal processes was observed in the retinal ganglion cell layer (Figure 10A). As the integrity of these processes varied throughout the retinal sections, we sought out sections with intact processes to better assess Ac-K123 SOD1 labeling within the retinal ganglion cell layer. Results from selected sections demonstrated Ac-K123 SOD1 distribution to both retinal ganglion cell bodies and neurites (Figure 10B). Closer examination of this layer indicated Ac-K123 SOD1 labeling of retinal ganglion cell axons, the long processes emerging from the retinal ganglion cell bodies (Figure 10B, inset).

In summary, our immunostaining results demonstrated that Ac-K123 SOD1 was localized to cell bodies within the inner nuclear and ganglion cell layers, as well as cone cells of the outer nuclear layer. Ac-K123 SOD1 was also distributed along retinal ganglion cell axons and processes coursing through the inner plexiform layer. It was previously shown that SOD1, because of its superoxide scavenging activity, is indispensable to retinal ganglion cells, and

SOD1 deficiency causes retinal ganglion cell vulnerability and death (Yuki et al., 2011). SOD1 has also been shown to play an important neuroprotective role against N-methyl-d-aspartate-induced cytotoxicity in retinal ganglion and inner nuclear layer cells (Yuki et al., 2013). Because our immunostaining results indicated high levels of Ac-K123 SOD1 within these regions, it will be worthwhile to investigate if there is a correlation between SOD1 K123 acetylation and retinal neuron survival.

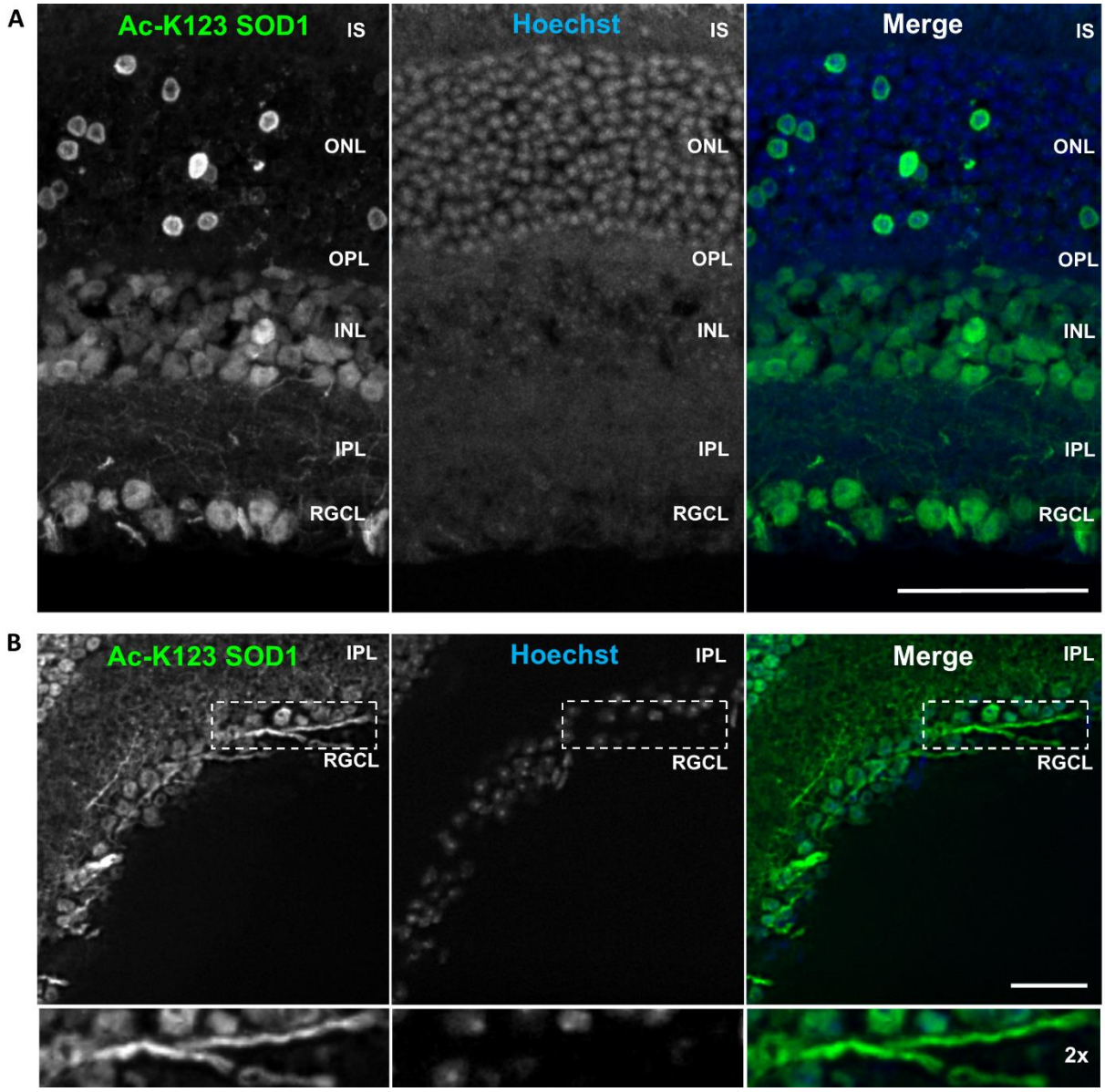

Figure 10. Ac-K123 SOD1 localization to retinal ganglion cells, outer and inner nuclear layer cell bodies, and inner plexiform layer neurites.

A. Confocal micrograph (scale bar, 50 µm) of a vertical section through the mouse retina showing Ac-K123 SOD1 (R26) immunostaining with nuclear counterstaining by Hoechst 33342. Identified retinal layers include the inner segments of photoreceptor (IS), outer nuclear layer (ONL), outer plexiform layer (OPL), inner nuclear layer (INL), inner plexiform layer (IPL), and retinal ganglion cell layer (RGCL). B. Fluorescence micrograph (scale bar, 50 µm) of a vertical section through the mouse retina demonstrating Ac-K123 SOD1 (R26) distribution within RGCL and IPL. Inset shows a 2x zoom of the boxed region containing a labeled RGC axon. A. Kennedy

performed immunostaining (Figure 10A), confocal microscopy (Figure 10A), and wide-field microscopy (Figure 10B). S. Blaes performed tissue embedding and cryosectioning (Figure 10A-B) and immunostaining (Figure 10B).

2.3.8 Ac-K123 SOD1 localizes to neurites and the nucleus in cortical neurons

To determine the localization of Lys123 acetylated SOD1 within neurons, we immunostained pure rat cortical neuron cultures with our antibody against Ac-K123 SOD1. Our findings show acetylated Lys123 SOD1 is predominantly found within the nucleus and neurites of primary cortical neurons (Figure 11A). The staining pattern of the neurites was noteworthy, as a strong but discontinuous staining pattern was observed within the neuronal processes (Figure 11B).

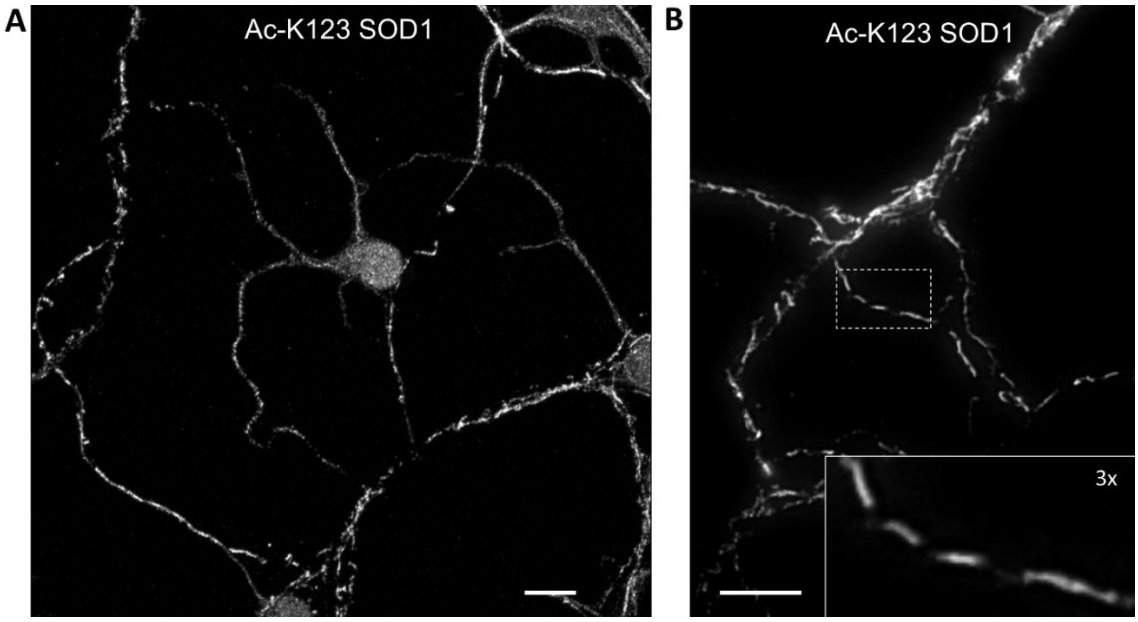

Figure 11. Lys123 acetylated SOD1 is localized within somata and neurites of cortical neurons.

A. Fluorescent micrograph (scale bar, 10 µm) of cultured rat primary cortical neurons immunostained for Ac-K123 SOD1. B. Fluorescent micrograph (scale bar, 30 µm) of cultured rat primary cortical neurons immunostained for Ac-K123 SOD1. Inset shows a 3x zoom of the boxed region demonstrating a discontinuous staining pattern of neurites. A. Kennedy performed immunostaining and wide-field microscopy (Figure 11A-B).

Additional immunostaining was done to evaluate whether Ac-K123 SOD1 detected in neurites was restricted to dendrites or axons. Immunostaining of neuron and astrocyte mixed cultures showed that Ac-K123 SOD1 localized to both the nucleus and dendrites of cortical neurons. Dendritic staining was confirmed by co-localization with microtubule-associated protein 2 (MAP2), while nuclear localization was confirmed by Hoechst counterstaining (Figure 12A). The Ac-K123 SOD1 labeled primary cilia observed in these cultures are from surrounding astrocytes (Figure 12A). These surrounding cells were confirmed to be astrocytes by positive co-labeling for GFAP (Figure 12B), and the origination of Ac-K123 SOD1 labeled primary cilia from astrocytes was clearly demonstrated through analysis of z-series confocal micrographs. However, Ac-K123 SOD1 localization to neuronal primary cilia should not be excluded. Most neurons contain primary cilia, and co-labeling with a neuronal ciliary marker was not performed. Unlike in astrocytes and many other cell types, Ac-K40 α-tubulin is not a marker for neuronal primary cilia. It should be noted that primary cilia were shown to be present in these cultured primary cortical neurons by immunostaining for type III adenylyl cyclase (ACIII), a marker for neuronal primary cilia (Figure 12C). Unfortunately ACIII and Ac-K123 SOD1 co-labeling was not performed due to both antibodies originating from the same host species.

Analysis of immunostained astrocyte and neuron mixed cultures also revealed long processes staining for Ac-K123 SOD1, but not MAP2. To evaluate whether Ac-K123 SOD1 localizes to axons, neurons were transfected with an expression plasmid for GFP-tagged Tau and immunostained for Ac-K123 SOD1 three days post transfection. Immunostaining of transfected

primary cortical neurons expressing Tau-GFP confirmed the axonal localization of Ac-K123 SOD1 (Figure 12D).

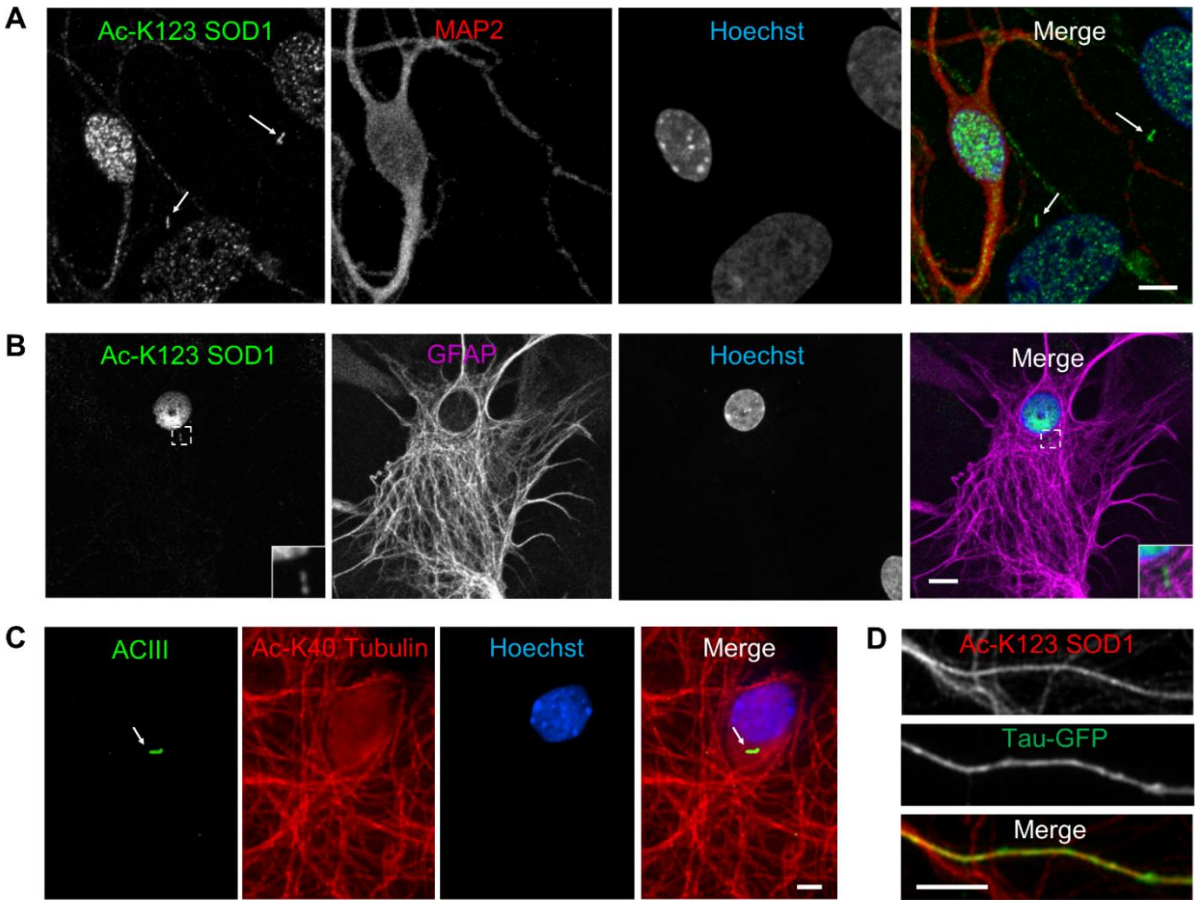

Figure 12. Lys123 acetylated SOD1 is localized within dendrites and axons of cortical neurons.

A. Confocal micrograph (scale bar, 10 µm) of primary cortical neurons co-cultured with primary astrocytes and immunostained for Ac-K123 SOD1 and the dendritic marker MAP2. Ac-K123 SOD1 labeling of primary cilia is also shown (arrows). B. Confocal micrograph (scale bar, 10 µm) of primary cortical neurons co-cultured with primary astrocytes and immunostained for Ac-K123 SOD1 and the astrocytic marker GFAP. Inset shows a 3x zoom of the boxed region demonstrating a primary cilium labeled for Ac-K123 SOD1 originating from an astrocyte. C. Confocal micrograph (scale bar, 10 µm) of primary cortical neurons immunostained for Ac-K40 α-tubulin and ACIII, a marker for neuronal primary cilia. ACIII labeling of a primary cilium is also shown (arrow). D. Confocal micrograph (scale bar, 10 µm) of transfected primary cortical neurons expressing Tau-GFP and immunostained for Ac-K123 SOD1. H. Hauser performed transfection (Figure 12D). A. Kennedy performed confocal microscopy (Figure 12D).

2.4 Discussion

SOD1 is acetylated at K123 within the electrostatic loop, a functional domain critical to enzymatic function and structural stability. Prior to our current study, the impact of this PTM had yet to be investigated. To gain a better understanding of SOD1 K123 acetylation, we generated rabbit polyclonal antibodies against Ac-K123 SOD1. Herein, we demonstrated specificity of this new antibody and described the distribution of Ac-K123 SOD1 within the normal nervous system.

In the cerebellar cortex, strongest Ac-K123 SOD1 immunoreactivity was observed in the glutamatergic granule cells. The soma of glutamatergic dentate granule cells and CA1 pyramidal cells were strongly stained for Ac-K123 SOD1 within the hippocampal formation. The strongest Ac-K123 SOD1 labeling of the olfactory bulb was along olfactory sensory neuron fibers and axons of glutamatergic tufted and mitral cells. In the retina, the glutamatergic ganglion cells exhibited the highest levels of Ac-K123 SOD1. Inner nuclear layer cell bodies and glutamatergic outer nuclear layer cone cells also exhibited considerable Ac-K123 SOD1 immunoreactivity. This would suggest that SOD1 K123 acetylation is optimized within functionally distinct neuronal subtypes.

Another key finding was the localization of Ac-K123 SOD1 within processes of major afferent and efferent neurons. In the hippocampal formation, tracts of the subiculum and fimbria were strongly labeled, as were apical dendrites of the efferent CA1 pyramidal cells. Strong Ac-K123 SOD1 labeling was also noted within mitral and tufted cell axonal projections of the olfactory

bulb, along fibers coursing through the lateral olfactory tract, and in the efferent axons of retinal ganglion cells. The propensity of Ac-K123 SOD1 to localize within long axonal projections of afferent and efferent neurons, as opposed to the shorter processes of interneurons, merits further study. It is possible that Ac-K123 SOD1 interacts with proteins specific to these axons, such as phosphorylated neurofilament heavy chain proteins, which are predominantly found in larger axons.

A noteworthy finding from the immunostaining of primary cortical neurons is the unique localization pattern observed within neuronal processes. This pattern is of interest because discontinuous staining is often indicative of microtubule-based transport. Mutant SOD1 has an increased propensity to interact with microtubule motor proteins and cargo linkers, resulting in impaired axonal transport (De Vos et al., 2007; Warita et al., 1999; Williamson and Cleveland, 1999). Because one of the effects of protein acetylation is altered protein-protein interaction, it will be interesting to investigate how SOD1 acetylation impacts axonal transport in neurons.

Finally, identification of Ac-K123 SOD1 in cells associated with CSF is an interesting finding. Ac-K123 SOD1 was highly localized to choroid plexus cuboidal cells and ventricle wall ependymal cells, the cells responsible for CSF production and circulation within the brain. Ac-K123 SOD1 antibody also strongly stained ependymal cells of the central canal within the spinal cord, an area continuous with the ventricular system of the brain and filled with CSF. Ependymal cells are responsible for regulating CSF, where interestingly SOD1 has been detected in patients.

Collectively, our findings provide a new understanding of the regional and cell-specific distribution of Ac-K123 SOD1 in the central nervous system. PTMs profoundly affect the structure and function of proteins, and substantial evidence suggests a role for aberrant PTMs in many neurodegenerative diseases. Significantly, PTMs have been shown to promote SOD1 misfolding in ALS. Because of the critical role of SOD1 and the distribution patterns of Ac-K123 SOD1 within the central nervous system that we have identified, our observations lay the foundation for future investigations into the function of acetylation in normal physiology and pathophysiology.

CHAPTER THREE: SOD1 ACETYLATION AND THE CELL CYCLE

3.1 Protein acetylation and the cell cycle

Acetylation and deacetylation of proteins is regulated by several families of acetyltransferase and deacetylase proteins. Among other factors, nutrient availability and cell cycle phase affect the acetylation status of proteins (Schwer et al., 2009).

3.1.1 SOD1 and the cell cycle

The process of cell proliferation is tightly controlled and highly sensitive to damages resulting from oxidative stress. To ensure fidelity during cell division, the cell relies on an antioxidant system to combat reactive oxygen species as well as a surveillance system to detect oxidative damage and initiate cell cycle checkpoint responses (Shackelford et al., 2000). It has been shown that SOD1 plays an important role in both these cellular systems.

The importance of SOD1 as an antioxidant has been demonstrated by *in vivo* studies utilizing *Sod1*$^{-/-}$ mice. Biochemical analysis of various organs showed an accumulation of oxidative molecules such as oxidized nucleic acids, lipid peroxidants, and advanced glycation end products (Watanabe et al., 2014). Data from tissues also shows induction of the DNA damage response via upregulation and activation of tumor suppressor p53 (Han et al., 2008a). Work in cultured cells further demonstrated this link with p53, as Sod1 deficient fibroblasts exhibited

This chapter includes material from the article “Primary cilia and autophagic dysfunction in Huntington's disease” previously published in *Cell Death and Differentiation* by Nature Publishing Group

superoxide accumulation which led to p53-mediated growth arrest and apoptosis (Watanabe et al., 2013). SOD1 has also been shown to take a more direct role with regard to protection of the genome. A recent report describes how SOD1, in response to ROS, translocates to the nucleus where it acts as a transcription factor to regulate the expression of oxidative resistance and repair genes (Tsang et al., 2014). Disturbed intracellular redox signaling and numerous alterations in the expression or activation of cell cycle proteins have also been described in various models of ALS involving mutant SOD1 (Cova et al., 2010; Nguyen et al., 2003), further demonstrating an intricate link between SOD1 and cell cycle regulation.

3.1.2 Structure and function of primary cilia

Found in nearly all post-mitotic or growth-arrested mammalian cells, primary cilia are solitary structures that protrude into the extracellular environment (Wheatley et al., 1996) (Figure 13A-B). These highly conserved, non-motile, signaling organelles act like cellular antennae, receiving neuroendocrine and sensory signals from the environment and activating signaling cascades that communicate with the rest of the cell (Singla and Reiter, 2006).

In order to facilitate their specialized signaling functions, primary cilia are compartmentalized from the rest of the cell by unique structures that include an ordered membrane-bound septin ring structure, a transition zone at the base of the cilium, and a specialized receptor-dense ciliary membrane (Garcia-Gonzalo et al., 2011; Hu et al., 2010). A microtubule-based axoneme extends out from the basal body which is anchored to the plasma membrane by transition fibers (Figure 13C). A unique bidirectional intraflagellar transport (IFT) system is utilized for the

trafficking of signaling and structural components along the axoneme (Rosenbaum and Witman, 2002). A complex of Bardet-Biedl Syndrome proteins (BBSome) and IFT proteins coordinates cargo attachment to microtubule motors, creating multi-protein IFT complexes that travel along the axoneme (Wei et al., 2012). IFT complex A is utilized for dynein-2-mediated retrograde transport and IFT complex B is used for kinesin-2-mediated transport to the ciliary tip (Figure 13C).

Primary cilia are essential for the regulation of critical signals during embryonic development and tissue homeostasis. Their presence is required for Sonic hedgehog signal transduction, and they have essential roles in Wnt, platelet-derived growth factor and transforming growth factor-β signaling pathways (Clement et al., 2013; Corbit et al., 2005, 2008; Rohatgi et al., 2007; Schneider et al., 2005). Primary cilia are also essential for mechanosensory signal transduction, such as in the detection of fluid flow in the kidney epithelium (Nauli et al., 2003; Pazour et al., 2002). Receptors and signaling cascades essential for olfaction, vision, hearing, and taste are also localized to primary cilia, demonstrating a key role in sensory perception (Jenkins et al., 2009; Kulaga et al., 2004; Sun et al., 2012; Wheway et al., 2013; Zhang et al., 2013). Primary cilia also play important roles in hormonal regulation with implications in dopamine, somatostatin, serotonin, and leptin signaling (Brailov et al., 2000; Domire et al., 2011; Han et al., 2014; Händel et al., 1999).

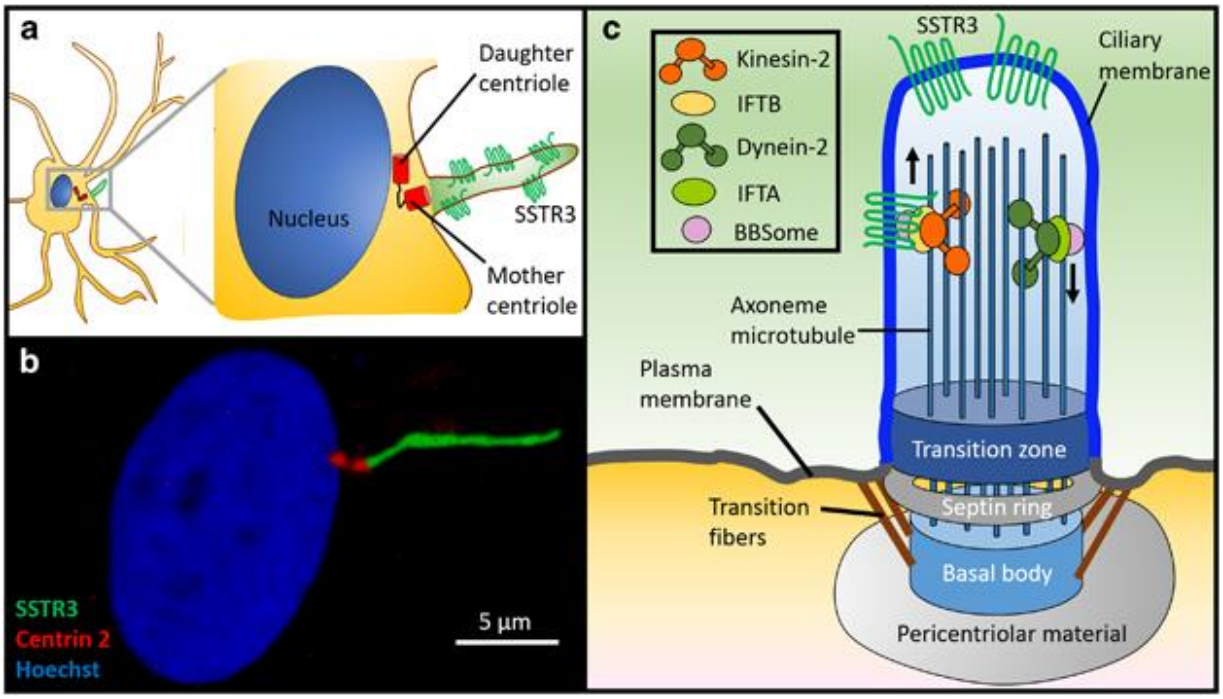

Figure 13. The primary cilium is a specialized signaling organelle.

A. Schematic of an astrocyte with a primary cilium. B. Fluorescent micrograph of a rat spinal primary astrocyte expressing dsRed-Centrin 2 (centriole marker) and somatostatin receptor type III (SSTR3)-GFP (primary cilia marker) that was fixed and stained with Hoechst dye (nucleus marker). C. Schematic of a primary cilium highlighting compartmentalization from the rest of the cell by unique structures, including the septin ring, transition zone, and ciliary membrane. The axoneme nucleates out from the basal body, which is anchored to the plasma membrane by transition fibers. Signal transduction is mediated by the receptor dense ciliary membrane and a specialized intraflagellar transport system (IFT) along the axoneme. The primary ciliary membrane is enriched in membrane receptors that include SSTR3. Cargo transport within the primary cilium is coordinated by the Bardet-Biedl Syndrome (BBSome) complex, IFT complex A, and IFT complex B. Figure adapted from Kaliszewski, M., Knott, A. B., & Bossy-Wetzel, E. (2015). Primary cilia and autophagic dysfunction in Huntington's disease. *Cell Death and Differentiation*, 22(9), 1413–1424.

3.1.3 Primary cilia in the nervous system

In the brain primary cilia are evident on virtually all brain cells including progenitors, neurons, and astrocytes. (Guemez-Gamboa et al., 2014; He et al., 2014).

Present in neurons, astrocytes and progenitors, primary cilia play important roles in the nervous system; these include neurodevelopment, neuronal homeostasis, differentiation and survival (Guemez-Gamboa et al., 2014). Neurological defects associated with ciliopathies, multi-system genetic disorders stemming from primary ciliary dysfunction, underscore the critical role of primary cilia in the nervous system. Primary cilia also maintain important functions in the adult nervous system, including neural stem cell regulation, neuronal signaling and regeneration (Han et al., 2008b). Recently, primary cilia dysfunction has also been implicated in late-onset neurodegenerative disorders such as Alzheimer's disease and Huntington's disease (Armato, 2012; Chakravarthy et al., 2012; Keryer et al., 2011; Liu and Zeitlin, 2011; Sotthibundhu et al., 2009).

3.1.4 Primary cilia and the cell cycle

Primary cilia are connected to cell cycle progression and play an important role in regulating cellular proliferation. These post-mitotic structures only form in quiescent cells, when during the G_0 and G_1 phases of the cell cycle the mother centriole moves to the cell membrane where it differentiates into the basal body, the structure from which the microtubule-based axoneme extends to form the primary cilium (Tang et al., 2013).

Prior to cell cycle entry and progression, the primary cilium must be disassembled (Ke and Yang, 2014). Ciliary disassembly is regulated by Aurora A kinase, localized at the basal body, which activates HDAC6 and promotes deacetylation of α-tubulin, ciliary resorption and axoneme disassembly (Pugacheva et al., 2007). It is the subsequent liberation of the basal body, required

for reutilization in the formation of the mitotic spindles, that regulates cell cycle re-entry (Seeley and Nachury, 2010). Recent studies have shown that ciliary length can also influence cell cycle time. Cells with longer primary cilia exhibit delayed re-entry into cell cycle based on signaling to the cytosol concerning the length of axoneme (Kim et al., 2011). The involvement of a ciliary length-based signal in regulation of cell cycle further demonstrates that primary cilia may function as a structural checkpoint in cell cycle re-entry.

Primary cilia also influence cell cycle through cross talk with autophagy, the major intracellular degradation system that mediates the turnover and recycling of proteins and organelles (Baehrecke, 2005). Autophagy occurs at low basal levels to perform homeostatic functions such as the recycling of damaged organelles. During adverse conditions, such as nutrient deprivation, induced autophagy acts as a pro-survival mechanism, making it essential for maintenance of the cell cycle in a nutrient-dependent manner. As environmental sensors of the cell, primary cilia transmit signals to the cell regarding conditions of the extracellular space that include information such as growth factor and nutrient availability (Boehlke et al., 2010). In cultured cells autophagy and primary cilia biogenesis are both triggered upon the growth arrest induced by nutrient withdrawal (Kiprilov et al., 2008), and recent findings describe a functional relationship between these pathways.

The induction of autophagy is dependent on Sonic hedgehog (Shh) signaling through the primary cilium, and primary cilia dysfunction results in impaired autophagy (Pampliega et al., 2013). Conversely, compromised autophagy alters primary cilia growth and structure. Basal

autophagy inhibits primary cilia formation through the degradation of proteins required for intraflagellar transport and the trafficking of components required for cilium growth (Figure 14A), and blocking autophagy results in enhanced primary cilia growth (Pampliega et al., 2013). By contrast, induced autophagy targets the specific degradation of the centriolar satellite protein OFD1 and is required for the formation of primary cilia (Tang et al., 2013) (Figure 14B).

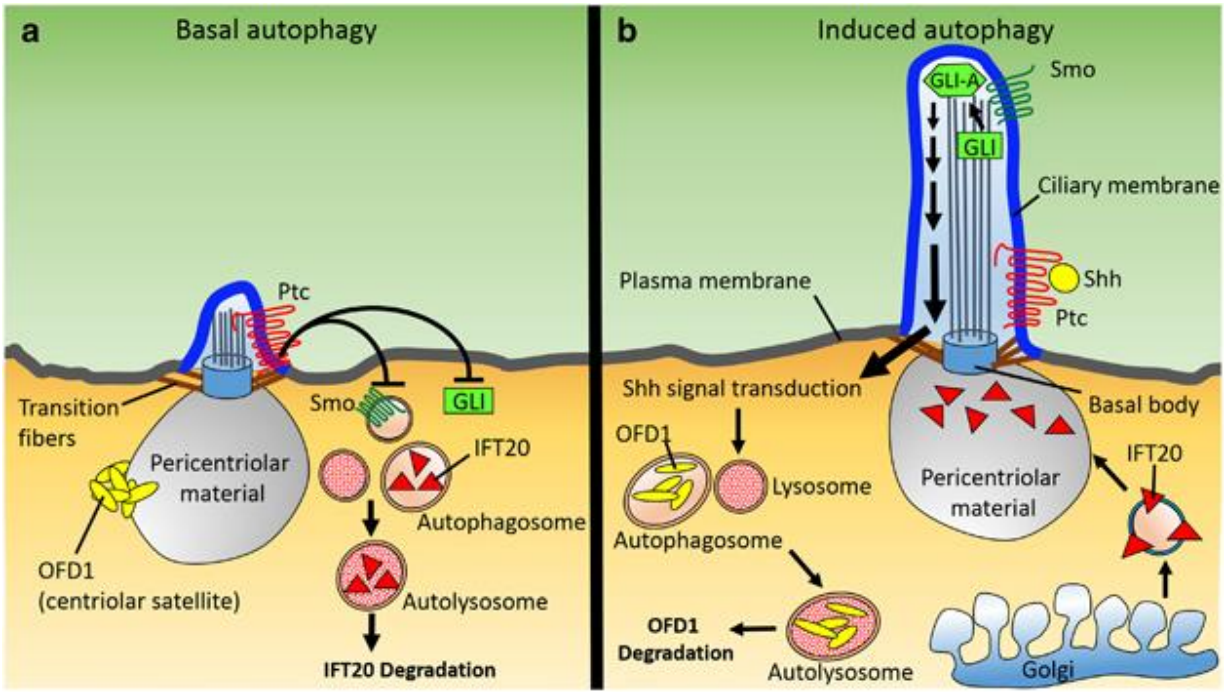

Figure 14. The functional relationship between primary cilia and autophagy.

A. In the absence of Sonic Hedgehog (Shh), the Patched (Ptc) receptor restricts Smoothened (Smo) entry into the primary cilium, which results in processing of the transcriptional effector GLI into its repressor form or targeting for degradation. Autophagy is not induced, OFD1 at centriolar satellites is not degraded and ciliogenesis is impaired. Basal autophagy degrades IFT20 when nutrient levels are normal. This reduces trafficking of IFT components to the pericentriolar material, thus impairing the ciliary transport required for growth of primary cilia. B. Primary ciliogenesis and autophagy are induced during starvation or periods of low-nutrient availability. Autophagy induction is dependent on Shh signaling through the primary cilium. Shh signal transduction is mediated by Smo, which undergoes localization to the primary cilium following Shh binding to Ptc. Smo accumulation within primary cilia promotes GLI protein processing into its transcriptional activator form (GLI-A), enabling downstream signal transduction. Shh-mediated signal transduction promotes the autophagic degradation of OFD1 at centriolar satellites, which is required for ciliogenesis. Figure adapted from Kaliszewski, M., Knott, A. B., & Bossy-Wetzel, E. (2015). Primary cilia and autophagic dysfunction in Huntington's disease. *Cell Death and Differentiation*, 22(9), 1413–1424.

3.1.5 Histone deacetylase 6

Histone deacetylase 6 (HDAC6) is a predominantly cytoplasmic enzyme that regulates many important biological processes, including cell migration, formation of the immune synapse, induction of heat-shock proteins, and clearance of misfolded proteins. HDAC6 is a unique deacetylase, as it the only member of the deacetylase family that contains two catalytic domains as well as an ubiquitin-binding domain. The first discovered physiological function of HDAC6 was the deacetylation of α-tubulin (Hubbert et al., 2002; Matsuyama et al., 2002), a process that reduces microtubule stability and promotes depolymerization. HDAC6 also regulates motor protein and cargo recruitment to microtubules and is required for efficient clearance of misfolded protein aggregates from the cytoplasm (Kawaguchi et al., 2003; Lee et al., 2010).

Previous studies have shown that HDAC6 plays critical roles in autophagy, apoptosis, and cell cycle progression (Ding et al., 2013; Pandey et al., 2007). A recent report described mutant SOD1 selectively interacting with HDAC6 and inhibiting its α-tubulin deacetylase activity (Gal et al., 2013), yet to date HDAC6 interaction with wild type SOD1 has not been described.

3.1.6 α-Tubulin acetyltransferase 1

α-Tubulin acetyltransferase 1 (αTAT1) is a predominantly cytoplasmic protein and member of the Gcn5-related *N*-acetyltransferase superfamily. It is the major enzyme responsible for acetylation of α-tubulin at Lys40 (Akella et al., 2010), a modification that is enriched in stable or

long-lived microtubules such as found within the ciliary axoneme. Tubulin acetylation plays a conserved role in many microtubule-based processes such as cell locomotion, cell division, and chemotaxis, and recent evidence shows that α-TAT1 is required for normal assembly of primary cilia (Shida et al., 2010).

3.2 Materials and Methods

3.2.1 Reagents

Lipofectamine 2000, Tissue protein extraction reagent (TPER), DMEM containing 4500 mg/L D-glucose, GlutaMax-1, N-2 supplement, 100x penicillin/streptomycin, sodium pyruvate, One Shot fetal bovine serum (FBS), TurboFect transfection reagent, 10% Tween-20 Surfact-Amps detergent solution, Halt protease and phosphatase inhibitor cocktail, Bolt LDS sample buffer, Bolt MES sodium dodecyl sulfate (SDS) running buffer, Bolt Bis-Tris Plus 4%–12% gradient gels, iBlot Gel transfer stacks, iBolt Dry Blotting System, Pierce Western Blotting Substrate, 20 mM Hoechst 33342 solution, Cytoseal 60, and premium cover glass were all obtained from Thermo Fisher Scientific. Phosphate buffered saline, pH 7.4 (PBS), EDTA, gelatin from cold water fish skin 45% in H_2O, Triton X-100, Ponceau S solution 0.1% w/v and 5% acetic acid, and poly-L-lysine, were obtained from Sigma-Aldrich. EM grade paraformaldehyde was obtained from Ted Pella Inc. Neutralized bacteriological peptone was obtained from Oxoid. HEPES-free acid, NaCl, and KCl were obtained from OmniPur/Calbiochem. β-Mercaptoethanol-proteomic grade was obtained from AMRESCO. CHAPS was obtained from G-Biosciences. Tissue culture dishes (100

and 145 mm) were obtained from Greiner Bio. Costar cell scrapers were obtained from Corning. Amersham Hyperfilm ECL high performance chemiluminescence films were obtained from GE Healthcare Limited. VECTAShield fluorescent mounting medium was obtained from Vector Laboratories, Inc.

3.2.2 Antibodies

Ac-K123 SOD1 antibodies were custom-made by Yenzym Antibodies. Rabbit polyconal SOD1 (rat) (10011387) was obtained from Cayman Chemical. Mouse monoclonal SOD1 (G-11), rabbit polyclonal SOD1 (FL-154), and rabbit polyclonal adenylyl cyclase 3 (ACIII) antibodies (C-20) were obtained from Santa Cruz Biotechnology. Mouse monoclonal α-tubulin (DM1A) and rabbit monoclonal HDAC6 (D2E5) antibodies were purchased from Cell Signaling. Mouse monoclonal acetylated α-tubulin (6-11B-1), mouse monoclonal FLAG (M2), and mouse monoclonal MAP2 (HM-2) antibodies were obtained from Sigma. Rabbit polyclonal GFP (ab6556) antibody and chicken polyclonal glial fibrillary acidic protein (GFAP) antibody (ab4674) was acquired from Abcam. Peroxidase-conjugated AffiniPure donkey anti-rabbit IgG (H+L), peroxidase-conjugated AffiniPure donkey anti-mouse IgG (H+L), and Alexa Fluor 594 AffiniPure Fab fragment donkey anti-rabbit IgG (H+L) secondary antibodies were obtained from Jackson ImmunoResearch Laboratories, Inc. Alexa Fluor 488 goat-anti-rabbit IgG (H+L), highly cross-absorbed, Alexa Fluor 594 goat anti-mouse IgG (H+L), Alexa Fluor 594-donkey anti-goat IgG (H+L), and Alexa Fluor 647 donkey-anti-chicken IgG (H+L) were obtained from Molecular Probes.

3.2.3 Mouse embryonic fibroblasts

Mouse embryonic fibroblasts (gift from David Sinclair, Harvard University) were seeded onto glass coverslips in a 24 well plates at a density of 1 x 10^5 cells per well and grown in DMEM supplemented with 4500 mg/L glucose, 10% FBS, 4 mM L-glutamine, 1 mM sodium pyruvate, and penicillin/streptomycin. For nutrient depletion treatment, growth medium was removed and replaced with nutrient deprivation buffer (1X HBSS, 10 mM HEPES pH 7.4, 2 mM $MgCl_2$, 2 mM $CaCl_2$) for 3 hours.

3.2.4 Rats

Timed-pregnant Sprague Dawley rats (Charles River) were used for the isolation of primary spinal cord astrocytes.

3.2.5 Isolation and transfection of spinal astrocytes

Primary astrocytes were isolated from spinal cords of one litter of E18 embryos from a timed-pregnant Sprague Dawley rat (Charles River). Spinal cord tissues were isolated, minced, and digested in 0.025% trypsin in Earle's Balanced Salt Solution (EBSS) at 37°C for 20 minutes. Tissues were transferred into a 50 mL tube containing 45 mL pre-warmed astrocyte medium (DMEM containing 4500 mg/L D-glucose, GlutaMax-1, N-2 supplement, 10% FBS, and penicillin/streptomycin) and allowed to sink. After tissues settled, medium was removed and replaced with 10 mL fresh astrocyte medium. Tissues were then triturated 20 times using a

P1000 micropipette. All dissociated cells were seeded onto three 75 cm^2 Cellgro culture flasks (Corning) and cultured at 37 °C, 5% CO_2. Medium was replaced the next day and astrocytes were grown until confluent. Upon reaching confluency, astrocytes were trypsinized with 0.25% trypsin and seeded at 2×10^5 cells/cm^2 onto 12 mm diameter #1 glass coverslips (Chemglass Life Sciences, Vineland NJ) coated with poly-L-lysine (50 µg/mL in ddH_2O). Prior to immunostaining, confluent astrocytes were treated for 5 hours with either deacetylase inhibitors (10 mM NAM, 1 µM TSA) or vehicle control (DMSO).

3.2.6 Nutrient depletion and recovery of astrocytes

Spinal cord astrocyte cultures were isolated from E18 rat embryos and seeded DIV6 at a density of 4 x 10^5 cells onto 12 mm diameter German glass coverslips (Chemglass Life Sciences) pre-coated with poly-L-lysine. Cells were cultured for 24 hours in astrocyte medium (DMEM containing 4500 mg/L D-glucose, GlutaMax-1, N-2 supplement, 10% FBS, and penicillin/streptomycin) within a tissue culture incubator at 37°C in 5% CO_2. For nutrient depletion treatment, astrocyte medium was removed and replaced with nutrient deprivation buffer (1X HBSS, 10 mM HEPES pH 7.4, 2 mM $MgCl_2$, 2 mM $CaCl_2$) for 1 or 3 hours. For recovery, starvation buffer was replaced with fresh media and incubated for one hour.

3.2.7 Immunocytochemistry

Cells were fixed in freshly prepared 4% paraformaldehyde in PBS pH 7.4 for 10 minutes at room temperature followed by 3 five minute PBS washes. Cells were permeabilized in 0.10% Triton X-

100 in PBS pH 7.4 for 10 minutes. Cells were then washed with PBS 3 times for 5 minutes. Blocking was performed by incubating cells with 1% gelatin from cold water fish in PBS for 30 minutes at room temperature. Incubation with primary antibodies was performed in 1% fish gelatin in PBS at 4°C overnight in a humidified chamber. Primary antibodies included custom-made anti-Ac-K123 SOD1 polyclonal, anti-rat SOD1 rabbit polyclonal, anti-acetylated-α-tubulin clone 6-11B-1 mouse monoclonal, anti-MAP2 clone HM-2 mouse monoclonal, and anti-glial fibrillary acidic protein (GFAP). Goat-anti-rabbit Alexa Fluor 488, goat-anti-mouse Alexa Fluor 594, and goat-anti-chicken Alexa Fluor 647 conjugated secondary antibodies (1:250) were diluted in 1% fish gelatin in PBS and applied to coverslips for 1 hour incubation in the dark at room temperature. Nuclei were counterstained with 1 μg/mL Hoechst. Controls performed with omission of the primary antibodies did not reveal significant immunostaining, nor did incubation with pre-immune serum collected from rabbits prior to immunization. In antibody preabsorption controls, purified antibody was incubated for two hours at room temperature in the primary antibody blocking buffer with the acetylated immunizing peptide (VVHE-acK-ADDLGKGGC) or the unmodified peptide (VVHEKADDLGKGGC). Immediately following preabsorption, the antibody/peptide mix was used for immunocytochemical staining. Coverslips were mounted onto Vectashield mounting and sealed onto glass slides with Cytoseal 60.

3.2.8 Microscopy

Imaging was carried out with a Zeiss LSM 710 Inverted Axio Observer confocal laser scanning microscope with six laser excitation lines (405, 458, 488, 514, 543, and 633 nm), a 34 channel QUASAR detector for spectral analysis, and several objectives including a EC Plan-Neofluar 10x 0.3 numeric aperture (NA) air objective, Plan-Apochromat 20x 0.8 NA air objective, EC Plan-Neofluar 40x 1.3 NA oil objective, and a Plan-Apochromat 63x 1.4 NA oil objective. Image acquisition and processing were performed using Zen 2012 software from Zeiss. To visualize Hoechst 33342, the excitation/emission wavelength was 405/495 nm using the diode laser. For Alexa Fluor 488, the excitation/emission wavelength was 488/540 nm using the multiline argon laser. For Alexa Fluor 594, the excitation/emission wavelength was 543/660 nm using a diode pumped solid state laser plus a QUASAR detector for all emission wavelengths. On average 25 z-stacks of 0.5 µm step-size were acquired for 354 µm x 354 µm scaled image size. The z-stacks were maximally projected and the gamma value adjusted to 0.70−0.85 using the ZEN 2012 software.

For comparison of the mean fluorescent intensities of inhibitor treated astrocytes to the vehicle control treated astrocytes, the following confocal acquisition settings were maintained for all conditions:

Alexa Fluor 488 laser =2.0, Pinhole = 1.75, Gain = 535, Digital gain = 1.0, Interval = 0.35

Alexa Fluor 594 Laser = 2.0, Pinhole = 3.62, Gain = 874, Digital gain = 1.0, Interval = 0.35

3.2.9 Expi293 cells

Expi293F cells were grown in suspension using vent-cap shaker flasks. Initially, 0.3×10^6 cells/mL were seeded in Expi293 Expression Medium and grown in a tissue culture incubator at 37°C in a humidified atmosphere of 8% CO_2 in air on an orbital shaker platform rotating at 125 rpm. Cultures were incubated until cell density reached at least 3×10^6 viable cells/mL (typically 3–4 days), at which time transfections are carried out.

3.2.10 Pharmacologic inhibitor treatment against HDAC6

Cells were treated for 6 hrs with either 10 µM Tubastatin A, 10 µM Tubacin, or 0.1% DMSO (vehicle control). Following inhibitor treatment, HEK293 cells were harvested for western blot analysis and cultured astrocytes were processed for immunocytochemistry.

3.2.11 HDAC6/α-TAT1 siRNA mediated knockdown

HEK293T cells were seeded into 6 well culture plates in DMEM, high glucose supplemented with 10% FBS + P/S. At approximately 70% confluency, DNA plasmids and/or siRNA are delivered into cells by cationic lipid-mediated transfection utilizing Lipofectamine 2000 transfection reagent. For each well to be transfected 5 µl of Lipofectamine 2000 is diluted into 150 µl OptiMEM. In a separate tube, 0.75 µg DNA and/or 20 pmol ON-TARGETplus SMARTpool™ siRNA against HDAC6, α-TAT1, or scrambled siRNA control is also diluted into 150 µl OptiMEM. After 5 minutes, both solutions are mixed together and incubated for 20 minutes

at room temperature. The DNA/siRNA lipid complexes are then added dropwise to each well containing cells in 2 mL growth medium. Transfected cells are thn cultured at 37°C in 5% CO_2. After 48-72 hours cells are washed very gently with PBS to remove serum proteins. Cells are then harvested with cell scraper, pelleted by a 5 minute centrifugation at 800 rpm, and resuspended in ice cold lysis buffer (TPER containing Halt protease and phosphatase inhibitor cocktail, Tubastatin A, TSA, and NAM). Cells were lysed by freezing on dry ice followed by rapid thaw, followed by one cycle of sonication at 50% output for 20 seconds. Lysates were cleared by centrifugation at 14,000 x g at 4°C for 10 minutes and total protein concentrations were determined by a Bradford assay kit.

3.2.12 SOD1 and HDAC6/α-TAT1 overexpression

Expi293F cells were transfected by electroporation using an Amexa Nucleofector system (Lonza). For each transfection $1x10^6$ cells were resuspended in 100 uL prewarmed electroporation buffer (12.5 mM NaCl, 123 mM KCl, 20 mM KOH, 10 mM EGTA, 4.5 mM $MgCl_2$, 20 mM PIPES pH 6.9, and 20% FBS) and mixed with 5 ug plasmid DNA in a cuvette. Cells were electroporated using program Q-01. Immediately after transfection, cells were removed from cuvette and seeded into 100 mm dish in 10 mL medium and grown for 72 hours.

3.2.13 Immunoprecipitation

1 mg of lysates of Expi293 cells transiently expressing SOD1, SOD1 and HDAC6-FLAG, or SOD1 and α-TAT1-EGFP were incubated with 5 µg of anti-Ac-K123 SOD1, 5 uL anti-FLAG, or 5 uL anti-

GFP antibody overnight. 50 µl of protein G-Dynabeads magnetic beads were added to the lysates and rotated at room temperature for 1 hour. The immune complexes were collected by magnet, washed 3 times with lysis buffer, quickly rinsed with ddH_2O, and resolved by SDS PAGE using gradient 4%–12% Bolt Bis-Tris Plus gels. Proteins were transferred to nitrocellulose membranes using the iBlot western blotting system and probed with anti-Ac-K123 SOD1, anti-HDAC6, or anti-GFP antibody.

3.3 Results

3.3.1 Antibodies are specific for K123-acetylated SOD1 by immunocytochemistry

It was important to first show that the Ac-K123 SOD1 antibody does not cross-react with unacetylated SOD1 when used in immunocytochemistry. Therefore, we performed antibody-peptide pre-incubation experiments using rat primary spinal astrocytes. We found that antibody preabsorption with the acetylated synthetic immunizing peptide abolished binding. In the antibody alone condition, we observed immunostaining of Ac-K123 SOD1 antibody in the nucleus of astrocytes (Figure 15A, column 1). Antibody incubated with acetylated peptide at 1:1 and 1:5 molar ratio blocked immunoreactivity (Figure 15A, columns 2 and 3). Preabsorption with unacetylated peptide did not block immunoreactivity (Figure 15A, columns 4 and 5). Finally, antibody incubated with acetylated peptide (1:1) and unacetylated peptide (1:100) blocked immunoreactivity (Figure 15A, column 6). As a control for experimental conditions, we also immunostained for total SOD1 using a commercial antibody against SOD1. As expected, this resulted in diffuse staining of the cytoplasm, identified as the area of the cell surrounding

the Hoechst counterstained nucleus (Figure 15A, column 7). Quantification of nuclear mean fluorescence intensity was also performed for three independent experiments (Figure 15B). Pre-incubation with acetylated peptide blocked antibody recognition while no significant reduction in signal was observed when antibody was pre-incubated with unacetylated peptide at high molar excess.

Omission of primary antibody from other samples undergoing immunostaining in parallel also resulted in the absence of staining. These controls confirm that immunostaining results were not due to primary antibody binding to substrates other than Lys123 acetylated SOD1 or from non-specific binding of secondary antibodies. Immunostaining with pre-immune serum (serum collected prior to injection of Ac-K123 SOD1 immunizing peptides) from the corresponding rabbit was also performed as a negative control. This resulted in a lack of cellular staining and demonstrated background staining for the antibody.

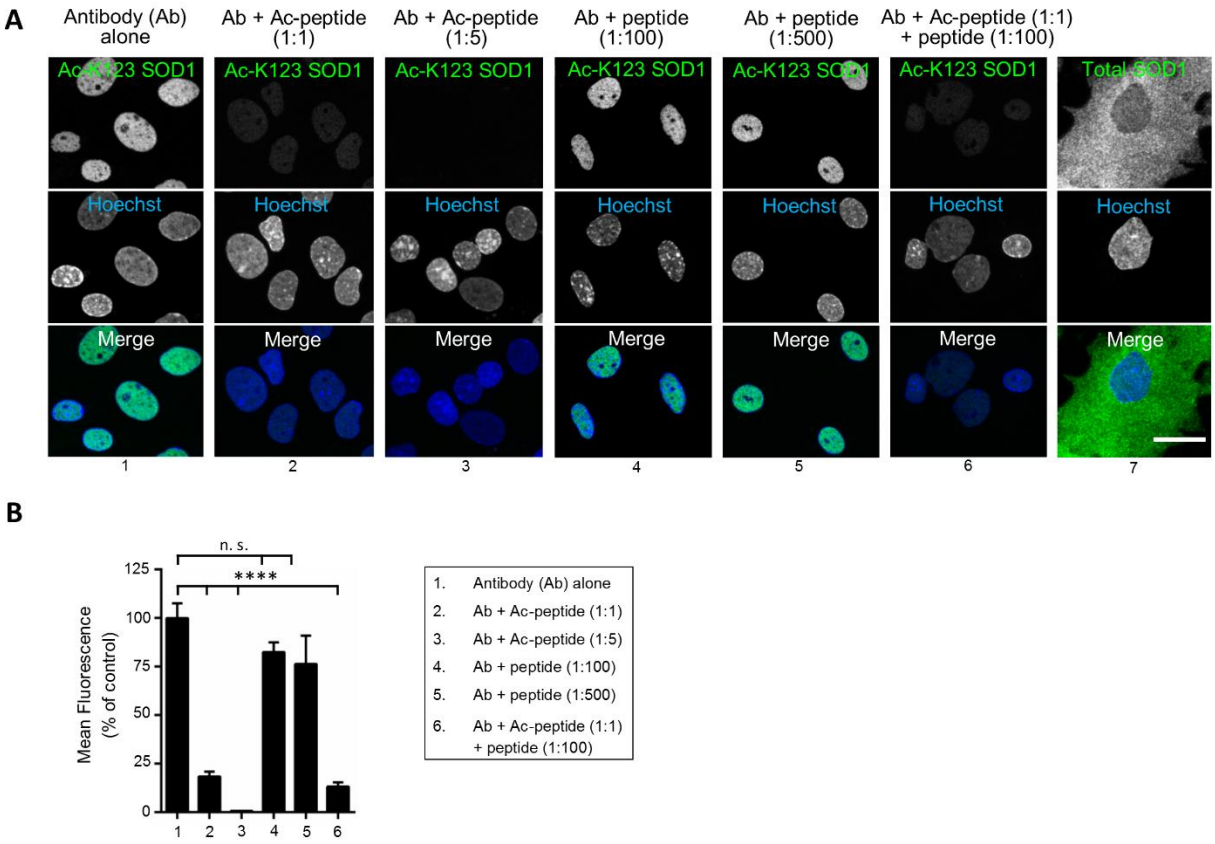

Figure 15. Ac-K123 SOD1 antibodies demonstrate specificity for use in immunohistochemistry

A. Confocal micrographs (scale bar, 20 µm) of primary spinal astrocytes immunostained with SOD1 or Ac-K123 SOD1 antibody that was pre-incubated with no peptide, acetylated peptide, unacetylated peptide, or a mixture of acetylated and unacetylated peptide (antibody:peptide molar rations as shown). Hoechst 33342 nuclear labeling and merged images are also shown. B**.** Quantification of antibody preabsorption immunocytochemistry results. Data are reported as percentage of nuclear mean fluorescence intensity relative to the antibody alone control of 150 (antibody alone), 100 (Ab + Ac-peptide 1:1), 100 (Ab + Ac-peptide 1:5), 100 (Ab + unacetylated peptide 1:100), 100 (Ab + unacetylated peptide 1:500) and 100 (Ab + Ac-peptide 1:1 + unacetylated peptide 1:100) astrocytes in three independent experiments (****significance at P<0.0001 by ANOVA).

3.3.2 Ac-K123 SOD1 localizes to nucleus and primary cilium in spinal astrocytes

SOD1 is ubiquitously expressed and predominantly found in the cytoplasm of cells. SOD1 also localizes to the nucleus and mitochondrial intermembrane (Okado-Matsumoto and Fridovich, 2001; Sturtz et al., 2001; Tsang et al., 2014). Interestingly, a recent proteomic study has identified SOD1 in isolated mammalian primary cilia (Ishikawa et al., 2012). Due to the role of PTMs in the regulation of subcellular localization of proteins, we investigated whether Ac-K123 SOD1 was preferentially localized to particular regions of the cell. We performed immunostaining of primary rat spinal astrocytes with either a commercially available SOD1 antibody or our customized antibody against Ac-K123 SOD1.

Immunostaining with commercial SOD1 antibody resulted in diffuse cytoplasmic staining, identified as the area of the cell surrounding the Hoechst counterstained nucleus (Figure 15A). Unexpectedly, we found that Ac-K123 SOD1 localized to the nucleus and primary cilium of cultured rat primary spinal astrocytes (Figure 16A). We identified primary cilia, which are solitary non-motile microtubule-based signaling organelles protruding from most quiescent or interphase mammalian cells including neurons and astrocytes (Singla and Reiter, 2006), by co-staining with an antibody for Lys40 acetylated α-tubulin, a marker for primary cilia (Figure 16A).

To confirm Ac-K123 SOD1 antibody specificity with regards to the ciliary labeling, primary astrocytes were immunostained with either untreated Ac-K123 SOD1 antibody or antibody preabsorbed with the acetylated immunizing peptide. The immunostaining performed with

preabsorbed antibody resulted in a loss of both nuclear and ciliary staining, demonstrating antibody specificity to Ac-K123 SOD1 within both the nucleus and primary cilium (Figure 16B).

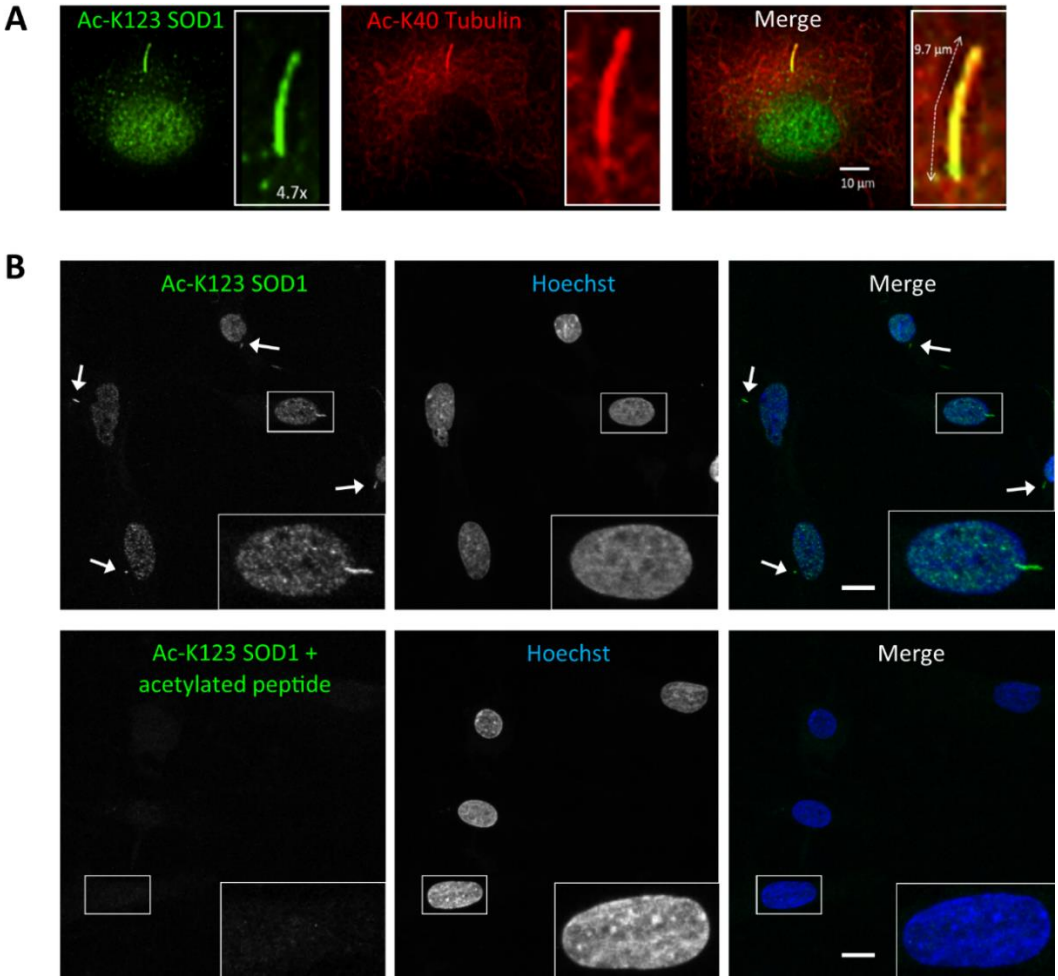

Figure 16. Ac-K123 SOD1 is localized to the primary cilium and nucleus.

A. Confocal micrograph (scale bar, 10 µm) of primary astrocytes immunostained with antibodies against Ac-K123 SOD1 and primary cilia marker Ac-K40 α-tubulin. Nuclei are counterstained with Hoechst 33342 dye. Inset shows a 4.7x zoom of the boxed region demonstrating Ac-K123 SOD1 and Ac-K40 tubulin co-labeling within the primary cilia. B. Confocal micrograph (scale bar, 20 µm) of nutrient withdrawn primary astrocytes with untreated Ac-K123 SOD1 antibody or Ac-K123 SOD1 antibody preabsorbed with the acetylated synthetic peptide. Nuclei are labeled by Hoechst and Ac-K123 SOD1 labeled primary cilia are identified (arrow). Inset shows a 2.5x zoom of the boxed region demonstrating abolishment of ciliary labeling in cells immunostained with preabsorbed Ac-K123 SOD1 antibody.

3.3.3 Ac-K123 SOD1 localization is dependent on cell cycle phase

The localization of Ac-K123 SOD1 to the nucleus and primary cilium is of particular interest because of the intimate relationship between these organelles and the cell cycle. The nucleus is home to cellular DNA in the form of chromosomes, and it must disassemble and reform each time the cell divides. The primary cilium is unique in that it only forms in resting cells. In fact, because its axoneme nucleates out from the basal body (a modified mother centriole docked to the plasma membrane upon cell cycle exit), the primary cilium must retract and disassemble in order to make both centrioles available for spindle formation and subsequent cell division (Pugacheva et al., 2007). To investigate Lys123 acetylated SOD1 localization in arrested astrocytes, we induced cellular quiescence through nutrient deprivation. The total elimination of nutrients and growth factors reduces basal cellular activity and makes the population of cells more homogenous as they withdraw from the cell cycle and enter the quiescent G_0/G_1 phase (Pirkmajer and Chibalin, 2011).

Our initial study of Ac-K123 SOD1 localization in growth arrested cells employed mouse embryonic fibroblast cells (MEFs). Cells were cultured in normal growth medium until near confluency. Once cultures were nearly confluent, serum-containing medium was removed and replaced with a nutrient deprivation buffer lacking growth factors and nutrients while the control cells continued being cultured in normal growth medium. After 3 hours MEFs were fixed and immunostained with our antibody against Ac-K123 SOD1. We found that MEFs grown in normal medium demonstrated strong nuclear localization of Ac-K123 SOD1 (Figure 17A, upper

panel). After cell cycle arrest induced by total nutrient deprivation, Ac-K123 SOD1 was no longer predominantly found within the nucleus but rather in the cytoplasm (Figure 17A, lower panel). Quantification of the percentage of cells with nuclear Ac-K123 SOD1 from 3 independent experiments shows that growth arrest promotes a significant loss of Ac-K123 SOD1 localization to the nucleus (Figure 17B). Whether the cell cycle arrest of MEFs is promoting the translocation of Ac-K123 SOD1 from the nucleus to the cytoplasm or the deacetylation of nuclear SOD1 and acetylation of cytoplasmic SOD1 remains to be determined.

Another key finding from the MEFs immunostaining was that Ac-K123 staining of the primary cilium is increased after cells underwent nutrient deprivation (Figure 17C). Quantification of percentage of cells with Ac-K123 SOD1 labeled primary cilia demonstrates that there is a significant increase from less than 5% of cells under normal conditions to nearly 20% of cells after nutrient deprivation. Based on these findings, we found that Ac-K123 SOD1 subcellular localization in MEFs was clearly responsive to the nutritional status of the cell. We next explored whether this finding extends to primary astrocytes.

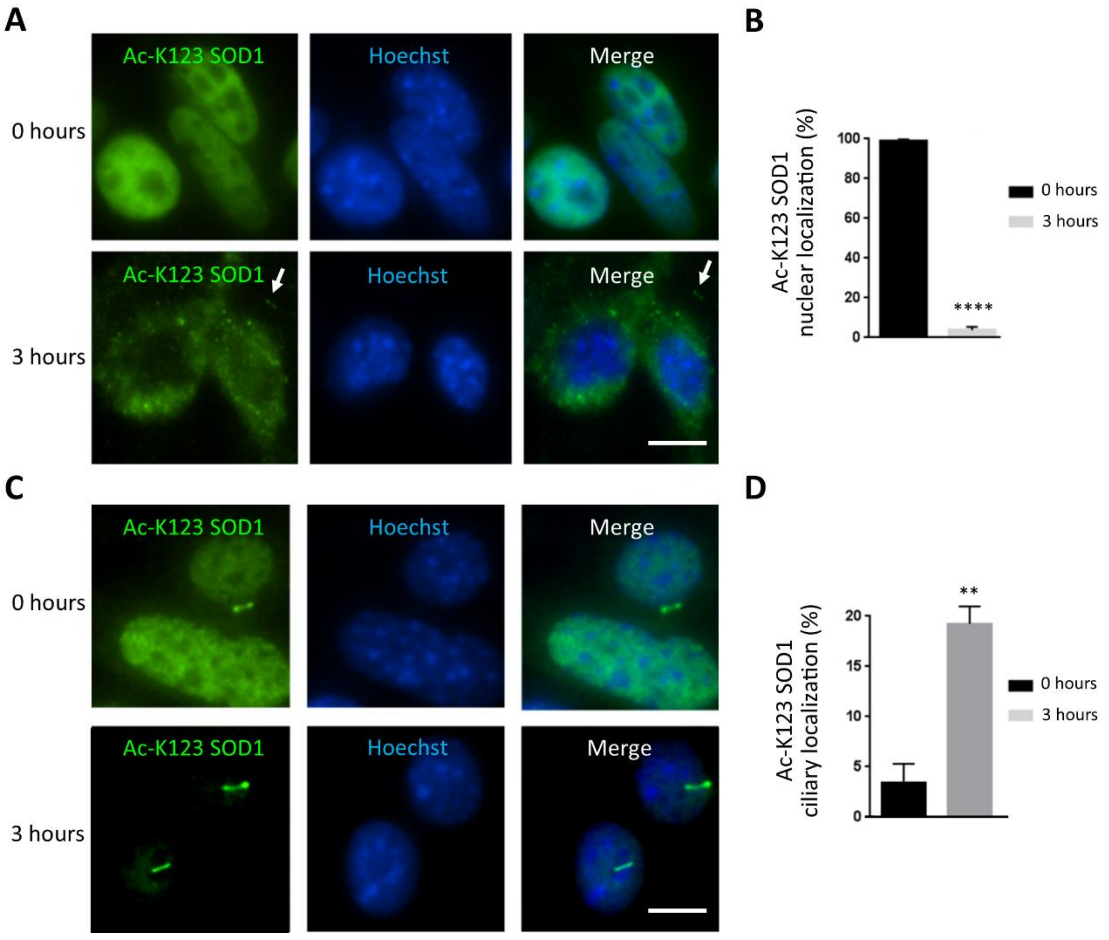

Figure 17. Cell cycle withdrawal decreases nuclear Ac-K123 SOD1 while promoting ciliary localization in mouse embryonic fibroblasts.

A. Fluorescent micrographs (scale bar, 20 µm) of mouse embryonic fibroblasts immunostained for Ac-K123 SOD1 with Hoechst nuclear counterstain. Cells were cultured to near confluency and then subjected to 0 or 3 hours of total nutrient withdrawal. A labeled primary cilium is marked by an arrow. B. Quantification of percentage Ac-K123 SOD1 nuclear localization in control versus nutrient depletion conditions shown with standard error of the mean error bars from three independent experiments (****significance at P<0.0001 by ANOVA). Nuclear Ac-K123 SOD1 was determined to be present if the intensity of immunostaining was comparable to or greater than the intensity in the surrounding cytoplasm. C. Fluorescent micrographs (scale bar, 20 µm) of Ac-K123 SOD1 immunostained mouse embryonic fibroblasts demonstrating ciliary localization. Cells were cultured to near confluency and then subjected to 0 or 3 hours of total nutrient withdrawal. D. Quantification of percentage of cells with ciliary Ac-K123 SOD1 in control versus nutrient depletion conditions shown with standard error of the mean error bars from three independent experiments (**significance at P<0.01 by ANOVA).

After removal of normal astrocyte growth medium, primary astrocytes were cultured in a nutrient deprivation buffer lacking nutrients and growth factors. Astrocytes were then fixed and the subcellular localization of Lys123 acetylated SOD1 was determined by immunocytochemistry. Similar to our findings from MEFs, we found that the ciliary localization of Ac-K123 SOD1 dramatically increased in astrocytes undergoing cell cycle arrest while nuclear localization decreased (Figure 18A). We also observed a decrease in the nuclear pool of Ac-K123 SOD1 that corresponded to duration of nutrient withdrawal, with astrocytes withdrawn for 3 hours showing less nuclear staining than those withdrawn for 1 hour (Figure 18A). Unlike in MEFs, Ac-K123 SOD1 localization to the cytoplasm after nutrient deprivation was not observed in astrocytes. To determine how robust the change in Ac-K123 SOD1 localization was in response to nutrient availability, we performed a recovery condition where the growth medium was added back to astrocytes that had undergone 3 hours of nutrient deprivation. Rescuing astrocytes from non-senescent arrest by returning complete medium lead to rapid retraction of Ac-Lys123 SOD1 labeled primary cilia and recovery of nuclear staining (Figure 18A). Thus, nutrient withdrawal evokes selective targeting of Lys123 acetylated SOD1 to primary cilia which is reversible upon recovery from nutrient withdrawal.

Quantification of our immunostaining results shows there is a significant increase in the number of cells with Ac-K123 SOD1 localized to the primary cilium after just 1 hour of nutrient deprivation (Figure 18B). Remarkably, after recovery the percentage of astrocytes with Ac-K123 SOD1 labeled primary cilia decreased back to the baseline levels observed in the control.

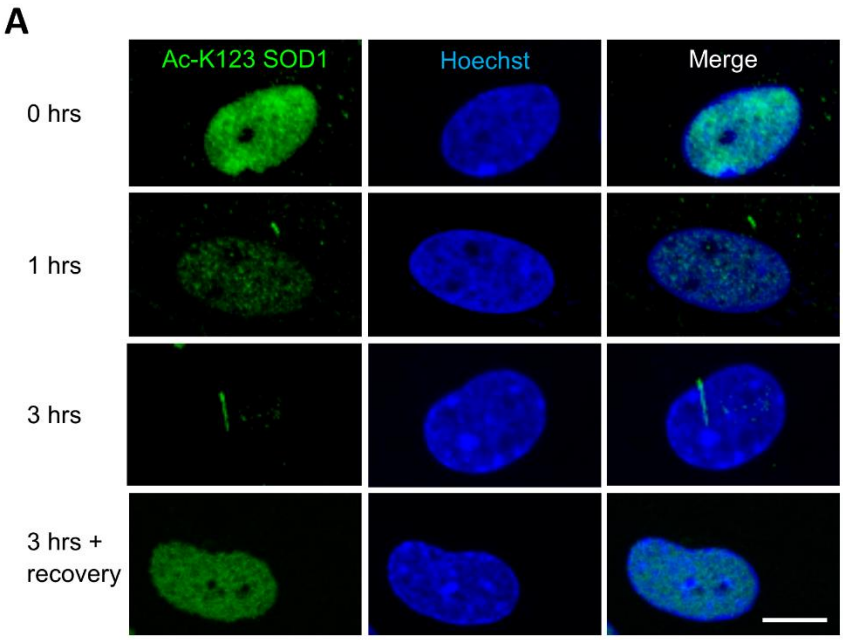

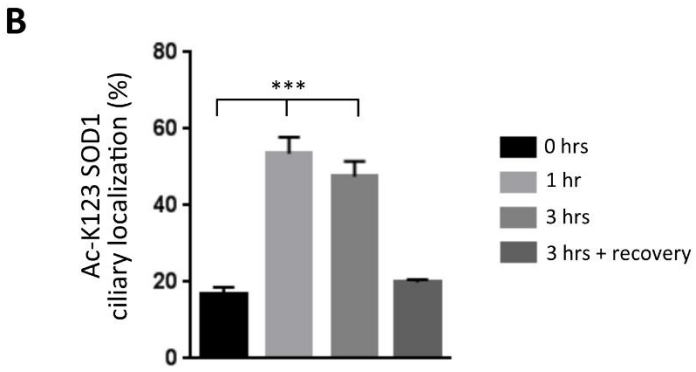

Figure 18. Cell cycle arrest promotes Ac-K123 SOD1 ciliary localization in primary astrocytes.

A. Confocal micrographs (scale bar, 20 µm) of primary astrocytes immunostained for Ac-K123 SOD1 with Hoechst nuclear counterstaining. Cells were cultured to near confluency and then subjected to 0, 1 or 3 hours of total nutrient withdrawal or 3 hours of nutrient withdrawal followed by 1 hour recovery with complete growth medium. B. Quantification of percentage of astrocytes with ciliary Ac-K123 SOD1 in control, nutrient depletion, or nutrient depletion with recovery conditions is shown with standard error of the mean error bars from three independent experiments (**significance at $P<0.001$ by ANOVA).

Ac-K123 SOD1 ciliary localization is best observed in arrested cells, but is still evident in astrocytes growing in normal culture medium. Under these conditions the correlation between ciliary localization and a decreased nuclear pool of Ac-K123 SOD1 is best demonstrated as not all cells are synchronized in cell cycle arrest. Immunostaining of primary astrocytes growing in normal medium shows neighboring cells with distinct Ac-K123 SOD1 localization (Figure 19). In one astrocyte there is a labeled primary cilium and no nuclear staining, while in the neighboring astrocyte there is significant nuclear Ac-K123 SOD1 localization and no ciliary labeling.

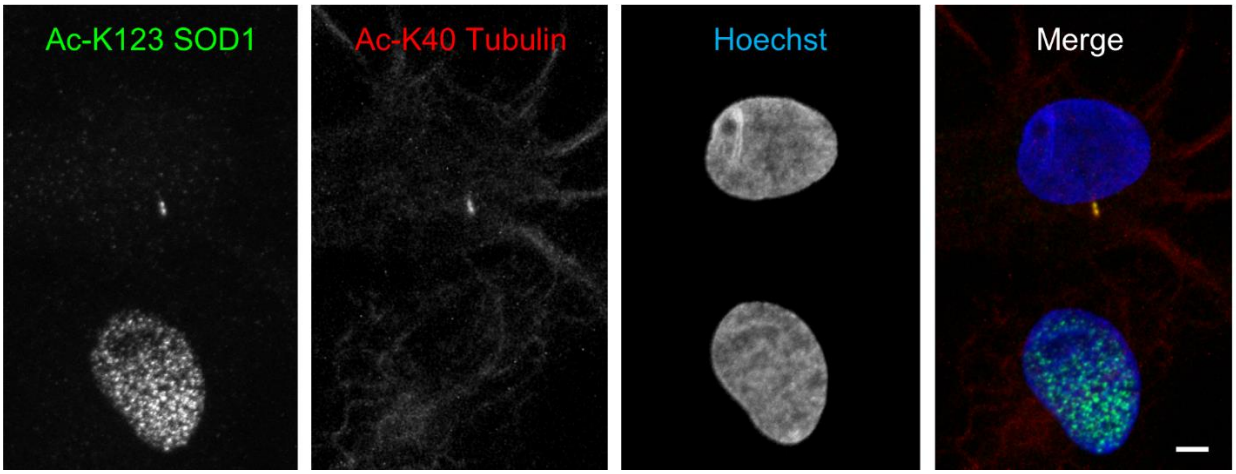

Figure 19. Ac-K123 SOD1 localization to primary cilium correlates to decreased nuclear signal. Confocal micrograph (scale bar, 10 µm) of neighboring primary astrocytes immunostained with antibodies against Ac-K123 SOD1 and primary cilia marker Ac-K40 Tubulin. Nuclei are counterstained with Hoechst 33342 dye.

When mitosis begins chromosomes condense, the nucleolus disappears, the nuclear envelope dissolves, and mitotic spindle fibers align the chromosomes at the metaphase plate along the middle of the cell in preparation for chromosome separation. During metaphase of mitosis, Ac-

K123 SOD1 was closely associated with chromosomes along the metaphase plate in cultured rat primary spinal astrocytes (Figure 20A). This co-localization of Ac-K123 SOD1 and chromosomes continues into anaphase as sister chromatids are separated from each other and pulled towards opposite ends of the cell (Figure 20B). It is also worth noting that during metaphase, Ac-K123 SOD1 does not co-localize with acetylated α-tubulin comprising the microtubule polymers that form the mitotic spindle.

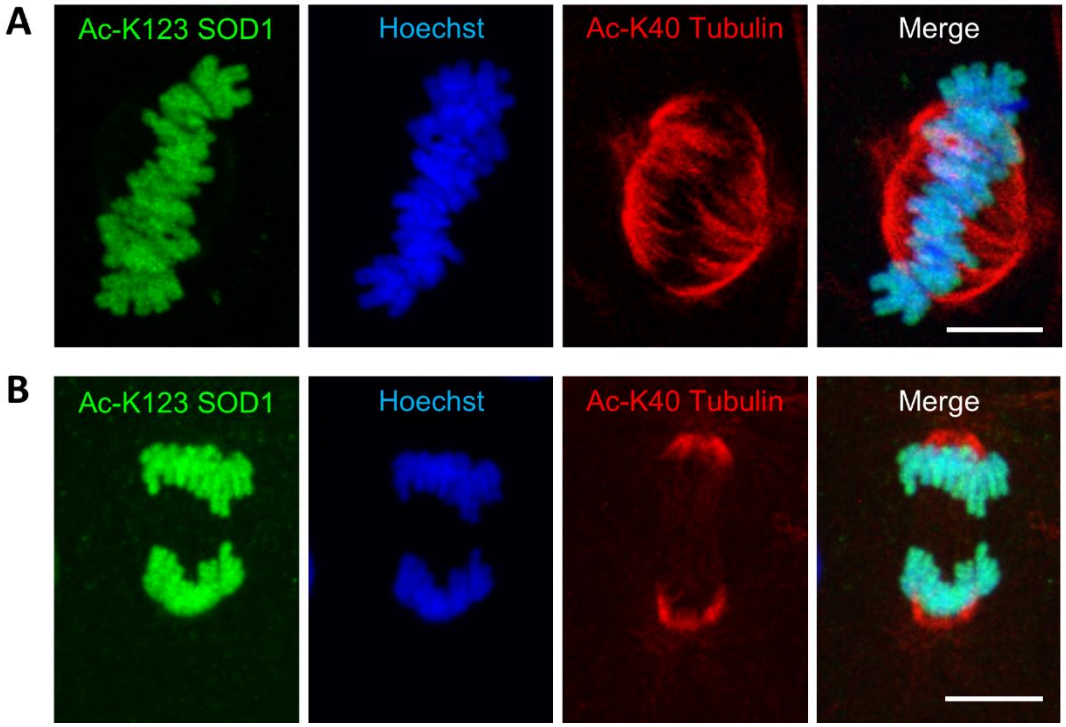

Figure 20. Lys123 acetylated SOD1 is associated with chromosomes during mitosis.

A. Confocal micrograph (scale bar, 10 µm) of an astrocyte during metaphase immunostained for Ac-K123 SOD1 and Ac-K40 α-tubulin with Hoechst counterstaining for DNA. B. Confocal micrograph (scale bar, 10 µm) of an astrocyte during anaphase immunostained for Ac-K123 SOD1 and Ac-K40 α-tubulin with Hoechst counterstaining for DNA.

At the end of mitosis, during telophase, chromosomes decondense into diffuse chromatin and new membranes form around the daughter nuclei. Spindle fibers disperse and the cell proceeds to cytokinesis, the physical process of cell division. Immunostaining of rat primary spinal astrocytes shows that Ac-K123 SOD1 was concentrated within the midbody during the end stage of telophase prior to cytokinesis (Figure 21). The microtubule-based midbody is a transient structure connecting two daughter cells with the principal function being to localize the site of abscission during cytokinesis (Hu et al., 2012). Despite the importance of the midbody, its assembly and regulation is not fully understood. Indeed, the localization of Ac-K123 SOD1 at the midbody and any potential interactions with microtubule interacting proteins merits further investigation. And although Ac-K123 SOD1 appears to be absent from the center of the midbody based on our immunostaining data, this may not be truly representative due to the presence of an antibody excluding region at the center that makes immunofluorescence problematic in this region of the midbody (Hu et al., 2012).

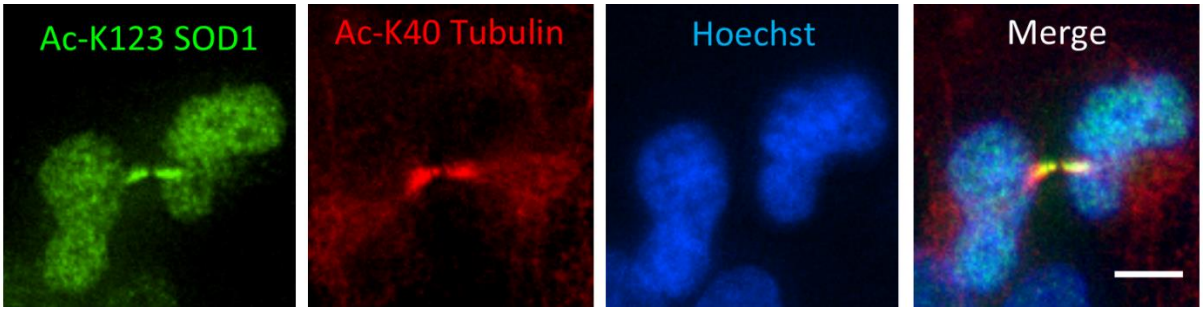

Figure 21. Lys123 acetylated SOD1 is concentrated within the transient midbody structure during the end stage of telophase.

Confocal micrograph (scale bar, 10 µm) of cultured rat primary spinal astrocytes immunostained for Ac-K123 SOD1 and Ac-K40 α-tubulin.

In summary, results from the immunostaining of primary astrocyte demonstrate that Ac-K123 SOD1 exhibits specific subcellular localization during the stages of interphase and mitosis (Figure 22).

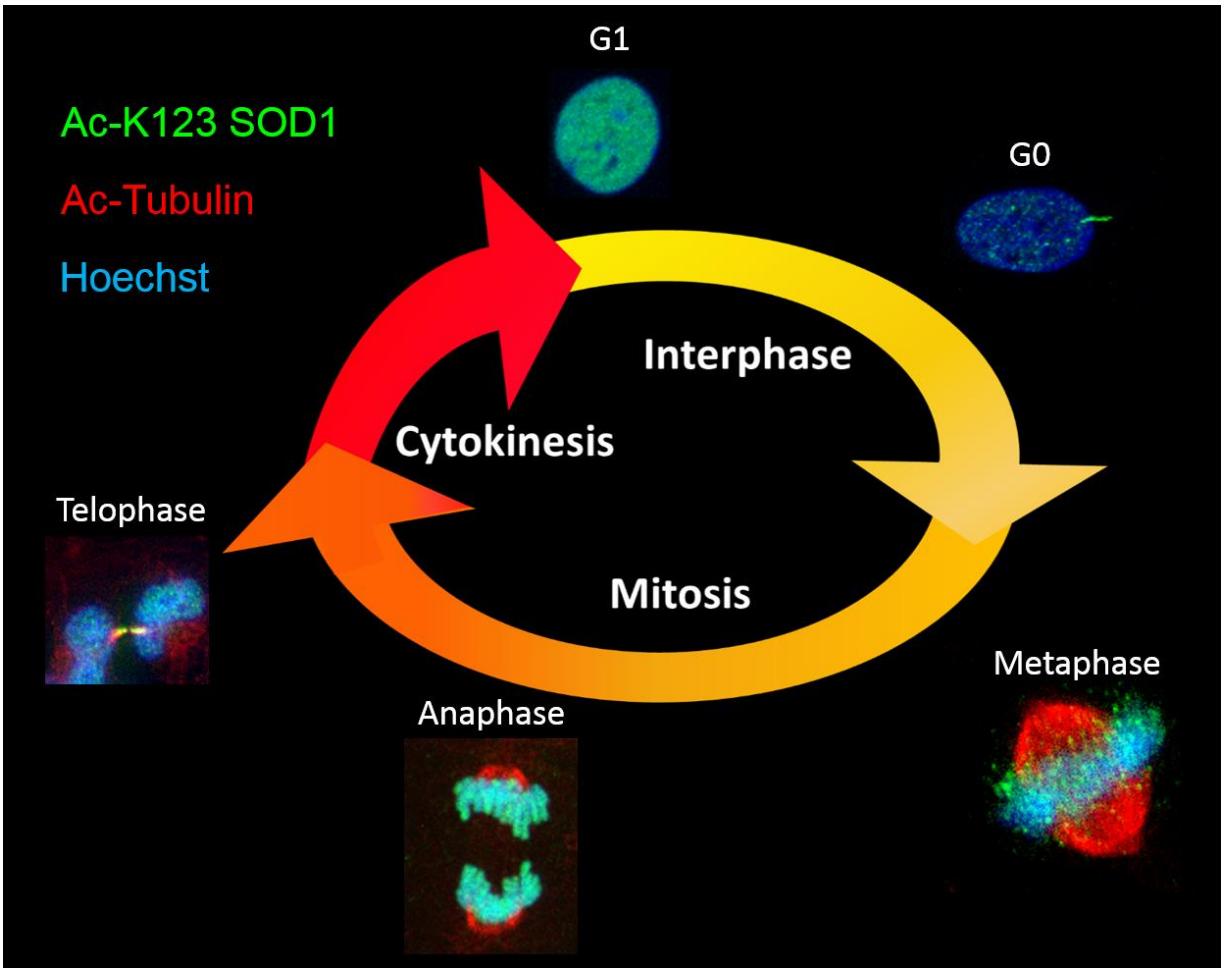

Figure 22. Ac-K123 SOD1 localization in astrocytes during specific stages of interphase and mitosis.

3.3.5 SOD1 interacts with HDAC6 in cells

We used a candidate approach to evaluate the potential regulators of SOD1 Lys123 acetylation. Given that HDAC6 and α-TAT1 are predominantly cytoplasmic enzymes, they would have access to SOD1 for modification. And similar to Ac-K123 SOD1, HDAC6 and α-TAT1 are also associated with primary cilia. HDAC6 is required for axoneme resorption and primary cilium disassembly while α-TAT1 promotes axoneme growth and primary cilium biogenesis (Pugacheva et al., 2007; Shida et al., 2010).

To confirm the interaction between Ac-K123 SOD1 and HDAC6 in cells, an expression vector encoding human SOD1 was co-transfected with an expression vector for FLAG-tagged human HDAC6 into Expi293F cells, a modified HEK293 cell line grown in suspension for higher protein yield. Cells were harvested and lysed 72 hours post transfection. Cell lysates were subsequently mixed with our anti-Ac-K123 SOD1 polyclonal antibody, which had been raised against the acetylated K123 of SOD1 protein, and the resulting immune complexes were collected and analyzed by immunoblotting with anti-FLAG antibody. We found that immunoprecipitation of Ac-K123 SOD1 from lysates of these co-transfected cells resulted in co-precipitation of HDAC6 (Figure 23). We also detected this interaction reciprocally by using the anti-FLAG antibody for immunoprecipitation and our anti-Ac-K123 SOD1 antibody for probing of the blotted precipitate (Figure 23). These observations provided the first indications that Ac-K123 SOD1 and HDAC6 can form physical complexes with one another in vivo.

Figure 23. HDAC6 and SOD1 interact in cells.

Co-immunoprecipitations of Expi293 cells transfected with SOD1 WT or SOD1 WT + HDAC6-FLAG were performed using Ac-K123 SOD1 or FLAG antibody, and subsequent western blots were performed using antibodies against Ac-K123 SOD1, FLAG, or α-Tubulin (loading control). Experimental data from B. Bossy, figure preparation by M. Kaliszewski.

3.3.6 HDAC6 inhibition or knockdown increases SOD1 K123 acetylation

We next assessed whether HDAC6 inhibition can block SOD1 deacetylation in cells. Cultured spinal cord astrocytes were pre-treated with HDAC6 pharmacological inhibitors tubastatin A and tubacin or a vehicle control, fixed, and immunostained with our Ac-K123 SOD1 antibody. Our results showed that both tubstatin A and tubacin potently blocked HDAC6 deacetylation of SOD1 in astrocytes and resulted in significantly increased immunolabeling of Ac-K123 SOD1 (Figure 24A). Co-labeling with antibodies against Ac-Tubulin demonstrate that Ac-K123 SOD1 detection predominantly within the nucleus. Quantification of the mean fluorescence intensity

of 3 independent experiments showed that HDAC6 inhibitor treatment resulted in significant increase in Ac-K123 SOD1 signal, with more than a 4-fold increase in tubastatin A and tubacin treated cells compared to the vehicle control (Figure 24B). Western blot analysis of Expi293 cells treated with tubastatin A or tubacin also showed increased detection of Ac-K123 SOD1 when compared to vehicle control treated cells (Figure 24C).

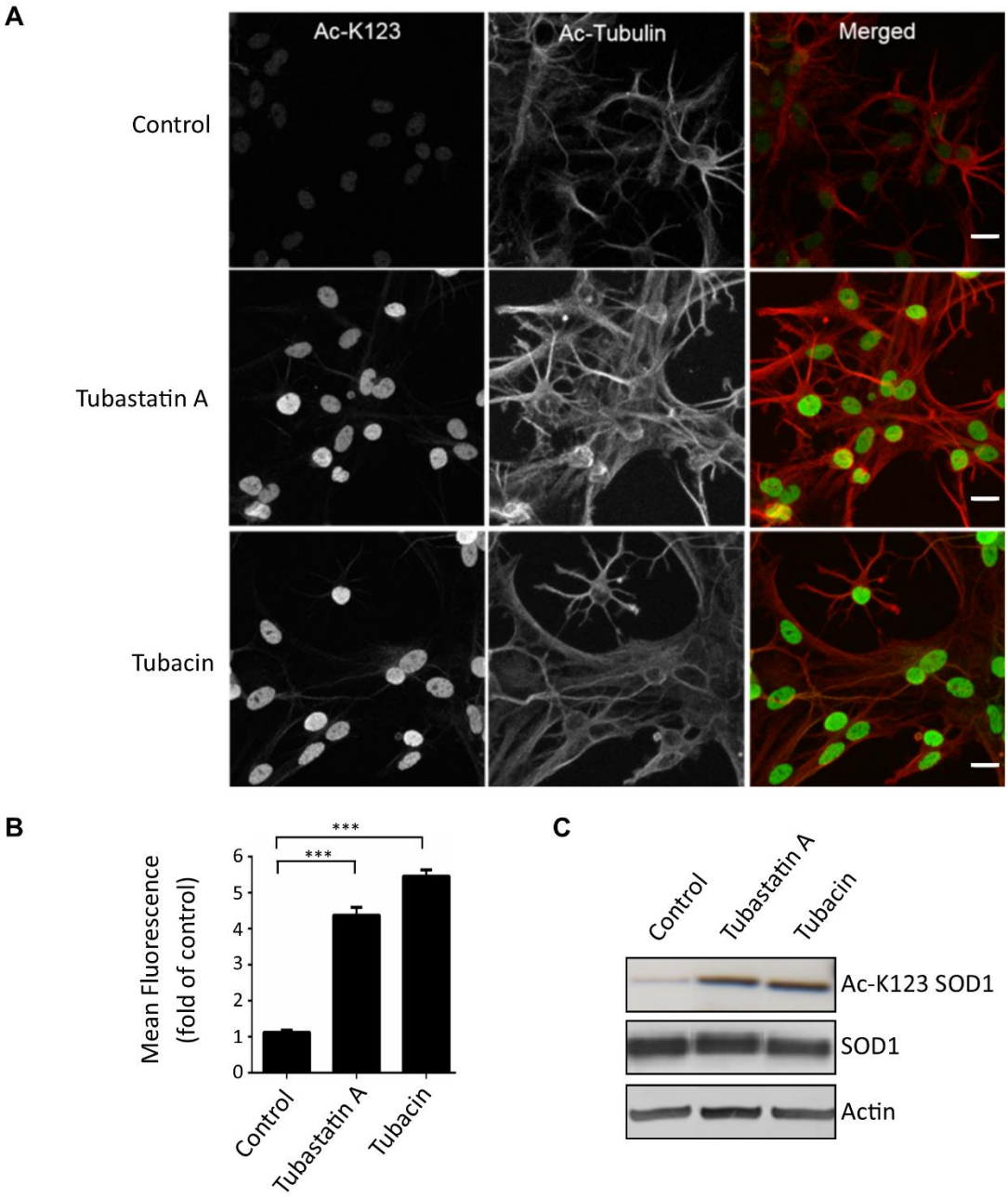

Figure 24. HDAC6 inhibitor treatment increases immunodetection of Ac-K123 SOD1.

A. Confocal micrographs (scale bar 10 µm) of rat primary spinal cord astrocytes treated with DMSO (control), tubastatin A (10 µM), or tubacin (10 µM) for 6 hours. B. Quantification of immunostaining data from 3 independent experiments (***, significance of $p<0.001$ by ANOVA). C. Western blot analysis of Expi293 cells treated with HDAC6 pharmacological inhibitors tubastatin A (10 µM), tubacin (10 µM), or vehicle control.

To confirm the specific effects of HDAC6 inhibition on SOD1 acetylation levels, we used HDAC6 siRNA knockdown in our study. HEK293 cells were co-transfected with a plasmid encoding SOD1 and siRNA targeting HDAC6. Transfected cells were cultured for 72 hours and then analyzed by western blot. Our results showed increased detection of Ac-K123 SOD1 in cells subjected to siRNA knockdown of HDAC6 when compared to control cells transfected with SOD1 plasmid and scrambled siRNA (Figure 25A). Quantification of three independent experiments demonstrates that HDAC6 knockdown resulted in a significant increase in SOD1 K123 acetylation (Figure 25B).

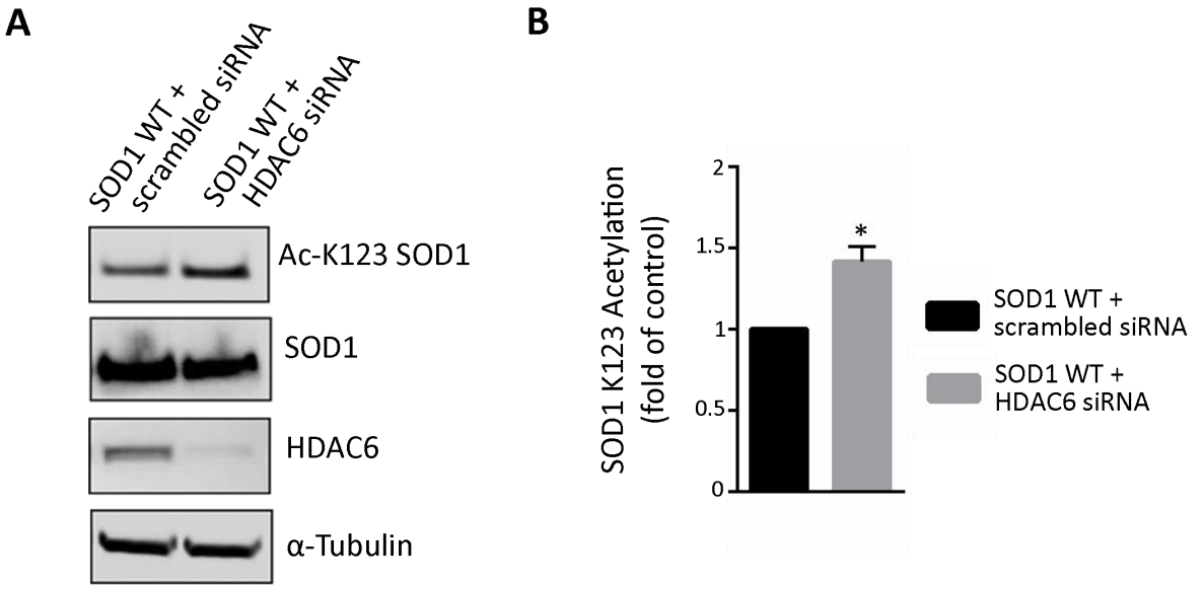

Figure 25. HDAC6 knockdown increases SOD1 K123 acetylation.

A. Representative western blot of lysate from HEK293 cells transfected with either scrambled siRNA or siRNA against HDAC6 and probed for Ac-K123 SOD1, SOD1, HDAC6, or α-Tubulin (loading control). B. Quantification by T-test (n=3, * signifies P value < 0.05). Experimental data from B. Bossy, quantification and figure preparation by M. Kaliszewski.

In summary, both pharmacological inhibitor treatment and HDAC6 knockdown inhibited HDAC6-mediated deacetylation of SOD1 and resulted in increased detection of Ac-K123 SOD1.

3.3.7 Deacetylation of SOD1 by HDAC6 in vivo

Next we proceeded to test the ability of HDAC6 to deacetylate SOD1 in vivo. We used the Expi293 expression system to transiently express SOD1 alone or in combination with HDAC6, and then compared the processed lysates by western blot analysis. To gauge the levels of SOD1 acetylation at Lys123, we used our rabbit anti-Ac-K123 SOD1 antibody.

Co-transfection of the SOD1 and HDAC6-FLAG plasmids substantially decreased the acetylated SOD1 that could be detected by the Ac-K123 SOD1 antibody (Figure 26A) when compared to SOD1 alone, and quantification of three independent experiments demonstrated a significant decrease (nearly 75%) of the Ac-K123 SOD1 signal in these samples (Figure 26B) . We therefore concluded that HDAC6 acts in vivo to specifically reduce the level of the K123 acetylated form of SOD1.

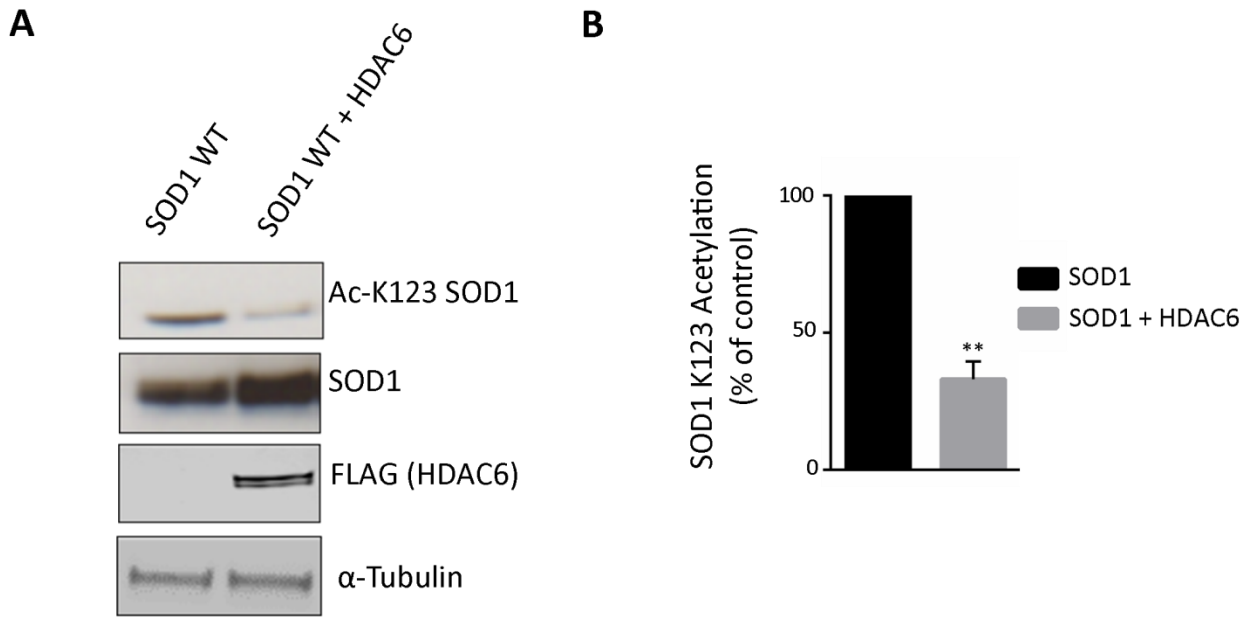

Figure 26. HDAC6 deacetylates Ac-K123 SOD1.

A. Western blot of lysate from Expi293 cells transfected with either SOD1 WT or SOD1 WT + HDAC6 and probed for Ac-K123 SOD1, SOD1, HDAC6, or α-Tubulin (loading control). B. Quantification (n=3, P value=0.0093). Experimental data from B. Bossy and R. Shaffer, quantification and figure preparation by M. Kaliszewski.

3.3.8 SOD1 interacts with α-TAT1 in cells

To determine if SOD1 and αTAT1 interacted in cells, Expi293 cells were transfected with plasmids expressing human SOD1 WT alone or in combination with human αTAT1-EGFP and analyzed by co-immunoprecipitation. When we performed western blot analysis of the immunoprecipitation of SOD1, we were able to also detect α-TAT1 (through its GFP tag) from the lysate of co-transfected cells (Figure 27). We also detected the reciprocal interaction by using an anti-GFP antibody for immunoprecipitation of α-TAT1 and an anti-SOD1 antibody for

immunoblotting (Figure 27). These results demonstrate that SOD1 and α-TAT1 can form physical complexes and interact within the cell.

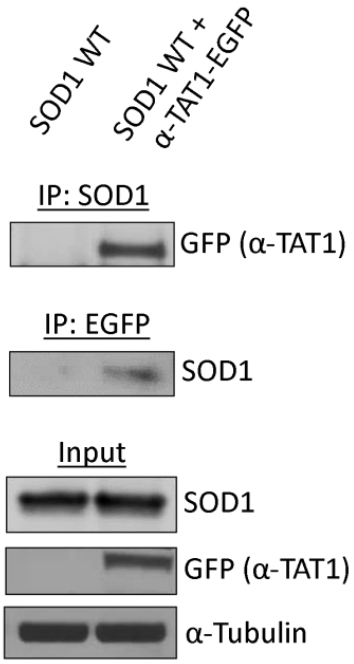

Figure 27. α-TAT1 and SOD1 interact in cells.

Co-immunoprecipitations of Expi293 cells transfected with either SOD1 WT or SOD1 WT + αTAT1-EGFP were performed using SOD1 or EGFP antibody, and subsequent western blots were performed using antibodies against SOD1, EGFP, or α-Tubulin (loading control). Experimental data from B. Bossy, figure preparation by M. Kaliszewski.

3.3.9 α-TAT1 knockdown decreases SOD1 K123 acetylation

To assess how depletion of α-TAT1 depletion affects the acetylation of SOD1, we examined Lys123 acetylation in HEK293 cells after siRNA-mediated knockdown of α-TAT1. We found that α-TAT1 depletion resulted in decreased SOD1 K123 acetylation levels (Figure 28), supporting our hypothesis that SOD1 is acetylated by αTAT1 *in vivo*.

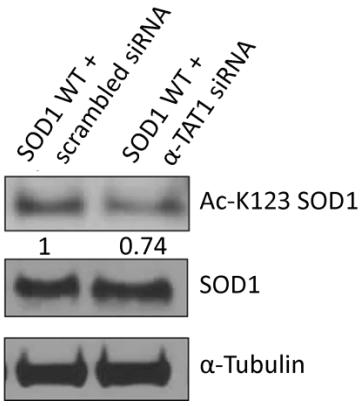

Figure 28. α-TAT1 siRNA mediated knockdown decreases SOD1 K123 acetylation.

Western blot of lysate from Expi293 cells transfected with either scrambled siRNA or siRNA against αTAT1 and probed for Ac-K123 SOD1, SOD1, or α-Tubulin (loading control). Numbers beneath the Ac-K123 SOD1 bands represent the relative integrated density values normalized to total SOD1. Experimental data from B. Bossy, figure preparation by M. Kaliszewski.

3.3.10 α-TAT1 acetylates SOD1 K123

To confirm that α-TAT1 is involved in the in vivo acetylation of SOD1, we evaluated Ac-K123 SOD1 levels in lysates from cells transfected with either SOD1 plasmid alone or in combination with α-TAT1 plasmid. Western blot analysis showed that Ac-K123 SOD1 detection is increased in cells co-expressing α-TAT1 (Figure 29A). Quantification of the normalized data from three separate experiments confirms that we observed an increase of Lys123 acetylated SOD1 in the cells co-transfected with α-TAT1 (Figure 29B).

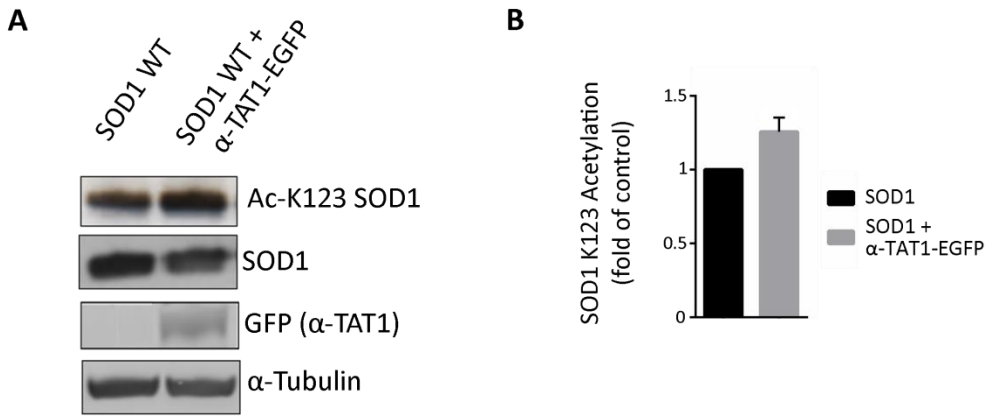

Figure 29. α-TAT1 acetylates SOD1 K123.

Western blot of lysate from Expi293 cells transfected with either SOD1 WT or SOD1 WT + αTAT1-EGFP and probed for Ac-K123 SOD1, SOD1, EGFP, or α-Tubulin (loading control). Experimental data from B. Bossy, quantification and figure preparation by M. Kaliszewski.

3.4 Discussion

To date, the effect of SOD1 lysine acetylation on protein localization has not been extensively characterized. In this study, we employed a custom antibody against acetyl-Lys123 SOD1 (Ac-K123 SOD1) to examine the subcellular localization of Ac-K123 SOD1 in primary astrocytes and neurons.

We found that primary astrocytes demonstrated Ac-K123 SOD1 localization to the nucleus and primary cilium. Interestingly, cellular quiescence promoted a loss of nuclear localization with increased localization to primary cilia after just one hour of total nutrient deprivation. This rapid ciliary localization can be explained by two likely scenarios: either Ac-K123 SOD1 is traveling into the primary cilia or an existing ciliary pool of SOD1 is becoming acetylated. Because the

primary cilium itself is not present in the majority of cells prior nutrient deprivation, the Ac-K123 SOD1 immunostaining of primary cilia in arrested astrocytes is most likely due to translocation. As the ciliary localization of Ac-K123 SOD1 rapidly occurs in parallel to the formation of primary cilia, it may also be possible that SOD1 has an undiscovered role in primary cilia biogenesis such as modulating communication between the cilia and cell body or influencing the IFT-dependent transport of materials required for axonemal growth.

The immunostaining of non-interphase astrocytes also yielded interesting results. We found that Ac-K123 SOD1 remains associated with the DNA during mitosis. This is an interesting observation because most contents of the nucleus are released into the cytoplasm following breakdown of the nuclear envelope. Rather than diffusing into the entire cytoplasm, Ac-K123 SOD1 remains close to the chromosomes. This finding raises the following question: does acetylated SOD1 play a role in mitosis, possibly aiding chromosome alignment, kinetochore attachment, or chromatid separation to daughter cell nuclei? SOD1 has been shown to directly interact with DNA in a transcription factor-like manner in response to oxidative stress (Tsang et al., 2014), but other roles outside of transcriptional regulation have yet to be described.

It is important to note that our analysis of Ac-K123 SOD1 localization within primary astrocyte cultures was performed in cells derived from spinal cords of Charles River Spraque-Dawley rats. This distinction is important, as previous studies have shown that the response to starvation of primary astrocytes varies based on the rat substrain. When compared to Charles River Spraque-Dawley rats, primary astrocytes derived from Harlan Spraque-Dawley rats showed a greater cell

response to starvation and more similarity to human astrocytes (Codeluppi et al., 2011). Therefore, it may be beneficial to explore if this rat substrain-dependent difference in response to nutrient deprivation extends to more pronounced ciliary and nuclear localization of Ac-K123 SOD1.

One key result from our custom antibody immunocytochemical staining experiments is the nuclear localization of Ac-K123 SOD1 in astrocytes. SOD1 localization and function within the nucleus has been previously described. Specifically, in response to elevated levels of reactive oxygen species, SOD1 translocates to the nucleus, binds to promoters, and regulates the expression of oxidative resistance and repair genes (Tsang et al., 2014). However, our finding that this nuclear pool of SOD1 is highly acetylated is novel. Acetylation of K123 may play a role in SOD1 translocation to the nucleus or it may act in retaining it there. Acetylation of K123 may also alter SOD1 interaction with other proteins or with DNA. Based on findings in other proteins, it is likely that K123 acetylation promotes the translocation of SOD1 into the nucleus. An example of a protein undergoing acetylation-mediated translocation is the glycolytic enzyme glyceraldehyde-3-phosphate dehydrogenase (GAPDH), where upon acetylation the predominantly cytoplasmic GAPDH undergoes translocation to the nucleus to regulate transcription and DNA repair (Ventura et al., 2010). It will be interesting to determine if SOD1 acetylation plays a role in the translocation of itself or other proteins, as studies have demonstrated nucleocytoplasmic transport dysfunction in motor neurons of ALS mouse models and patients (Kinoshita et al., 2009; Zhang et al., 2006). If Ac-K123 SOD1 does indeed have a physiological role in the nuclear transport of SOD1 or other proteins, the next step would be to

determine if there is a link between SOD1 K123 acetylation and the aberrant protein accumulation observed in ALS.

Another interesting finding from our primary astrocyte immunostaining was the localization of Ac-K123 SOD1 to primary cilia. To date very little is known with regards to SOD1 and primary cilia, and our data is the first evidence linking SOD1 acetylation to ciliary localization. This raises important questions, such as: what is the function of SOD1 K123 acetylation within the primary cilium, and where (in the cell) does SOD1 acetylation occur? The subcellular location is important, because SOD1 acetylation may act as a localization signaling domain, mediating translocation to the primary cilia, or it may behave as a ciliary retention signal, keeping SOD1 within the primary cilium. These are important questions that need to be addressed in future investigations, and the findings from such studies will help us better understand how post-translational modification regulates SOD1 subcellular localization. And based on the continued discovery of new roles for SOD1 within the cell, further inquiry into SOD1 acetylation may reveal previously unknown cellular functions of SOD1.

The localization of Ac-K123 SOD1 to primary cilia may be significant to ALS pathogenesis. Primary cilia number is reduced in motor neurons from mutant SOD1 ALS mice (Ma et al., 2011). There is also evidence that mutant SOD1 disrupts primary cilia-mediated signaling, as Sonic hedgehog agonist treatment confers neuroprotection in a cellular model of ALS (Peterson and Turnbull, 2011). With these points in mind, the relationship between disrupted primary cilia function in ALS and the ciliary localization of Ac-K123 SOD1 merits further investigation.

It is worth noting that in our present study we have focused exclusively on the subcellular localization of wildtype SOD1. This is an important point because previous studies have shown a low nuclear presence of endogenous SOD1 in mouse brain and spinal cord, with higher levels of SOD1 nuclear accumulation observed in SOD1 WT and ALS mutant transgenic mice (Gertz et al., 2012). Recent findings from another group describe levels of mutant SOD1 as lower than those of wildtype SOD1 within the nuclei of both cortical neurons and astrocytes derived from transgenic mice (Lee et al., 2015). Taken together, it will be of interest to next explore how acetylation impacts the localization of mutant SOD1 in neurons and astrocytes.

The other goal of this study was to evaluate the potential regulators of SOD1 Lys123 acetylation. Based on our novel immunocytochemical findings that demonstrated Ac-K123 SOD1 localization with the primary cilium, we used a candidate approach to come up with potential acetyltransferases and deacetylases that have known associations with both the cytoplasm and primary cilia. We showed that α-TAT1 interacts with and acetylates SOD1 within cells, while HDAC6 is responsible for the deacetylation of Ac-K123 SOD1. Interestingly, depletion or dysfunction of both α-TAT1 and HDAC6 are implicated in several disease processes, including neurodegenerative disorders. It will therefore be of interest to examine whether aberrant SOD1 acetylation is linked to cellular toxicity. Given that SOD1 misfolding plays a major role in ALS pathogenesis, an investigation of how Lys123 acetylation impacts SOD1 structure and stability will be highly merited.

CHAPTER FOUR: SOD1 LYS123 ACETYLATION PROMOTES MISFOLDING AND CILIARY TARGETING

4.1 SOD1 and ALS

4.1.1 Overview of ALS

Amyotrophic lateral sclerosis (ALS) is a disease of the motor neurons in the spinal cord, brain stem, and motor cortex that control voluntary muscle movement. Progressive degeneration of these motor nerves leads to progressive muscle weakness, atrophy, paralysis, and eventually death by respiratory failure. ALS is incurable and patient treatment remains primarily palliative. The glutamate antagonist Riluzole, the only drug approved for the treatment of ALS, has a small effect on disease progression and extends the median survival by 2–3 months (Bensimon et al., 1994).

The onset of disease is typically in midlife (between 45 and 60 years of age) with a median survival period of 3 years after onset of symptoms (Hardiman et al., 2011). The incidence, or frequency of new cases per year, is 1–2 per 100,000 and the prevalence, or proportion of affected individuals in the population, is 4–6 per 100,000. Unfortunately, these epidemiologic statistics understate the true impact of ALS. A better indicator of one's risk to develop ALS is the estimated lifetime risk, which is about 1 in 350 in men and 1 in 450 in women (Alonso et al., 2009).

The vast majority of ALS cases (approximately 90%) are sporadic (SALS) and of unknown etiology. The remaining 5-10% of cases are due to inheritable, mostly autosomal dominant, genetic mutations and are classified as familial ALS (FALS).

Mutations within a wide variety of genes have been implicated in FALS. Important genes involved in ALS include SOD1, TAR DNA-binding protein 43 (TDP43), fused in sarcoma/translocated in liposarcoma (FUS), dynactin, optineurin, ubiquilin 2, and a repeat expansion within the non-coding region of the open reading frame 72 of chromosome 9p (C9ORF72) (DeJesus-Hernandez et al., 2011; Deng et al., 2011; Kwiatkowski et al., 2009; Maruyama et al., 2010; Münch et al., 2004; Neumann et al., 2006; Rosen et al., 1993; Vance et al., 2009).

To date, over 180 mutations identified in SOD1 have been found to cause ALS, accounting for about 20% of inherited cases (http://alsod.iop.kcl.ac.uk). At least 75 of the 153 amino acids in SOD1 are mutated and there are no mutational hot spots (Saccon et al., 2013). Mutations are scattered throughout the protein and can be found within the beta-barrel, the dimer interface, and the active site channel.

4.1.2 SOD1 toxic gain of function

Due to its important function of protecting the cell from oxidative damage, it was initially proposed that loss of SOD1 activity may contribute to the pathogenesis of SOD1-linked ALS. Several key findings from previous investigations have resoundingly put this theory to rest. *In*

vitro studies showed that several SOD1 mutant proteins have diminished enzymatic activities, while at least some mutants linked to ALS retain full enzyme activity (Borchelt et al., 1994). In mice, the expression of mutant human SOD1 in transgenic mice causes motor neuron disease, while the expression of wild type human SOD1 does not (Bruijn et al., 1998; Gurney et al., 1994). And most importantly, Sod1 $^{-/-}$ mice do not develop motor neuron disease (Reaume et al., 1996). These important findings support the hypothesis that mutant SOD1 toxicity arises from a gain of function as opposed to a loss of function.

The toxic properties of mutant SOD1 are believed to arise from mutation-induced conformational changes that cause misfolding and aggregation. Inherited SOD1 mutations promote structural instability, unfolding, and dimer dissociation; changes that are enhanced by the release of zinc. Conformational changes alter configuration of the active site channel and allow non-conventional substrates to interact with copper. As a result mutant SOD1 is more prone to aberrant redox chemistry, such as the interaction of peroxynitrite or hydrogen peroxide with reduced copper that results in SOD1 tyrosine nitration and hydroxyradical formation (Beckman et al., 1993; Wiedau-Pazos et al., 1996). The backward catalysis of molecular oxygen generates superoxide anions after the loss of zinc, and zinc-defiecient SOD1 is sufficient for inducing apoptosis in cultured motor neurons (Estévez et al., 1999).

Mutant SOD1 also demonstrates altered subcellular localization and has been identified within the nucleus, mitochondria, endoplasmic reticulum (ER), Golgi, peroxisomes, and cytoplasm. The

selective loss of motor neurons reflects a disturbance of several different pathways, and many pathologic processes attributed to ALS pathogenesis are mediated by mutant SOD1.

Several lines of evidence indicate mutant SOD1-mediated mitochondrial dysfunction. Mutant SOD1 displays and increased tendency to localize within mitochondria, and abnormal mitochondrial morphology and cristae vacuolization are observed in ALS patient samples and mouse models (Kong and Xu, 1998; Wong et al., 1995). Mutant SOD1 blocks mitochondrial protein import through inhibition of the translocator outer membrane (TOM) complex, diminishes ATP production by impairing respiration, promotes the release of free calcium, and decreases the calcium buffering capacity (Damiano et al., 2006; Israelson et al., 2010; Li et al., 2010; Mattiazzi et al., 2002). Mutant SOD1 alters mitochondrial dynamics, with evidence from a variety of cellular models demonstrating increased mitochondrial fragmentation and impaired mitochondrial transport along axons (De Vos et al., 2007; Magrané et al., 2009, 2014; Song et al., 2013). Additionally, the mitochondrial localization of mutant SOD1 contributes to activation of the apoptotic pathway. On the mitochondrial surface SOD1 aggregates inhibit the anti-apoptotic BCL2 protein and cause damage to the membrane, resulting in cytochrome c release and caspase activation (Kirkinezos et al., 2005; Pedrini et al., 2010).

Glutamate-induced excitotoxicity is a component of ALS that is caused by the failure to remove glutamate from synaptic clefts. This results in excessive stimulation of postsynaptic glutamate receptors and massive calcium influxes into the cell. Motor neurons exhibit a selective vulnerability to glutamate-induced excitotoxicity due to a diminished capacity to buffer calcium

and their expression of AMPA (α-amino-3-hydroxy-5-methyl-4-isoxazole propionic acid)/kainate receptors. Unlike NMDA (*N*-methyl-D-aspartate) receptors that are utilized by most neurons, AMPA/kainate receptors lack the GluR2 subunit that regulates calcium permeability and influx during glutamate stimulation. It has also been reported that mutant SOD1 increases the expression and function of AMPA receptors, further increasing motor neuron sensitivity to glutamate-induced toxicity (Spalloni et al., 2004). Additionally there is diminished expression of the excitatory amino acid transporter 2 (EAAT2) glutamate transporter in mutant SOD1 astrocytes (Howland et al., 2002), further exacerbating the excessive accumulation of glutamate observed in ALS.

Another characteristic of ALS is abnormal axonal transport, which has been described in both patients and transgenic mouse models (Sasaki and Iwata, 1996; Sasaki et al., 2005). With axons that can extend up to one meter in length, motor neurons depend on a functional axonal transport system for maintaining synaptic function, neurotransmitter release, vesicle recycling, and mitochondrial calcium buffering. Mutant SOD1 interaction with microtubule motor protein complexes has been shown to perturb anterograde and retrograde axonal transport (Shi et al., 2010; Ström et al., 2008), and it has been proposed that impaired axonal transport is an early event mediating the toxicity of ALS-linked SOD1 mutants in motor neurons (Williamson and Cleveland, 1999).

Proteasome dysfunction and defective removal of toxic proteins are also features of ALS. Aggregated SOD1 has been shown to inhibit both chaperone and proteasome activity, resulting

in the subsequent misfolding and insufficient clearance of other toxic proteins (Bendotti et al., 2012; Urushitani et al., 2002). Mutant SOD1 also interacts with unfolded protein response components and is recruited to the ER, adversely effecting ER function and causing sustained ER stress (Atkin et al., 2006; Kanekura et al., 2009; Wang et al., 2011a).

4.1.3 Misfolding of modified wild-type SOD1

It has recently been suggested that misfolded wild-type SOD1 plays a role in the more prevalent, sporadic form of the disease (SALS) (Bosco et al., 2010; Rotunno and Bosco, 2013). In transgenic mice the onset of paralysis is accelerated when wild type SOD1 is co-expressed with mutant SOD1 (Wang et al., 2009). Evidence from mice shows wild-type SOD1 was induced to aggregate with mutant SOD1 (Prudencio et al., 2009a), demonstrating wild type SOD1 as a potential pathogenic link between FALS and SALS. Oxidation, an exogenous post-translational modification (PTM) of wild-type SOD1, promotes misfolding of the protein (Rakhit et al., 2002), hinting at the possibility that endogenous PTMs might similarly contribute to misfolding and SOD1-mediated toxicity in SALS.

4.1.4 Conformation specific misfolded SOD1 (C4F6) antibody

The anti-misfolded SOD1 (C4F6) antibody is conformation specific and is widely used in studies to identify misfolded SOD1. Studies have shown that the C4F6 monoclonal antibody, which was produced using standard procedures after immunization of mice with mutant SOD1 G93A recombinant protein, recognizes epitopes normally buried in the native conformation of SOD1.

C4F6 antibody shows strong immunoreactivity to SOD1 mutants with little to no reactivity to wildtype SOD1 (Urushitani et al., 2007). A recent study showed that C4F6 recognizes wild type SOD1 modified by *in vitro* oxidation, and furthermore linked wild type SOD1 to SALS by showing C4F6 immunoreactivity to spinal motor neurons in SALS patients (Bosco et al., 2010). For these reasons we employed the C4F6 antibody during our investigation into the relationship between SOD1 acetylation and misfolding.

4.1.5 ALS and non-cell autonomous toxicity

Although the selective degeneration and death of motor neurons is a defining feature of ALS, recent studies have shown that non-neuronal cells also contribute to the pathogenesis of ALS (Boillée et al., 2006a). Neuroinflammation arising from activated glial cells and infiltrated immune cells has been described in both mutant SOD1 mouse models and ALS patients (Endo et al., 2015; Engelhardt et al., 1993). Moreover, the selective reduction of mutant SOD1 expression in microglia or astrocytes has been shown to significantly extend the survival time of ALS mice (Beers et al., 2006; Boillée et al., 2006b; Wang et al., 2011b; Yamanaka et al., 2008).

4.1.6 Prion-like spreading of SOD1 in ALS

Increasing evidence supports a model of neurodegenerative disease in which pathological progression is driven by the formation of aberrant protein aggregates that are propagated in a self-templating manner. This process resembles the replication of infectious prions, and is therefore often referred to as “prion-like” protein seeding and propagation (Goedert et al.,

2010). The prion theory of neurodegeneration postulates that fibrillary protein seeds taken up by neighboring cells in the brain or spinal cord induce the aggregation of normally structured proteins, resulting in the spreading of misfolded proteins (Frost and Diamond, 2010). Most neurodegenerative diseases are characterized by dysfunction in discrete brain regions during the early stages with more widespread dysfunction in later stages, suggestive of a spreading pathology (Frost and Diamond, 2010). Furthermore, spreading of protein aggregates has been shown to mirror the overall clinical pathophysiology of neurodegeneration (Frost and Diamond, 2010).

Mechanistically, the prion-like theory postulates that ALS pathological progression is driven by the formation of aberrant SOD1 aggregates which are propagated in a self-templating manner (Figure 30). Misfolded SOD1 acts as seeds of aggregation that sequester and convert natively folded SOD1 to form growing fibrils. Subsequent fragmentation amplifies the misfolded SOD1 seeds available for repetition of the cycle. The release of seeds into the extracellular environment and uptake by neighboring cells represents a mechanism of cell-to-cell transfer, and seeded nucleation within the new cell furthers the repetition of the propagation cycle. The characteristics of a prion-like spreading mechanism are observed during the progression of ALS and apply to SOD1.

Clinical observations and mouse model studies describe a contiguous spreading of the disease that can be explained by propagation of misfolded protein via a prion-like mechanism. Typically, a focal onset of motor weakness (in the spinal cord and bulbar regions) is followed by regional

spreading of motor symptoms with exacerbation of local motor symptoms (Ravits, 2014). This pattern of disease progression suggests that the pathology is propagating neuroanatomically, starting discretely within one area of the neuraxis and then spreading outward to contiguous regions. Furthermore, when also taking into consideration the non-cell autonomous nature of ALS, it is possible that such a spreading mechanism underlies the toxic interplay between astrocytes and motor neurons.

Another feature of ALS supporting a prion-like spreading is the presence of fibrillary protein aggregates that can act as structural templates for converting SOD1 from a native to misfolded protein. Mutant SOD1 aggregation has been demonstrated in human tissues, mouse models, cultured cells, and *in vitro* with purified proteins. Spinal cords from ALS patients and FALS mouse models are characterized by SOD1-positive inclusions within neurons and glial cells (Bruijn et al., 1998; Chia et al., 2010; Kato, 2007; Matsumoto et al., 1996; Shibata et al., 1994).

Perhaps the most important feature of ALS, with regards to prion-like spreading, is the actual cell-to-cell transmission and propagation of misfolded proteins. Several cell culture studies investigating this process showed misfolded SOD1 aggregates promoted further misfolding and transmission to neighboring cells (Grad et al., 2014; Münch et al., 2011). Interestingly, seeding of cell cultures with mutant SOD1 aggregates also resulted in misfolding of endogenous wildtype SOD1 (Münch et al., 2011; Silverman et al., 2016). Furthermore, this aggregation was self-perpetuating and continued for many passages following removal of aggregate seeds from the culture medium. In an astrocyte and motor neuron mixed culture study exosomes derived

from astrocytes were shown to effectively transfer mutant SOD1 to motor neurons and induce selective cell death (Basso et al., 2013), demonstrating that mutant SOD1 expression in astrocytes impacts protein secretion pathways and the spread of disease. Recently, in vivo transmission of mutant SOD1 has been demonstrated in a study using mouse models. Motor neuron disease was induced by injection of mutant SOD1 spinal cord homogenate into the spinal cords of unaffected animals (Ayers et al., 2014), providing the first evidence of misfolded SOD1 intra-organismal transmission.

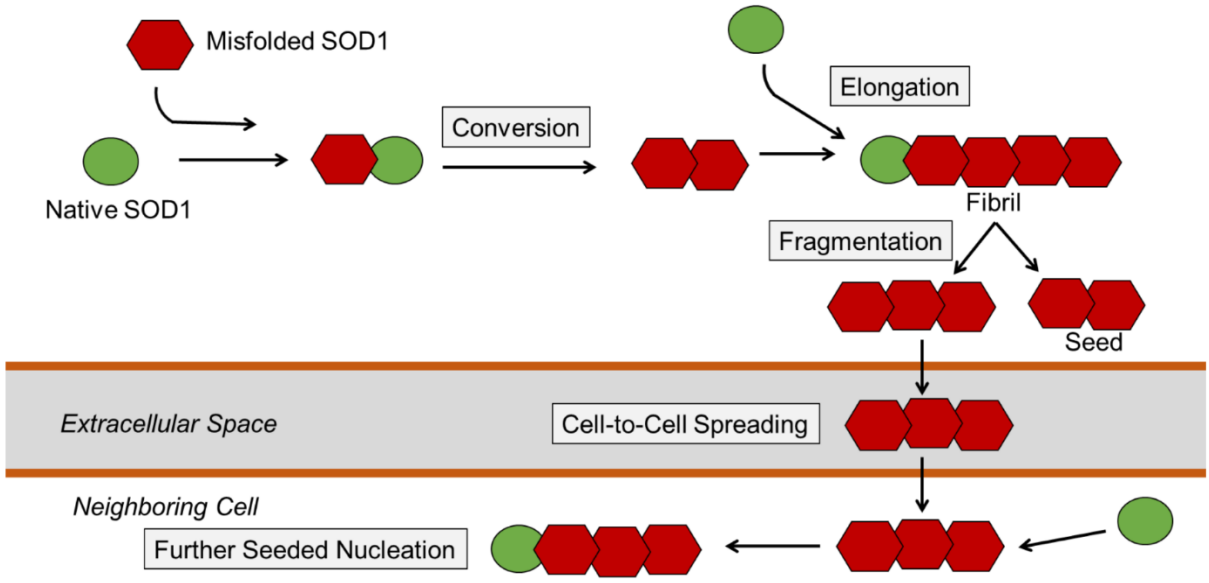

Figure 30. Model of the prion-like transfer of misfolded SOD1.

4.1.7 Evidence of vesicle secretion from primary cilia

There has been several findings supporting the notion that primary cilia may participate in the intercellular transfer of materials. One recent study showed that primary cilia of adjacent cells

contact and form adhesions, allowing for a direct communication between two neighboring cells (Ott et al., 2012). Although the secretory capabilities of primary cilia in humans remain uncertain, several lines of evidence suggest that cilia might act as secretory organelles.

Studies of simple organism model systems have identified release of extracellular vesicles from ciliary structures. EM analysis showed that distal ends of the primary cilia-like flagella of *Chlamydomonas*, a unicellular green alga, secrete bioactive vesicles containing a proteolytic enzyme (Wood et al., 2013). This finding is of potential relevance to human primary cilia because green algae flagella have traditionally served as a reliable model of mammalian cilia; other ciliary components first identified in algae and later found to be conserved in mammals include the IFT proteins (Avasthi and Marshall, 2013; Wood et al., 2013). In addition, ciliated sensory neurons in *Caenorhabditis elegans* were recently shown to release extracellular vesicles (Wang et al., 2014). A recent study of the developing central nervous system in vertebrates also described membrane budding from primary cilia. Using high-resolution live-cell imaging of chick neural tube, investigators elegantly describe a form of cell remodeling in which constriction and abscission of the apical membrane is used for dismantling of the primary cilium and termination of Shh signal transduction (Das and Storey, 2014).

Early studies in mammalian cells have also yielded indicators of protein secretion from primary cilia. For example, a study of neuroepithelial cells found that the distribution of prominin-1, a stem cell marker, on primary cilia was suggestive of budding of small membrane vesicles from the tips of differentiating cells (Dubreuil et al., 2007). In addition, extracellular membrane

particles released into neural tube fluid from neuroepithelial cells were found to be enriched in prominin-1. In humans, the protein contents of exosome-like vesicles purified from urine suggested that these structures originated from primary cilia (Chacon-Heszele et al., 2014).

In summary, the observations in simpler organisms and recent evidence from mammalian studies demonstrate that the primary cilium represents a novel source of extracellular membrane vesicles. Further exploration of primary cilia-mediated protein secretion is therefore highly warranted, especially when taking into consideration the prion-like propagation of misfolded SOD1 underlies the pathology of ALS. In light of the clues suggesting protein secretion from primary cilia, we speculate that primary cilia are important, as yet unexplored mediators of prion-like spreading of SOD1 in ALS.

4.1.8 Genes linking primary cilia to ALS

Genetic studies, including whole-exome analyses of familial ALS cases, have identified genetic factors contributing to ALS. Many of the identified genes are structurally or functionally critical to primary cilia.

Point mutations within the DCTN1 gene encoding the microtubule motor adapter protein dynactin causes defective transport and is a risk factor for ALS (Münch et al., 2004). Although dynactin does not interact with cytoplasmic dynein 2, the IFTB motor in primary cilia, it plays an important role in primary cilia dynamics through the dynein-dynactin complex-dependent recruitment of the Plk1 kinase to pericentriolar matrix for activation of HDAC6.

An exome-wide rare variant analysis identified TUBA4A mutations with FALS. Microtubules comprise the axoneme structure of primary cilia. TUBA4A mutants destabilize microtubules and diminish their repolymerization capability (Smith et al., 2014).

Studies examining OPTN mutations in ALS patients suggest that optineurin is involved in the pathogenesis of ALS (Maruyama et al., 2010). Optineurin is an autophagy adapter that interacts with Rab8 to mediate endocytic trafficking. Optineurin also plays an important role in ciliary membrane expansion and fusion with the plasma membrane during ciliogenesis.

Mutations within UBQLN2 have also been shown to cause ALS (Deng et al., 2011). The encoded ubiquilin 2 protein associates with both proteasomes and ubiquitin ligases to modulate *in vivo* protein degradation. Due to its important role in linking the ubiquitination machinery to the proteasome, ubiquilin 2 plays an important autophagic role functionally downstream of the primary cilia mediated Shh signaling required for induced autophagy. Another mutated protein functionally related to primary cilia is the actin-binding protein profilin-1. Exome sequencing demonstrated that PFN1 mutations cause FALS (Wu et al., 2012). Profilin-1 plays an important role in axon elongation through Shh pathway activation via the primary cilia.

The expanded hexanucleotide repeat within a noncoding region of chromosome 9 open reading frame 72 (C9ORF72) represents the most common cause of ALS to date (DeJesus-Hernandez et al., 2011). Although the protein has yet to be fully characterized, initial studies have suggested a role in endosomal trafficking and autophagy. Structural homology also suggests the C9ORF72 protein is a Rab GEF which activates Rabs. There is also indications that C9ORF72 interacts with

the primary cilia-associated Rab8, thereby regulating transport to primary cilia, playing a critical role in early cilia formation, and maintaining ciliary function through coordination with the intraflagellar transport system.

Interestingly, a recent study involving the screening of whole-exome sequencing data described the association of NEK1 variants with ALS at exome-wide significance (Kenna et al., 2016). NEK1 is a kinase linked to several cellular functions, including primary cilia formation.

4.2 Materials and Methods

4.2.1 Reagents

Neurobasal medium, Neuronal Supplement 21, GlutaMAX, 100x penicillin-streptomycin solution, Lipofectamine 2000, MagnaBind Protein G magnetic beads, and Expi293 Expression Medium were acquired from Thermo Fisher. Phosphate buffered saline, pH 7.4 (PBS), EDTA, Tubastatin A hydrochloride, gelatin from cold water fish skin 45% in H_2O, Ponceau S solution 0.1% w/v and 5% acetic acid, and poly-L-lysine were obtained from Sigma-Aldrich. Amaxa Nucleofector kits for rat neurons and rat glial cells were purchased from Lonza.

4.2.2 Antibodies

Ac-K123 SOD1 antibodies were custom-made by Yenzym Antibodies. Mouse monoclonal misfolded SOD1 (C4F6) antibody was obtained from MédiMabs. Mouse monoclonal SOD1 (G11) antibody was purchased from Santa Cruz Biotechnology. Mouse monoclonal acetylated α-tubulin (6-11B-1) antibody was obtained from Sigma. Peroxidase-conjugated AffiniPure donkey

anti-rabbit IgG (H+L) and peroxidase-conjugated AffiniPure donkey anti-mouse IgG (H+L) secondary antibodies were obtained from Jackson ImmunoResearch Laboratories, Inc. Alexa Fluor 488 goat-anti-rabbit IgG (H+L), highly cross-absorbed, and Alexa Fluor 594 goat anti-mouse IgG (H+L) were obtained from Molecular Probes.

4.2.3 Rats

Timed-pregnant Sprague Dawley rats (Charles River) were used for the isolation of primary spinal astrocytes and cortical neurons.

4.2.4 Site directed mutagenesis

Mutagenesis was performed using the QuikChange Lightning site-directed mutagenesis kit (Agilent Technologies, Santa Clara, CA). The SOD1 K123Q and SOD1 K123R mutants for mammalian expression were created using the pcDNA3.1 SOD1 WT vector (gift from Dr. Alvaro Estevez, University of Central Florida) as a template. The primers utilized for mutagenesis were as follows:

Table 2. The primers used for mutagenesis of SOD1 K123.

Primer	Sequence
K123Q Forward	5’-GCACACTGGTGGTCCATGAACAAGCAGATGACTTGGGC-3’
K123Q Reverse	5’-GCACAAGTCATCTGCTTGTTCATGGACCACCAGTGTGC-3’
K123R Forward	5’-GCACACTGGTGGTCCATGAAAGAGCAGATGACTTGGGC-3’
K123R Reverse	5’-GCCCAAGTCATCTGCTCTTTCATGGACCACCAGTGTGC-3’

The DNA template-primer mix was amplified using an Eppendorf Mastercycler Gradient 531 PCR machine. After PCR amplification, template DNA was digested by incubation with DpnI at 37^{o}C for 5 minutes. For bacterial transformation, 22.5 µL of XL10-Gold Ultracompetent bacteria were incubated with 2 µL of PCR-amplified DNA on ice for 30 minutes, heat-shocked at 42^{o} C for 30 seconds, and placed back on ice for 2 minutes. Bacteria were then resuspended in 500 µL pre-warmed super optimal broth (SOB) (0.5% yeast extract, 2% tryptone, 10 mM NaCl, 2.5 mM KCl, 20 mM $MgSO_4$) and then grown for one hour at 37^{o} C in a bacterial shaker at 225 rpm. Finally, 200 µL was plated on LB agar plates containing 100 µg/mL ampicillin. After 37°C overnight incubation, single colonies were picked and inoculated in 5 mL LB medium with ampicillin (100 µg/mL). Bacterial cultures were grown overnight at 37^{o} C in a bacterial shaker at 225 rpm. Plasmid DNA was isolated using a QIAprep Spin Miniprep kit and subjected to DNA sequencing to confirm mutagenesis (Eurofins Scientific). Large-scale endotoxin-free plasmid DNA was isolated using a Gene Jet Plasmid Maxiprep kit per manufacturer's instructions.

4.2.5 Expi293 cells

Expi293F cells were grown in suspension using vent-cap shaker flasks. Initially, 0.3×10^6 cells/mL were seeded in Expi293 Expression Medium and grown in a tissue culture incubator at 37°C in a humidified atmosphere of 8% CO_2 in air on an orbital shaker platform rotating at 125 rpm. Cultures were incubated until cell density reached at least 3×10^6 viable cells/mL (typically 3–4 days), at which time transfections are carried out using the ExpiFectamine 293 transfection kit per manufacturer's guidelines.

4.2.6 Immunoprecipitation and western blotting

Expi293F cells were harvested by centrifugation, resuspended in ice cold lysis buffer (TPER supplemented with protease, phosphatase, and deacetylase inhibitors), and lysed by freeze-thaw lysis and one cycle of sonication at 50% output for 30 seconds. 1 mg of lysate was mixed with 5 µg of antibody and rotated overnight at 4°C. Antibody-peptide complexes were then incubated with 25 µl of MagnaBind Protein G magnetic beads for 1 hour at room temperature under rotation. Immune complexes were isolated by magnet, washed 3 times in lysis buffer, quick rinsed one time in ddH_2O. Proteins were eluted from beads by boiling in SDS sample buffer, and collected eluate was removed and loaded onto gels for SDS-PAGE analysis.

4.2.7 Primary cortical neurons and transfection

Cortical neuronal cultures were prepared from embryonic day E18 rat embryos and seeded in D10C medium. After 4 hours the medium is changed to neuronal medium (Neurobasal medium supplemented with 2% Neuronal Supplement 21, 2 mM GlutaMAX, and penicillin/streptomycin).

Primary cortical neurons were isolated from fetal rat cortices dissected and prepared from one litter of E18 Sprague Dawley rat embryos. For expression of DsRed2-Mito (Clonetech) in combination with SOD1 WT or one of the various SOD1 mutants, cortical neurons were transfected by electroporation. For transfections, $5x10^6$ cells were resuspended in 100 µL of Primary Rat Neuron Nucleofector Solution (Lonza) and mixed with 2 µg plasmid DNA for both

DsRed2-Mito and SOD1 (pcDNA3.1 SOD1 WT, SOD1 K123R, SOD1 K123Q, SOD1 A4V, SOD1 A4V/K123R, or SOD1 A4V/K123Q). Neurons were electroporated using an Amaxa Nucleofector I device (Lonza) following an optimized protocol for primary rat neurons provided by the manufacturer.

4.2.8 Primary spinal astrocytes and transfection

Astrocytes were passaged 2-3 days before transfection and allowed to grow to about 80% confluency. After trypsinization, a volume of cell suspension containing 3 x 10^6 cells is transferred to a 15 mL tube and cells are pelleted by centrifugation at 100 x g for 10 minutes at room temperature. Cells were gently resuspended in 100 µL Nucleofector solution and mixed with 4 µg of total plasmid DNA. Cell suspensions were then transferred into electroporation cuvettes which were placed into the holder of an Amaxa Nucleofector electroporation device (Lonza) and run on program T-20. 500 µL of pre-warmed media was then immediately added to each sample in their cuvettes. Samples were removed from cuvettes using sterile custom pipettes from the Amaxa Nucleofector kit and seeded onto poly-D-lysine coated glass coverslips at a density of 2 x 10^5 cells per well of a 24 well tissue culture plate containing prewarmed astrocyte medium. Transfected astrocytes were grown in a humidified tissue culture incubator at 37°C in 5% CO_2 for 48-72 hours until processing for immunocytochemistry.

4.2.9 Confocal microscopy

Confocal imaging was carried out with a Zeiss LSM 710 Inverted Axio Observer confocal laser scanning microscope with six laser excitation lines (405, 458, 488, 514, 543, and 633 nm), a 34 channel QUASAR detector for spectral analysis, and several objectives including a EC Plan-Neofluar 10x 0.3 numeric aperture (NA) air objective, Plan-Apochromat 20x 0.8 NA air objective, EC Plan-Neofluar 40x 1.3 NA oil objective, and a Plan-Apochromat 63x 1.4 NA oil objective. Image acquisition and processing were performed using Zen 2012 software from Zeiss. To visualize Hoechst 33342, the excitation/emission wavelength was 405/495 nm using the diode laser. For Alexa Fluor 488, the excitation/emission wavelength was 488/540 nm using the multiline argon laser. For Alexa Fluor 594, the excitation/emission wavelength was 543/660 nm using a diode pumped solid state laser plus a QUASAR detector for all emission wavelengths. The acquired z-stacks were maximally projected and the gamma value adjusted using the ZEN 2012 software.

4.2.10 Live-cell imaging and quantification

Time-lapse imaging was performed using an Axiovert Zeiss 100 M inverted fluorescence microscope equipped with a motorized focus, a Plan-Apochromat 63 × 1.4 NA oil objective, a DG-4/Lambda 10–2 combo Xenon-arc illumination system (Sutter), a Ludl MAC 5000/bioprecision 2 linear encoded XY-motorized stage, and a Sensicam QE cooled CCD camera (PCO AG, Germany) and controlled by MetaMorph 7.5 software (Molecular Devices). During

imaging cells were housed in the Axiovert Incubator XL 100/135 in order to maintain a controlled environment (37°C, humidified 5% CO_2).

Cortical neurons were grown on Lab-Tek II 8-chamber slides (#1.5 German coverglass) in neuronal medium supplemented with 2% Neuronal Supplement 21, 2 mM GlutaMAX, and and 0.25% penicillin without phenol red. To visualize the DsRed2-Mito labeled mitochondria a S555/28x excitation filter (Chroma) and a S617/73m emission filter (Chroma) were used. 3D images were acquired using the Multi-Dimensional Acquisition module 45 in MetaMorph 7.5. Neurites of at least 100 µm in length were selected, and mitochondrial movement was recorded for 5 min at 3 second intervals (6 planes, 0.5 µm step size). Kymographs were generated by average projections of all planes without background subtraction using MetaMorph 7.5, and the mitochondrial velocity and moving distance measurements were exported to Microsoft Excel for further analysis.

Primary spinal astrocytes were grown on Lab-Tek II 8-chamber slides (#1.5 German coverglass) in normal astrocyte medium without phenol red. To visualize the primary cilia and ciliary vesicles labeled by SSTR3-EGFP, a S490/20× excitation filter (Chroma) and a S528/38m emission filter (Chroma) were used. 3D images were acquired using the Multi-Dimensional Acquisition module 45 in MetaMorph 7.5. Primary cilia that were well isolated with little background were selected, and ciliary movement and budding was recorded for 90 min at 30 second intervals (11 planes, 1 µm step size). Cilia images were filtered and maximum projected using MetaMorph 7.5, and journals were utilized for image looping and the creation of movies.

4.3 Results

4.3.1 ALS-linked SOD1 mutants demonstrate increased K123 acetylation

Protein dysfunction and accumulation into intraneuronal aggregates is observed in many neurodegenerative disorders, including ALS. It is now also appreciated that reversible lysine acetylation plays an important role in the pathologic misfolding of many proteins associated with neurodegeneration. One such example is the acetylation of tau, which recent studies has implicated in the pathogenesis of Alzheimer's disease and other related tauopathies (Cohen et al., 2011). For these reasons, and the fact that many SOD1 mutations cause an increased propensity for misfolding (Prudencio and Borchelt, 2011), we sought to assess Lys123 acetylation in several mutants associated with ALS.

In order to examine the baseline Lys123 acetylation of SOD1 in human cells, we transfected Expi293F cells with expression plasmids for wild type SOD1, the A4V, H46R, G37R, and G85R ALS-linked SOD1 mutants, and an empty pcDNA vector as a transfection control. Based on our previous results demonstrating an overall low level of Lys123 acetylation in SOD1 WT, we used our custom antibody to immunoprecipitate Ac-K123 SOD1 from the lysates of transfected cells. Immune complexes were then isolated by magnetic beads, washed, eluted, and resolved by SDS-PAGE. Immunoblotting using a SOD1 antibody revealed that the SOD1 mutants were more prone to Lys123 acetylation when compared to the wild type protein (Figure 31). Western blot analysis of total SOD1 within the input lysates confirmed that the increased acetylation level observed in the SOD1 mutants was not due to increased expression levels (Figure 31).

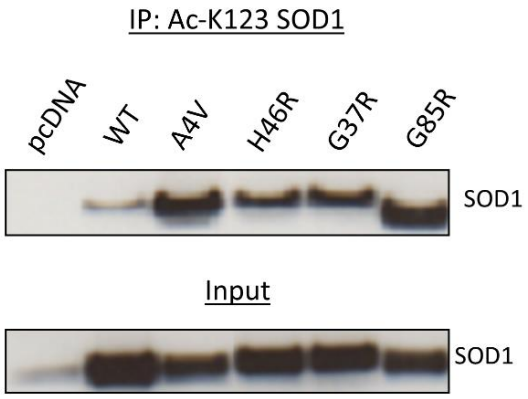

Figure 31. ALS-linked SOD1 mutants demonstrate increased K123 acetylation.

Lysates from transfected Expi293 cells were analyzed by IP-western blot with the indicated antibodies. Total SOD1 from the input control was analyzed by western bot. Experimental data from B. Bossy and S. Blaes, figure preparation by M. Kaliszewski.

4.3.2 Lys123 acetylation promotes mutant SOD1 misfolding

Once we discovered that ALS-linked SOD1 mutants are more likely to be acetylated at Lys123, we wished to explore how this modification impacts SOD1 misfolding. For this analysis we focused on the SOD1 A4V mutant, the most common mutation in North America and one associated with rapidly progressing disease and a very high propensity to aggregate (Prudencio et al., 2009b).

To examine if misfolded SOD1 is acetylated at Lys123, we transfected Expi1293 cells with vectors for mammalian expression of wild type SOD1, mutant SOD1 A4V, or empty pCDNA as a transfection control. We then performed immunoprecipitation of the lysate using the conformation-specific C4F6 monoclonal antibody raised against misfolded SOD1. Our western-IP results confirm that misfolded mutant SOD1 is Lys123 acetylated (Figure 32A). Next, we

looked into how Lys123 acetylation impacts the misfolding of mutant SOD1. Based on our previous findings demonstrating that α-TAT1 is responsible for K123 acetylation in SOD1 WT (Figures 27-29), we compared SOD1 misfolding in transfected cells expressing either SOD1 A4V alone or in combination with α-TAT1. Interestingly, we found that α-TAT1 overexpression promotes mutant SOD1 misfolding (Figure 32B). The experiment was repeated with the exception that α-TAT1 was replaced by HDAC6, the deacetylase we previously showed is responsible for Ac-K123 SOD1 deacetylation (Figures 23-26). In accordance with the α-TAT1 results, we found that HDAC6 overexpression decreases mutant SOD1 misfolding (Figure 32C).

Figure 32. Lys123 acetylation promotes mutant SOD1 misfolding.

A. Immunopreciptation of transfected Expi293 cells using misfolded SOD1 C4F6 antibody for pulldown and Ac-K123 SOD1 antibody for western blot. Cells were transfected with empty pcDNA vector or expression plasmids for SOD1 WT or mutant SOD1 A4V. B. Immunopreciptation of transfected Expi293 cells using misfolded SOD1 C4F6 antibody for pulldown and SOD1 antibody for western blot. Cells were transfected with mutant SOD1 A4V expression plasmid alone or in combination with α-TAT1-GFP. C. Immunopreciptation of transfected Expi293 cells using misfolded SOD1 C4F6 antibody for pulldown and SOD1 antibody for western blot. Cells were transfected with mutant SOD1 A4V expression plasmid alone or in combination with HDAC6. Experimental data from B. Bossy. Figure preparation by M. Kaliszewski.

4.3.3 Ciliary Ac-K123 SOD1 is misfolded

Based on the association of Lys123 acetylation with both SOD1 misfolding and ciliary localization, we next investigated whether misfolded SOD1 can be detected within primary cilia. For this analysis primary spinal astrocytes were fixed and immunostained with antibodies against Ac-K123 SOD1 and misfolded SOD1. Interestingly, we found that Ac-K123 SOD1 and misfolded SOD1 are co-localized within the primary cilia of astrocytes (Figure 33).

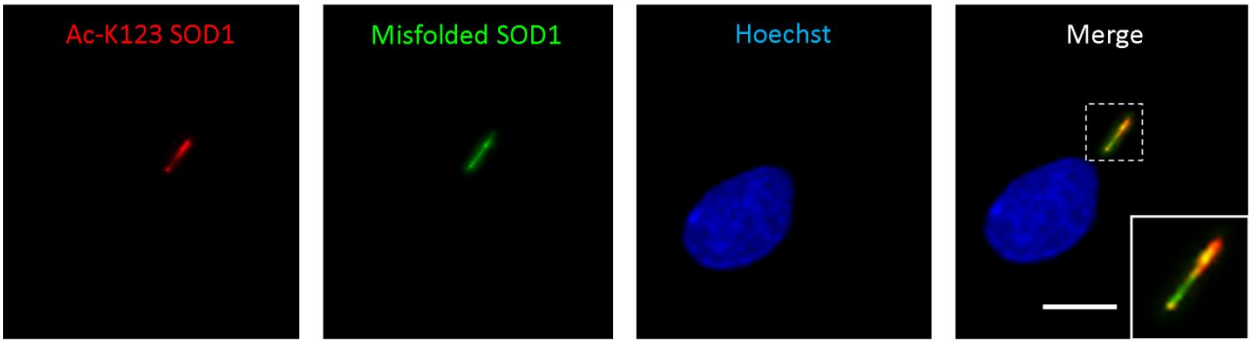

Figure 33. Ac-K123 SOD1 and misfolded SOD1 co-localize of within the primary cilium.

Confocal micrograph (scale bar, 10 µm) of a primary astrocyte immunostained with antibodies against Ac-K123 SOD1 and misfolded SOD1. Inset shows a 3x zoom of the boxed region demonstrating co-localization of Ac-K123 SOD1 and misfolded SOD1 within the primary cilium. Immunostaining and confocal microscopy by A. Kennedy, figure preparation by M. Kaliszewski.

4.3.4 Mutant SOD1 promotes primary cilia secretion

We next investigated how the expression of misfolded mutant SOD1 would affect primary cilia structure. Primary spinal astrocytes were transfected with expression plasmids for fluorescent protein-tagged markers of primary cilia (pEGFPN3-SSTR3 was a gift from Dr. Kirk Mykytyn, Ohio State University College of Medicine), centrioles (dsRed-cent2 was a gift from Joseph Gleeson,

Rockefeller University) and the nucleus (pECFP-N1-H2B was a gift from Wei Jiang, Burnham Institute) in combination with either untagged SOD1 WT or SOD1 A4V.

The results obtained from quantification of fixed astrocytes showed a significant increase in the ciliary budding of SOD1 A4V transfected astrocytes (Figure 34B). However, one can argue that a drawback of this analysis is the use of static representations of cells to assess a dynamic process. Membrane budding and vesicle release is a gradual process, and in order to identify ciliary budding the cells and primary cilia must be fixed during the actual process (or at the exact moment of vesicle release). Once vesicles are released into the extracellular environment they will diffuse away from the cilia and not be captured during fixation, becoming lost in subsequent washes during the immunostaining procedure. As a result, by limiting our analysis to one time point (the time of cell fixation) we may not be getting a true representation of how mutant SOD1 impacts primary cilia. This limitation may in fact undervalue the true increase of ciliary budding in SOD1 A4V astrocytes. In addition, it can be argued that what was observed to be ciliary budding was in fact an artifact of fixation. For these important reasons, we sought to confirm that our findings from fixed cells were representative of ciliary membrane budding by demonstrating the process of primary cilia-derived vesicle release *in vivo*.

In order to capture the process of secretion from primary cilia in living cells, we utilized time-lapse fluorescent microscopy with primary spinal astrocytes that were transfected with and expression plasmid for SOD1 A4V. In addition, the membranes of primary cilia were labeled by co-transfection with a plasmid encoding GFP-tagged somatostatin receptor 3 (SSTR3-

EGFP). The acquired micrographs were processed and used for creating time-lapse movies of labeled primary cilia. These resulting movies demonstrate that primary cilia undergo membrane budding and vesicle release. A representative time-lapse sequences of a SSTR3-EGFP labeled primary cilium from an astrocyte expressing SOD1 A4V shows the key steps of this process (Figure 34C). It begins with formation of a bulb-like “bouton”, followed by subapical membrane constriction, membrane abscission, and vesicle release into the surrounding environment.

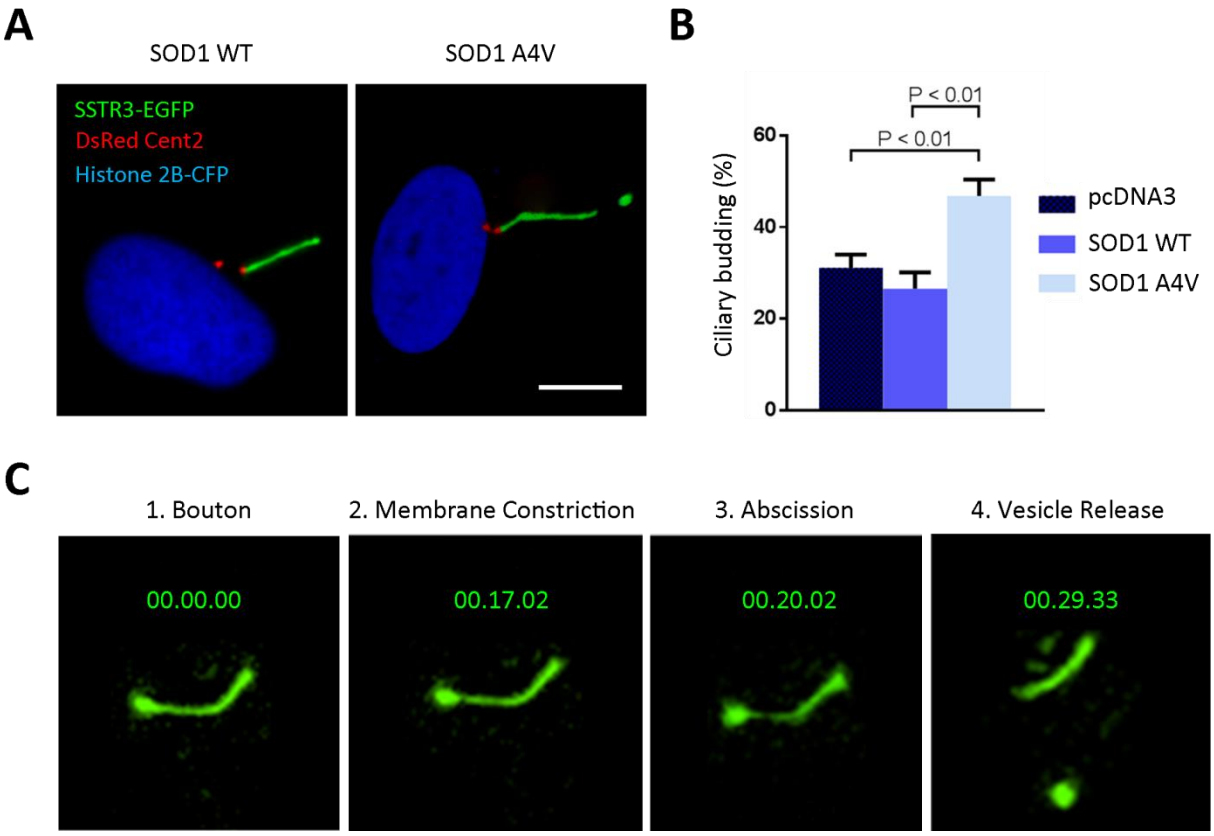

Figure 34. Mutant SOD1 promotes the release of ciliary vesicles from astrocytes.

A. Fluorescent micrograph (scale bar, 10 µm) of astrocytes transfected with expression vectors for SSTR3-EGFP, DsRed Cent2, and Histone 2B-CFP in combination with either SOD1 WT or SOD1 A4V. B. Quantification of ciliary budding in fixed astrocytes transfected with expression plasmids for SOD1 WT, SOD1 A4V, or pcDNA3 empty vector control. Data is shown with standard error of the mean error bars from three independent experiments (significance at $P<0.01$ by ANOVA). C. Time-lapse sequence of a primary cilium (identified with SSTR3-GFP) of an SOD1 A4V expressing astrocyte undergoing the distinct stages of bouton formation, membrane constriction, abscission, and vesicle release. Fluorescent microscopy and time-lapse imaging by A. Kennedy, quantification by A. Kennedy and K. Kleinschmidt, and figure preparation by M. Kaliszewski.

4.3.5 Ac-K123 SOD1 is found in primary cilia derived vesicles

After demonstrating that mutant SOD1 expression in astrocytes increased the secretion of vesicles from primary cilia, we next looked to investigate the contents of these vesicles. Based

on our astrocyte immunostaining data that demonstrates the SOD1 localized to the primary cilium is both Lys123 acetylated and misfolded, we were curious to see if Ac-K123 SOD1 can be found within primary cilia-derived vesicles. Having already shown that Lys123 acetylation promoted SOD1 misfolding, if Ac-K123 SOD1 is in fact secreted within these vesicles then primary cilia may represent a novel source for the cellular release of misfolded SOD1. And based on reports describing the fusion and reuptake of ciliary vesicles at distant cells, the primary cilia may represent a previously unknown conduit for the transfer of misfolded SOD1 between cells.

In order to assess whether Ac-K123 SOD1 can be found within budding ciliary vesicles, we first transfected primary astrocytes with expression plasmids for fluorescently-tagged markers of nucleus and primary cilia. After 3 days cells were fixed and immunostained for Ac-K123 SOD1. Our results show that Ac-K123 SOD1 is found within primary cilia undergoing membrane budding and vesicle release (Figure 35A).

To demonstrate that Ac-K123 SOD1 is localized within actual secreted vesicles, we analyzed the contents vesicles isolated from the conditioned medium of astrocytes transfected with the SSTR3-EGFP marker in combination with either SOD1 WT or SOD1 A4V. Western blot analysis showed that both Ac-K123 SOD1 and GFP, the fluorescent tag fused to the ciliary membrane protein SSTR3, are present within the isolated vesicles (Figure 35B). In addition, the detection of Ac-K123 SOD1 detection was higher in vesicles isolated from the conditioned medium of SOD1 A4V transfected astrocytes (Figure 35B). This hints at a defensive mechanism for the removal of

misfolded SOD1 from the primary cilia, possibly as a preventive measure to safeguard microtubule-dependent ciliary function from mutant SOD1-mediated impairment. Taken together, these findings demonstrate that Ac-K123 SOD1 is both localized to primary cilia undergoing membrane budding and is found within secreted vesicles derived from the ciliary membrane.

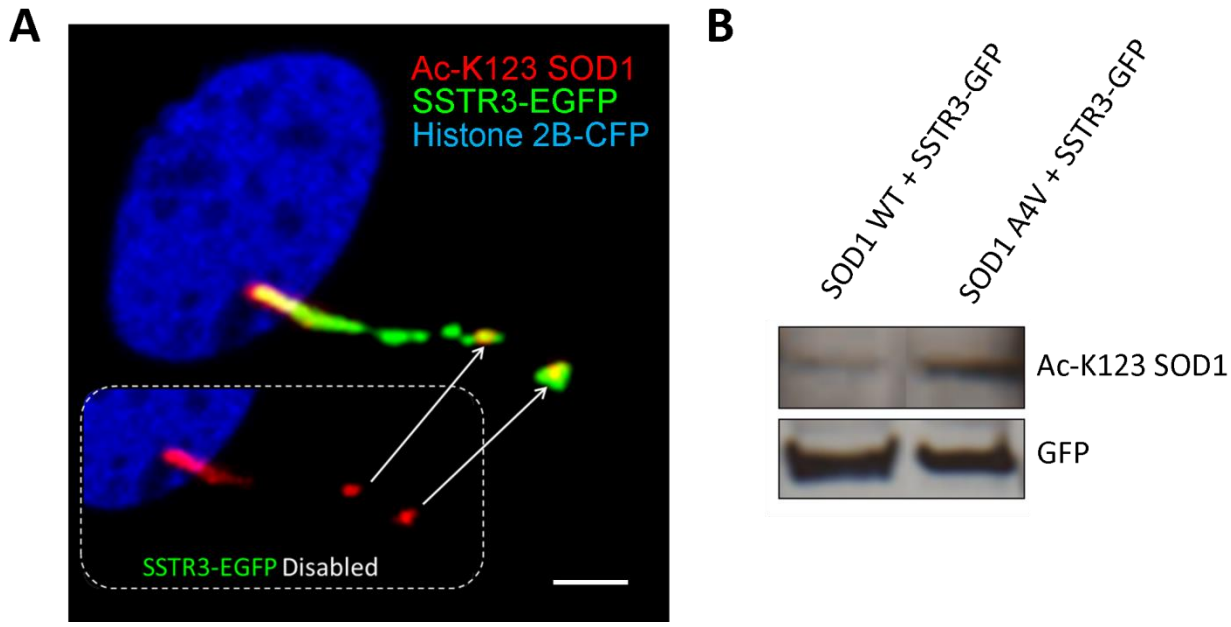

Figure 35. Ac-K123 SOD1 is found in primary cilia derived vesicles.

A. Fluorescent micrograph (scale bar, 2 µm) of a SSTR3-EGFP and histone 2B-CFP transfected primary astrocyte immunostained for Ac-K123 SOD1. Inset shows region of the primary cilium with the SSTR3-GFP channel disabled. Imaging performed by A. Kennedy. B. Western blot of vesicles isolated from astrocyte conditioned medium and probed for Ac-K123 SOD1 and GFP (tag for SSTR3). Western blot analysis by R. Shaffer.

4.3.6 Ac-K123 SOD1 in choroid plexus and ependymal cells of ventricle and central canal

A hallmark feature of ALS is the focality of clinical onset and regional spreading of symptoms. A popular theory explaining the spreading of ALS along the motor nervous system involves the prion-like propagation of misfolded SOD1, although the exact mechanism of misfolded SOD1 cell-to-cell transfer is not fully understood. Interestingly, SOD1 has been detected in human cerebral spinal fluid (CSF) samples (Winer L et al., 2013). A recent hypothesis suggests that the CSF might be involved in the regional spreading of ALS (Smith et al., 2015). Thus, we sought to explore whether Ac-K123 SOD1 was present in regions of the brain in contact with CSF.

Our findings show that Ac-K123 SOD1 was found within the choroid plexus and in ependymal cells lining the ventricles (section 2.3.5, Figure 8)**.** Interestingly, Ac-K123 SOD1 was localized within motile cilia of ependymal cells, as demonstrated by co-labeling of these structures for Ac-K123 SOD1 and the ciliary marker Ac-K40 α-Tubulin (Figure 36A). Because the 4th ventricle narrows caudally to eventually empty into the spinal cord, we next analyzed immunostained transverse spinal cord cryosections to assess Ac-K123 SOD1 distribution. Weak staining was noted in cell bodies throughout the white and gray matter, but the most prominent staining was observed in ependymal cells lining the central canal (Figure 36B), the CSF-filled space that is continuous with the ventricular system of the brain.

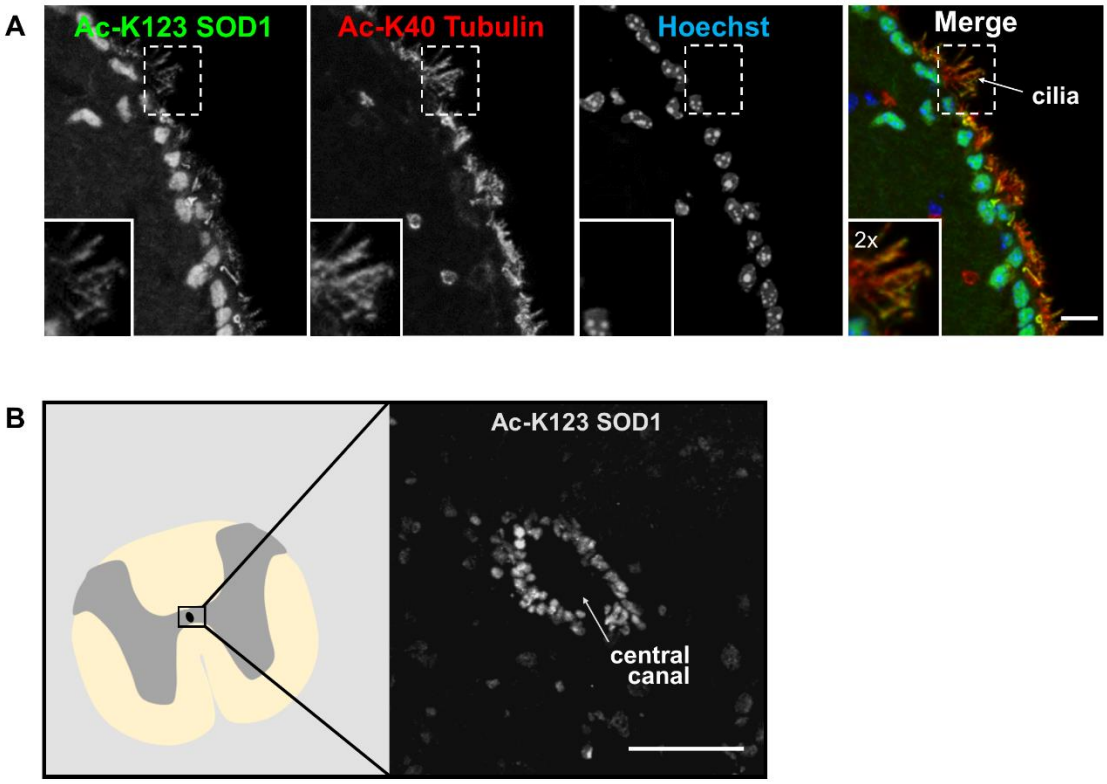

Figure 36. Ac-K123 SOD1 localization in choroid plexus and ependymal cells.

A. Sagittal view confocal micrograph (scale bar, 10 µm) of 4th ventricle wall immunostained for Ac-K123 SOD1 (R26) and Ac-K40 α-Tubulin. Nuclei were counterstained with Hoechst 33342. Cilia of the ependymal cells are labeled (arrow). Inset shows a 2x zoom of the boxed region demonstrating Ac-K123 SOD1 and Ac-K40 α-Tubulin co-labeling within the cilia. Tissue embedding and cryosectioning by S. Blaes. B. Confocal micrograph (scale bar, 50 µm) of a transverse section of spinal cord immunostained for Ac-K123 SOD1 (R26). On the left is a schematic of a transverse spinal cord section demonstrating the location of the central canal.

4.3.7 Acetyl mimetic SOD1 K123Q impairs axonal transport

Several previous studies have demonstrated defective axonal trafficking in ALS mouse models, stemming from the interaction between mutant SOD1 and motor proteins (De Vos et al., 2007; Warita et al., 1999; Williamson and Cleveland, 1999). Based on our observations that Ac-K123 SOD1 misfolds (similar to mutant SOD1) and is localized along axonal processes, we next

investigated if SOD1 acetylation impacts axonal transport in neurons. Primary cortical neurons were transfected with DsRed2-Mito, a mammalian expression vector that encodes red fluorescent protein fused to a mitochondrial targeting sequence, in combination with expression vectors for SOD1 WT, SOD1 K123R, or SOD1 K123Q. DsRed2-Mito was used for fluorescent labeling of mitochondria and allowed us to observe axonal transport of mitochondria in living cells. Fast acquisition fluorescence time-lapse imaging was used to measure mitochondrial movement over a period of 5 minutes.

Representative kymographs of cortical neurons expressing either SOD1 WT or SOD1 K123R show both vertical and horizontal lines, indicating mitochondria mobility and movement in both the anterograde and retrograde directions (Figure 37A, top and middle panels). By contrast, a kymograph for neurons expressing SOD1 K123Q displayed mostly vertical lines, indicating minimal movement of mitochondria and reduced axonal transport (Figure 37A, bottom panel). Quantitative analysis indicated a significant reduction in the velocity of mitochondrial transport in SOD1 K123Q neurons when compared to SOD1 WT and SOD1 K123R neurons (Figure 37B). Moreover, the mitochondrial mobility of SOD1 K123Q neurons was decreased by more than 80% (Figure 37C). These results demonstrate that SOD1 Lys123 acetylation, represented by acetyl-mimetic SOD1 K123Q, triggers mitochondrial axonal transport defects in cultured neurons.

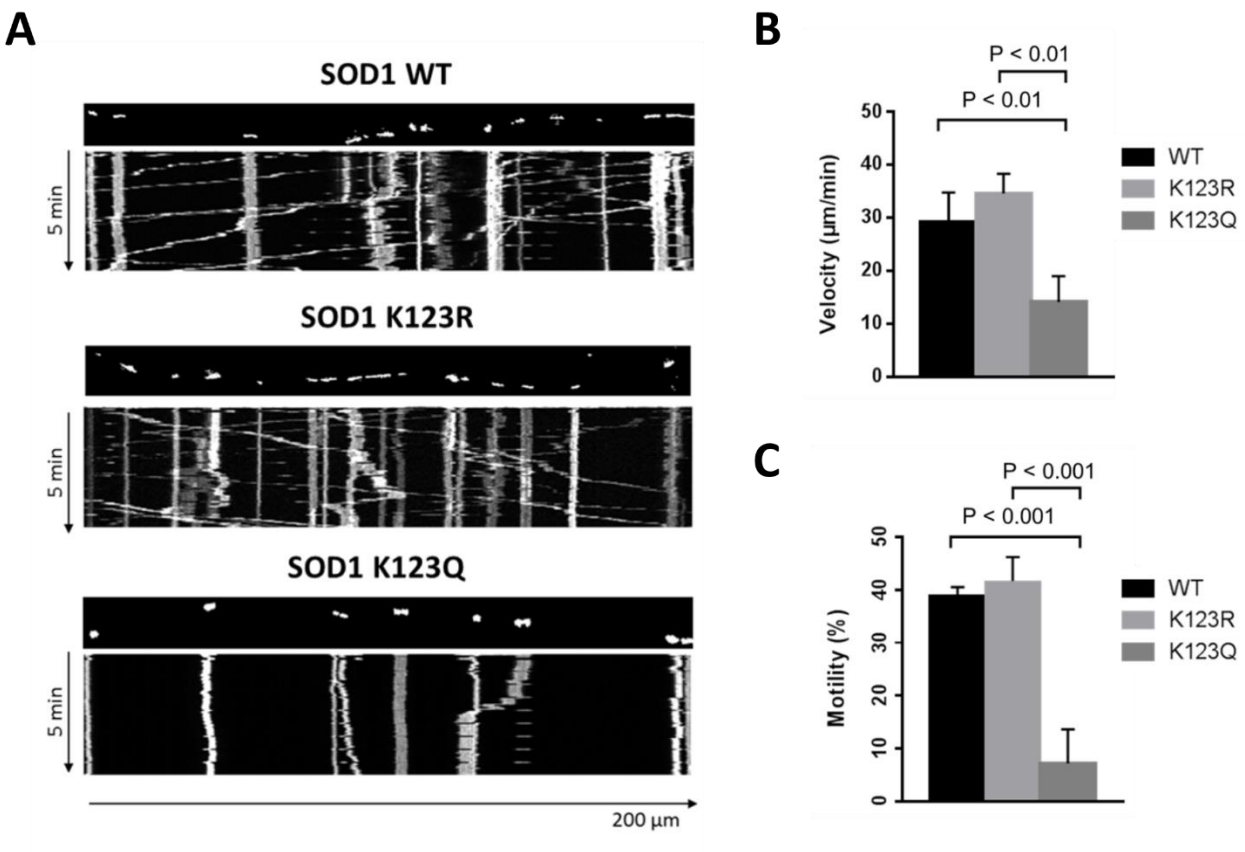

Figure 37. Lys123 acetylated SOD1 impairs axonal transport of mitochondria in cortical neurons.

A. Kymographs of cortical neurons expressing DsRed2-Mito and either SOD1 WT, SOD1 K123R, or SOD1K123Q. B. Mean velocity of mitochondria in the axons of cortical neurons expressing DsRed2-Mito and either SOD1 WT, SOD1 K123R, or SOD1K123Q. D) Mitochondrial mobility in cortical neurons expressing DsRed2-Mito and either SOD1 WT, SOD1 K123R, or SOD1K123Q. *P* value: ANOVA, n = 10. Live cell imaging by A. Kennedy. Kymographs processing, quantification, and analysis by M. Kaliszewski.

4.3.8 K123R mutation rescues SOD1 A4V from axonal transport defects

Based on our finding showing that SOD1 WT acetylation impaired axonal transport, we sought to test whether blocking Lys123 acetylation could rescue mutant SOD1-induced trafficking defects. To test this hypothesis we created mutant SOD1 Lys123 deacetylated and acetyl-

mimetics by cloning K123R and K123Q mutations into an expression vector for SOD1 A4V. We then co-transfected cortical neurons with SOD1 A4V, SOD1 A4V/K123R or SOD1 A4V/K123Q in combination with DsRed2-Mito. Neurons expressing the constitutively acetylated mutant SOD1 A4V/K123Q exhibited mitochondrial transport defects typical for mutant SOD1 A4V (Figure 38A, top and middle panels). Remarkably, mitochondrial transport was restored in the acetylation resistant SOD1 A4V/K123R neurons (Figure 38A, bottom panel). In addition, mitochondrial velocity and motility were rescued in neurons expressing the SOD1 A4V/K123R mutant (Figure 38B-C). This data collectively shows that mitochondrial transport, mean velocity, and overall mobility are regained by inhibiting Lys123 acetylation of mutant SOD1. Therefore, Lys123 acetylation explain the axonal transport defects observed in mutant SOD1 neurons.

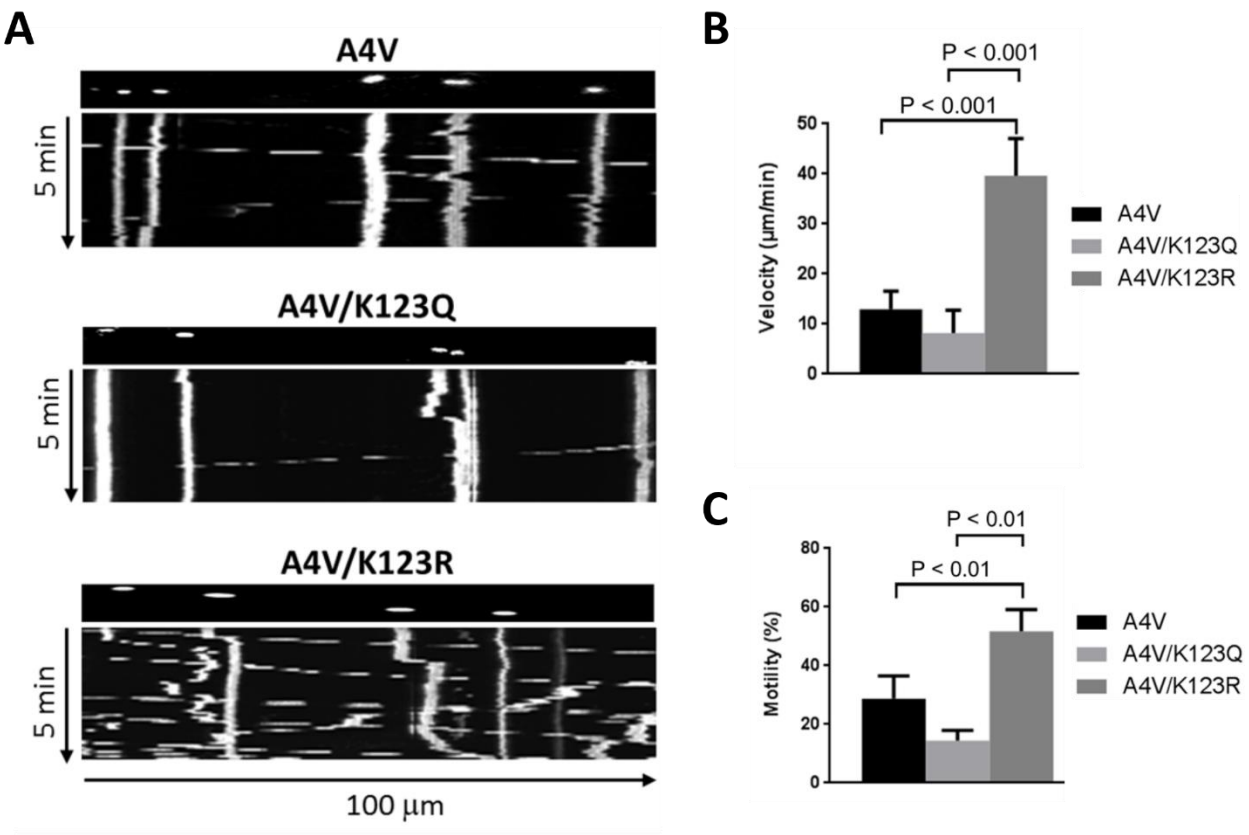

Figure 38. Mutant SOD1 Lys123 deacetylation rescues neurons from mitochondrial trafficking defects.

A. Kymographs of cortical neurons expressing DsRed2-Mito and either SOD1 A4V, SOD1 A4V/K123Q, or SOD1 A4V/K123R. B. Mean velocity of mitochondria in the axons of cortical neurons expressing DsRed2-Mito and either SOD1 A4V, SOD1 A4V/K123Q, or SOD1 A4V/K123R. D) Mitochondrial mobility in cortical neurons expressing DsRed2-Mito and either SOD1 A4V, SOD1 A4V/K123Q, or SOD1 A4V/K123R. *P* value: ANOVA, n = 10. Live cell imaging by A. Kennedy. Kymographs processing, quantification, and analysis by M. Kaliszewski.

4.4 Discussion

Mutations of the SOD1 gene are toxic to motor neurons and represent the first identified genetic component linked to the subset of rare inherited ALS cases (Rosen et al., 1993). Since

the identification of the first mutation in 1993, more than 180 mutations have been described in *SOD1.* Murine models based on mutant SOD1 expression develop ALS-like disease and have provided many mechanistic details with regards to mutant SOD1-mediated toxicity. Samples from patients with *SOD1* mutations and mutant SOD1 mice exhibit cytoplasmic inclusions containing SOD1 (Kato, 2007), indicating a role for SOD1 misfolding in ALS. Clinically, both SALS and FALS are very similar, suggesting a common downstream pathogenic mechanism. Recent evidence reports that SOD1 modification is implicated in the sporadic form of the disease (Bosco et al., 2010). For these reasons we investigated the impact of SOD1 acetylation at Lys123. This residue has been previously reported to be modified by acetylation (Choudhary et al., 2009; Zhao et al., 2010), and is located within the electrostatic loop, an important functional domain responsible for substrate recruitment to the active site. This investigation also expanded on our previous findings describing the regulation of SOD1 Lys123 acetylation by HDAC6 and α-TAT1 and the localization of Ac-K123 SOD1 to the primary cilium.

We showed that many ALS-linked SOD1 mutants exhibit increased Lys123 acetylation (Section 4.3.1, figure 31), and explored the impact that this modification may have with regards to ALS pathogenesis. Because the gain-of-function toxicity associated with mutant SOD1 often stems from conformational changes and misfolding, we assessed the relationship between Lys123 acetylation and misfolding. Interestingly, we found that Lys123 acetylation increased mutant SOD1 misfolding in a HDAC6 and α-TAT1-dependent manner. This is the first evidence showing acetylation promote SOD1 misfolding, and it is supported by findings that have demonstrated aberrant conformations of wild type SOD1 resulting from by oxidation, metal loss, and other

altered post-translational modifications (Bosco et al., 2010; Ezzi et al., 2007; Guareschi et al., 2012). It is important to note that we also showed α-TAT1 and HDAC directly interact with SOD1 and modify Lys123 through acetylation and deacetylation. However, it is possible that the altered detection of misfolded SOD1 is a result of secondary events not related to these proteins directly interacting with SOD1. For instance, in addition to being a deacetylase HDAC6 also possesses an ubiquitin-binding domain and is responsible for the disposal of misfolded protein aggregates (Kawaguchi et al., 2003). It is therefore possible that although we have shown HDAC6 deacetylates SOD1, the decline in misfolded SOD1 accompanying HDAC6 expression is simply a result of clearance via the lysosome-dependent degradative system. In this regard, contrary reports have been published concerning the role of HDAC6 in ALS pathogenesis. For example, in a cellular model study using live cell imaging and cellulose acetate membrane filtration HDAC6 knockdown was shown to increase mutant SOD1 aggregation (Gal et al., 2013), while in an animal model study *Hdac6* deletion was found to significantly extend the survival of SOD1 G93A mice (Taes et al., 2013). Based on the controversial role of HDAC6 in ALS, further studies examining the Lys123 acetylation and SOD1 misfolding is required. One such experimental modification would be to compare the detection of misfolded SOD1 in astrocytes when mutant SOD1 is expressed in combination with either wild type HDAC6, an HDAC6 mutant with a deleted ubiquitin-binding domain, or an HDAC6 mutant with deleted deacetylase domains. Results from such a study may guide us to a better understanding of the relationship between HDAC6, Lys123 acetylation, and SOD1 misfolding.

In addition to an expanded inquiry of HDAC6-mediated Lys123 deacetylation and SOD1 misfolding, a more in-depth analysis of the structural changes associated with Lys123 acetylation can also provide more insight into how this modification promotes misfolding of SOD1. The location of Lys123 within the electrostatic loop is of significance, as structural change and perturbation of the electrostatic loop are a common property of several FALS-associated SOD1 variants (Molnar et al., 2009). When this is considered in the context of Lys123 acetylation and SOD1 misfolding, there is an important question of causation versus correlation. Does Lys123 acetylation promote the conformational changes that alter electrostatic loop structure and lead to misfolding, or are SOD1 mutants simply more prone to acetylation due to an increased Lys123 accessibility to acetyl-transferases resulting from increased electrostatic loop dynamics? A spectroscopic structural analysis, such as circular dichroism, of SOD1 Lys123 acetylated mimetics and constitutively deacetylated mimetics may shed light on how acetylation affects SOD1 deacetylation and should be examined in in both wild type and ALS-linked mutant proteins. Based on previous studies that indicate electrostatic loop structural changes lead to intermolecular interactions and fibril formation, results from CD analysis of SOD1 Lys123 acetylation may provide a mechanism for SOD1 aggregation (Elam et al., 2003).

Based on our findings showing increased Lys123 acetylation in several ALS-linked SOD1 mutants (Section 4.3.1, figure 31), we explored how mutant SOD1 Lys123 acetylation impacts microtubule-based transport. Previous studies from our lab and other groups report axonal transport defects resulting from mutant SOD1 expression in neurons (De Vos et al., 2007; Song

et al., 2013; Warita et al., 1999; Williamson and Cleveland, 1999), and in this study we demonstrated that removal of Lys123 acetylation abolished the transport defects associated with mutant SOD1. It remains to be determined how mutant SOD1 Lys123 acetylation mechanistically impacts axonal transport. A common effect of protein acetylation is altered protein-protein interactions, and it is possible that Lys123 acetylation promotes mutant SOD1 interaction with the microtubule motor protein complex.

Another key finding was the localization of both misfolded and Lys123 acetylated SOD1 within the primary cilium. Previous studies have shown a decreased primary cilia number in G93A mice spinal cord primary culture and in situ (Ma et al., 2011), and mutant SOD1 overexpression was shown to decrease primary cilia-mediated Shh pathway signaling and render cells more susceptible to oxidative stress (Peterson and Turnbull, 2011). Treatment with Shh or Shh agonists proved to be cytoprotective to mutant SOD1 cells, further suggesting that defective primary cilia-mediated signaling may play a role in ALS. Based on these findings and the fact that primary cilia signaling is dependent on transport along the axoneme (Liem et al., 2012), we explored how mutant SOD1 Lys123 acetylation impacts microtubule-based transport. Previous studies from our lab and other groups reported axonal transport defects resulting from mutant SOD1 expression in neurons, and in this study we demonstrated that removal of Lys123 acetylation abolished the transport defects associated with mutant SOD1. When considered in the context of decreased Shh signaling mediated by mutant SOD1, the direct impact of mutant SOD1 Lys123 acetylation on primary cilia signaling merits further consideration. For these reasons, a study on the impact of SOD1 Lys123 acetylation on the function of microtubule-

based primary cilia is merited and has the potential to elucidate the mechanism behind the Shh signaling impairment observed in ALS models. Because the downstream effect of Shh signaling transduction is the activation of Gli transcription factors (Briscoe and Thérond, 2013), a simple study employing a Gli reporter assay (many Luciferase-based kits are commercially available) and astrocytes expressing either wild type SOD1, ALS-linked mutants, or the Lys123 acetylated and deacetylated mimetics of wild type and mutant SOD1 can be performed. These results can subsequently identify any disruptions to Shh signaling due to SOD1 Lys123 acetylation.

Furthermore, we have shown that expression of the acetyl-mimetic SOD1 K123Q impaired axonal transport in cortical neurons. These findings demonstrate that Lys123 acetylation of wild type SOD1 causes mutant SOD1-like microtubule-based transport impairments, providing a possible molecular mechanism that underlies both rare FALS and the more common SALS.

We also demonstrated that mutant SOD1 expression causes aberrant primary cilia morphology and promotes secretion of ciliary vesicles containing Ac-K123 SOD1. Considering that ALS is characterized by prion-like spreading of toxic misfolded proteins, our data indicate primary cilia-derived vesicles as a possible conduit for the intercellular transfer of misfolded SOD1 and further study is of high importance.

CHAPTER FIVE: DISCUSSION

The aim of this study was to examine SOD1 Lys123 acetylation within the central nervous system (on a regional, cellular level and eventually subcellular level) and determine if this modification has any implication in disease. In the course of this work, affinity-purified rabbit polyclonal antibodies were generated and validated as specific against Lys123 acetylated SOD1. The acetylated synthetic peptides used for immunization were based on the documented SOD1 acetylation site at Lys123 identified through mass spectrometry during previous high-throughput proteomic studies.

We used immunohistochemistry to assess Ac-K123 SOD1 distribution in the normal nervous system. Ac-K123 SOD1 was detected within distinct regions and cell types, and one commonality of the observed immunostaining was the prominent labeling in glutamatergic neurons within the cerebellar cortex, dentate gyrus, hippocampus, olfactory bulb, and retina. In the ventricular system, choroid plexus cuboidal cells and ependymal cells of the ventricle wall and spinal cord central canal also exhibited strong staining. This initial study demonstrated that SOD1 acetylation is confined to specific regions and cells, especially when considering that SOD1 is so abundant and ubiquitously expressed throughout the central nervous system(Pardo et al., 1995). However, in order to appreciate the relevance of these immunohistochemical findings it is pertinent to follow up this study with an examination of Ac-K123 SOD1 distribution in the nervous system of mouse models for disease or aging. It would be especially valuable to determine if there is any alteration in Ac-K123 SOD1 levels within the motor cortex, bulbar

region, or spinal cord of mutant SOD1 mice. Aside from the central canal of the spinal there was not significant labeling in these areas, so it would be interesting to see if Ac-K123 SOD1 is increased in mutant SOD1 mice.

Ac-K123 SOD1 antibody immunostaining of primary astrocyte and neuronal cultures demonstrated a distinct subcellular localization of SOD1 Lys123 acetylation. In contrast to the predominantly cytoplasmic localization of SOD1, Ac-K123 SOD1 was found within neuronal nuclei and neurites and in nuclei and primary cilia of astrocytes. The localization of Ac-K123 SOD1 within astrocytes was also cell cycle dependent, with nuclear localization strongest during G1 and G2 phases of interphase and weakest during cell cycle arrest. SOD1 has been shown to translocate to the nucleus and act as a transcription factor during cellular exposure to oxidative stress, but this function does not explain the nuclear localization of Ac-K123 SOD1 during G1 and G2. Further studies will be also required to elucidate the role of Lys123 acetylation with regards to SOD1 translocation and retention within the nucleus and primary cilia of astrocytes. The association of Ac-K123 SOD1 with chromosomes during metaphase and anaphase was also an interesting find, as diffusion into the rest of the cell would be expected after the break of the nuclear envelope. It is possible that acetylation supports directly maintains SOD1 interaction with chromosomes in order to allow close proximity and defense against DNA oxidative damage. There is also the possibility that extended nuclear localization of SOD1 can be detrimental to the genomic integrity of the cell. K123 acetylation may promote perturbation of the electrostatic loop, allowing non-specific substrates to enter the active site. This can result in

aberrant copper redox chemistry, and in the cellular environment this may cause reverse catalysis with the production of superoxide.

The localization within the primary cilium was an exciting discovery that was further explored. Using a candidate approach based on ciliary localization, we tested and confirmed that HDAC6 deacetylases Ac-K123 SOD1 and α-TAT1 acetylates SOD1 at Lys123. It should be noted that although we were able to provide evidence of the enzymes modifying Lys123 acetylation, we cannot exclude the possibility there are other regulators of SOD1 acetylation. Based on the reported implications of wild type SOD1 modification promoting misfolding, we investigated the relationship between SOD1 misfolding and Lys123 acetylation. We found that ALS-linked SOD1 mutants exhibit increased Lys123 acetylation and this misfolding was responsive to increased expression of HDAC6 or α-TAT1. In addition to acetylation, SOD1 Lys123 is also subject to other modifications such as ubiquitination (Wagner et al., 2011; Wu et al., 2015). In this regard, K123 acetylation may compete with ubiquitination and act as a means of delaying protein degradation. The increased K123 acetylation of ALS-linked mutants may prevent their degradation, thereby increasing their half-life. If this is the case, further studies into the impact of K123 acetylation on SOD1 stability and resistance to degradation is highly warranted.

Interestingly, we also found that SOD1 within the primary cilium is both Lys123 acetylated and misfolded through co-immunostaining with a conformation specific antibody against misfolded SOD1. The localization of misfolded SOD1 within the primary cilia was unexpected, and it is yet to be determined if this compartmentalization of misfolded SOD1 serves a physiologic role for

the cell. It is possible that this is a protective mechanism to isolate misfolded SOD1 from the rest of the cell. Interestingly, in addition to their role of signaling to the cell body, primary cilia are also secretory organelles that communicate with other cells. Due to the localization of misfolded SOD1, the primary cilia may represent a source of SOD1 aggregation seeds that can undergo intercellular transfer via ciliary membrane-bound vesicles. Importantly, mutant SOD1 expression increased primary cilia membrane budding in astrocytes and the detection of Ac-K123 SOD1 isolated from vesicles in conditioned medium. Based on these findings we have developed a model implicating Lys123 acetylation in the prion-like transfer of misfolded SOD1 (Figure 39). This model is also supported by the non-cell autonomous nature of ALS, as we speculate that ciliary-derived vesicles from astrocytes are the conduit for transferring Lys123 acetylated and misfolded SOD1 to motor neurons. Based on our findings in cortical neurons, we predict that acetylated SOD1 will also impair axonal transport within motor neurons.

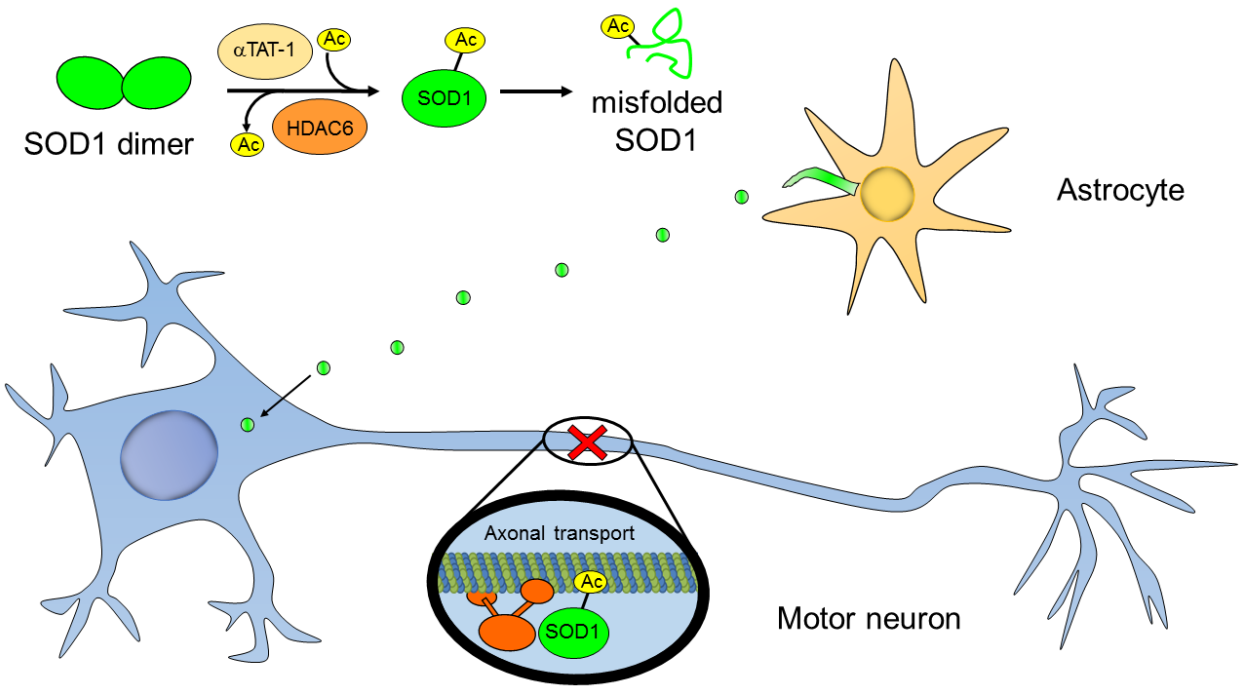

Figure 39. Current model for promotion of SOD1 misfolding and cell-to-cell transfer by K123 acetylation.

SOD1 Lys123 acetylation by α-TAT1 promotes monomerization and subsequent protein misfolding. Ac-K123 SOD1 localization has been observed within primary cilia of astrocytes and primary cilia-derived vesicles. These vesicles containing Ac-K123 SOD1 can be taken up by neurons. Within neurons, Ac-K123 SOD1 impairs axonal transport in a fashion similar to misfolded mutant SOD1.

Although we have described the relationship SOD1 Lys123 acetylation and misfolding, additional evidence beyond that derived from the use of a conformation-specific antibody will be needed. Data from structural studies, such as circular dichroism, and analysis of human samples (healthy versus ALS) with Ac-K123 SOD1 antibody will aid in supporting the notion that Lys123 acetylation promotes SOD1 misfolding. The other components of prion-like transfer that need to be addressed are the ability of Ac-K123 SOD1 to seed misfolding and aggregation

of natively folded SOD1, and confirmation that Ac-K123 SOD1 within primary cilia-derived vesicles is misfolded and taken up by neighboring cells.

Interestingly, results from a recent whole-exome screening study reported that variants of NEK1, a protein linked to microtubule stability and cilia formation, confers susceptibility to amyotrophic lateral sclerosis (Kenna et al., 2016). This data further supports a possible role for primary cilia in ALS pathogenesis, and it will be of interest to investigate how Lys123 acetylation impacts SOD1 interaction with NEK1.

This work examines the impact of Lys123 acetylation on SOD1 structure and localization, with the hope that a better understanding of these relationships will help to further elucidate the etiology of familial and sporadic ALS. This study also lays the groundwork for future studies investigating the intercellular transfer of misfolded SOD1 via primary cilia-derived vesicles. The antibodies developed during the course of this work have the potential to provide valuable tools for evaluating disease progression by assessing aberrant SOD1 acetylation through immunohistochemical analysis of tissue from animal models or post-mortem samples. Acetylated SOD1 also has the potential to be utilized as a biomarker ALS, possibly through detection within patient CSF samples.

APPENDIX: PERMISSION FOR REPRINT

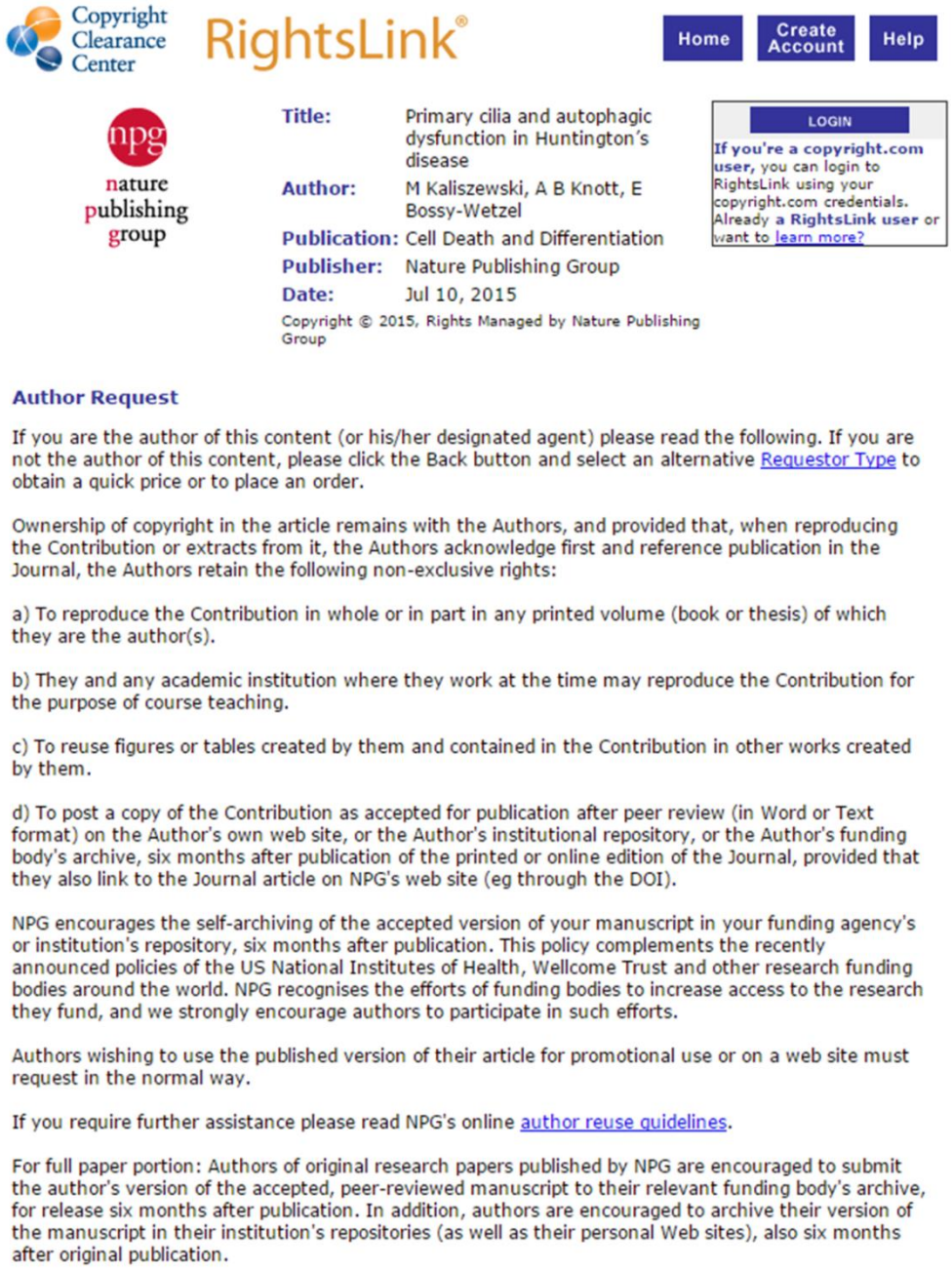

Copyright Clearance Center RightsLink®

Home | Create Account | Help

nature publishing group

Title: Primary cilia and autophagic dysfunction in Huntington's disease

Author: M Kaliszewski, A B Knott, E Bossy-Wetzel

Publication: Cell Death and Differentiation

Publisher: Nature Publishing Group

Date: Jul 10, 2015

Copyright © 2015, Rights Managed by Nature Publishing Group

LOGIN

If you're a copyright.com user, you can login to RightsLink using your copyright.com credentials. Already a RightsLink user or want to learn more?

Author Request

If you are the author of this content (or his/her designated agent) please read the following. If you are not the author of this content, please click the Back button and select an alternative Requestor Type to obtain a quick price or to place an order.

Ownership of copyright in the article remains with the Authors, and provided that, when reproducing the Contribution or extracts from it, the Authors acknowledge first and reference publication in the Journal, the Authors retain the following non-exclusive rights:

a) To reproduce the Contribution in whole or in part in any printed volume (book or thesis) of which they are the author(s).

b) They and any academic institution where they work at the time may reproduce the Contribution for the purpose of course teaching.

c) To reuse figures or tables created by them and contained in the Contribution in other works created by them.

d) To post a copy of the Contribution as accepted for publication after peer review (in Word or Text format) on the Author's own web site, or the Author's institutional repository, or the Author's funding body's archive, six months after publication of the printed or online edition of the Journal, provided that they also link to the Journal article on NPG's web site (eg through the DOI).

NPG encourages the self-archiving of the accepted version of your manuscript in your funding agency's or institution's repository, six months after publication. This policy complements the recently announced policies of the US National Institutes of Health, Wellcome Trust and other research funding bodies around the world. NPG recognises the efforts of funding bodies to increase access to the research they fund, and we strongly encourage authors to participate in such efforts.

Authors wishing to use the published version of their article for promotional use or on a web site must request in the normal way.

If you require further assistance please read NPG's online author reuse guidelines.

For full paper portion: Authors of original research papers published by NPG are encouraged to submit the author's version of the accepted, peer-reviewed manuscript to their relevant funding body's archive, for release six months after publication. In addition, authors are encouraged to archive their version of the manuscript in their institution's repositories (as well as their personal Web sites), also six months after original publication.

Ownership of copyright in the article "Primary cilia and autophagic dysfunction in Huntington's disease" published in *Cell Death and Differentiation* remains with the authors. Thus, the figures which have been published are allowed to be reproduced in this dissertation.

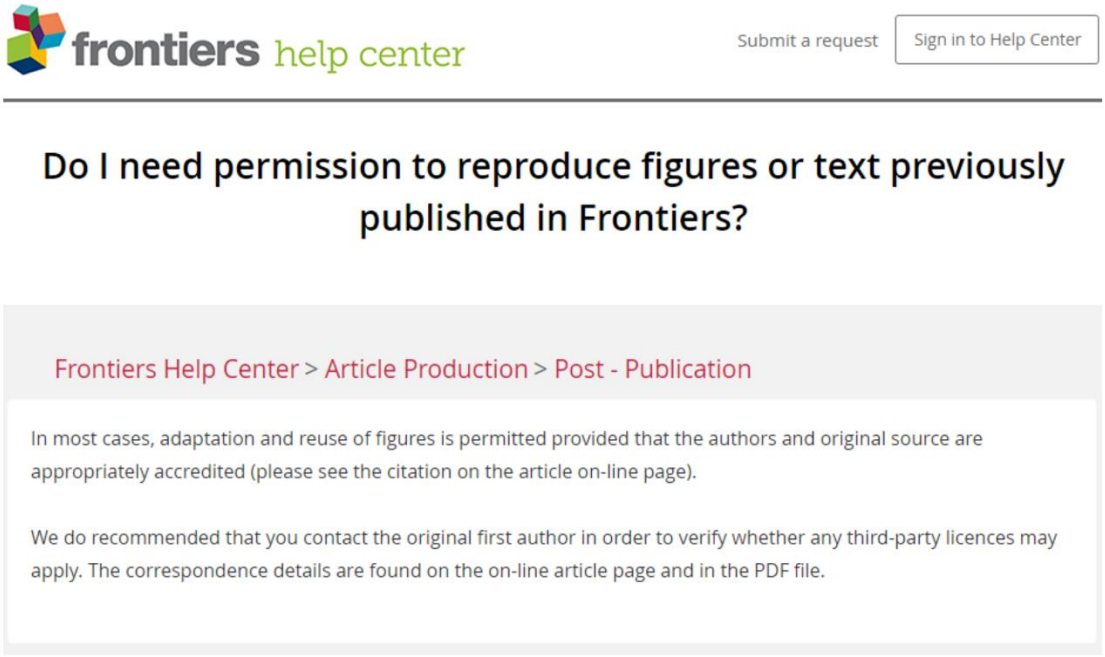

Adaption and reuse of figures from the article "SOD1 Lysine 123 Acetylation in the Adult Central Nervous System" published in *Frontiers in Cellular Neuroscience* is permitted provided that authors and original source are appropriately accredited. Thus, the figures which have been published are allowed to be reproduced in this dissertation.

LIST OF REFERENCES

Akella, J.S., Wloga, D., Kim, J., Starostina, N.G., Lyons-Abbott, S., Morrissette, N.S., Dougan, S.T., Kipreos, E.T., and Gaertig, J. (2010). MEC-17 is an α-tubulin acetyltransferase. Nature *467*, 218–222.

Aksenov, M.Y., Tucker, H.M., Nair, P., Aksenova, M.V., Butterfield, D.A., Estus, S., and Markesbery, W.R. (1998). The expression of key oxidative stress-handling genes in different brain regions in alzheimer's disease. J. Mol. Neurosci. *11*, 151–164.

Allfrey, V.G., Faulkner, R., and Mirsky, A.E. (1964). Acetylation and methylation of histones and their possible role in the regulation of RNA synthesis. Proc. Natl. Acad. Sci. U. S. A. *51*, 786–794.

Allis, C.D., Berger, S.L., Cote, J., Dent, S., Jenuwien, T., Kouzarides, T., Pillus, L., Reinberg, D., Shi, Y., Shiekhattar, R., et al. (2007). New Nomenclature for Chromatin-Modifying Enzymes. Cell *131*, 633–636.

Alonso, A., Logroscino, G., Jick, S.S., and Hernán, M.A. (2009). Incidence and lifetime risk of motor neuron disease in the United Kingdom: a population-based study. Eur. J. Neurol. Off. J. Eur. Fed. Neurol. Soc. *16*, 745–751.

Antinone, S.E., Ghadge, G.D., Lam, T.T., Wang, L., Roos, R.P., and Green, W.N. (2013). Palmitoylation of Superoxide Dismutase 1 (SOD1) Is Increased for Familial Amyotrophic Lateral Sclerosis-linked SOD1 Mutants. J. Biol. Chem. *288*, 21606–21617.

Armato, U. (2012). Alzheimer's disease: An update of the roles of receptors, astrocytes and primary cilia (Review). Int. J. Mol. Med. *31*, 3–10.

Arnesano, F., Banci, L., Bertini, I., Martinelli, M., Furukawa, Y., and O'Halloran, T.V. (2004). The Unusually Stable Quaternary Structure of Human Cu,Zn-Superoxide Dismutase 1 Is Controlled by Both Metal Occupancy and Disulfide Status. J. Biol. Chem. *279*, 47998–48003.

Arnesen, T., Damme, P.V., Polevoda, B., Helsens, K., Evjenth, R., Colaert, N., Varhaug, J.E., Vandekerckhove, J., Lillehaug, J.R., Sherman, F., et al. (2009). Proteomics analyses reveal the evolutionary conservation and divergence of N-terminal acetyltransferases from yeast and humans. Proc. Natl. Acad. Sci. *106*, 8157–8162.

Atkin, J.D., Farg, M.A., Turner, B.J., Tomas, D., Lysaght, J.A., Nunan, J., Rembach, A., Nagley, P., Beart, P.M., Cheema, S.S., et al. (2006). Induction of the Unfolded Protein Response in Familial Amyotrophic Lateral Sclerosis and Association of Protein-disulfide Isomerase with Superoxide Dismutase 1. J. Biol. Chem. *281*, 30152–30165.

Avasthi, P., and Marshall, W. (2013). Ciliary secretion: switching the cellular antenna to "transmit." Curr. Biol. CB *23*, R471-473.

Ayers, J.I., Fromholt, S., Koch, M., DeBosier, A., McMahon, B., Xu, G., and Borchelt, D.R. (2014). Experimental transmissibility of mutant SOD1 motor neuron disease. Acta Neuropathol. (Berl.) *128*, 791–803.

Baehrecke, E.H. (2005). Autophagy: dual roles in life and death? Nat. Rev. Mol. Cell Biol. *6*, 505–510.

Bannister, A.J., and Kouzarides, T. (1996). The CBP co-activator is a histone acetyltransferase. Nature *384*, 641–643.

Basso, M., Pozzi, S., Tortarolo, M., Fiordaliso, F., Bisighini, C., Pasetto, L., Spaltro, G., Lidonnici, D., Gensano, F., Battaglia, E., et al. (2013). Mutant Copper-Zinc Superoxide Dismutase (SOD1) Induces Protein Secretion Pathway Alterations and Exosome Release in Astrocytes IMPLICATIONS FOR DISEASE SPREADING AND MOTOR NEURON PATHOLOGY IN AMYOTROPHIC LATERAL SCLEROSIS. J. Biol. Chem. *288*, 15699–15711.

Bechara, E.G., Didiot, M.C., Melko, M., Davidovic, L., Bensaid, M., Martin, P., Castets, M., Pognonec, P., Khandjian, E.W., Moine, H., et al. (2009). A Novel Function for Fragile X Mental Retardation Protein in Translational Activation. PLOS Biol *7*, e1000016.

Beckman, J.S., Carson, M., Smith, C.D., and Koppenol, W.H. (1993). ALS, SOD and peroxynitrite. Nature *364*, 584–584.

Beers, D.R., Henkel, J.S., Xiao, Q., Zhao, W., Wang, J., Yen, A.A., Siklos, L., McKercher, S.R., and Appel, S.H. (2006). Wild-type microglia extend survival in PU.1 knockout mice with familial amyotrophic lateral sclerosis. Proc. Natl. Acad. Sci. *103*, 16021–16026.

Behndig, A., Karlsson, K., Reaume, A.G., Sentman, M.-L., and Marklund, S.L. (2001). In vitro photochemical cataract in mice lacking copper-zinc superoxide dismutase. Free Radic. Biol. Med. *31*, 738–744.

Bendotti, C., Marino, M., Cheroni, C., Fontana, E., Crippa, V., Poletti, A., and De Biasi, S. (2012). Dysfunction of constitutive and inducible ubiquitin-proteasome system in amyotrophic lateral sclerosis: Implication for protein aggregation and immune response. Prog. Neurobiol. *97*, 101–126.

Bensimon, G., Lacomblez, L., Meininger, V., and Group, the A.S. (1994). A Controlled Trial of Riluzole in Amyotrophic Lateral Sclerosis. N. Engl. J. Med. *330*, 585–591.

Boehlke, C., Kotsis, F., Patel, V., Braeg, S., Voelker, H., Bredt, S., Beyer, T., Janusch, H., Hamann, C., Gödel, M., et al. (2010). Primary cilia regulate mTORC1 activity and cell size through Lkb1. Nat. Cell Biol. *12*, 1115–1122.

Boillée, S., Velde, C.V., and Cleveland, D.W. (2006a). ALS: A Disease of Motor Neurons and Their Nonneuronal Neighbors. Neuron *52*, 39–59.

Boillée, S., Yamanaka, K., Lobsiger, C.S., Copeland, N.G., Jenkins, N.A., Kassiotis, G., Kollias, G., and Cleveland, D.W. (2006b). Onset and Progression in Inherited ALS Determined by Motor Neurons and Microglia. Science *312*, 1389–1392.

Borchelt, D.R., Lee, M.K., Slunt, H.S., Guarnieri, M., Xu, Z.S., Wong, P.C., Brown, R.H., Price, D.L., Sisodia, S.S., and Cleveland, D.W. (1994). Superoxide dismutase 1 with mutations linked to familial amyotrophic lateral sclerosis possesses significant activity. Proc. Natl. Acad. Sci. U. S. A. *91*, 8292–8296.

Bosco, D.A., Morfini, G., Karabacak, N.M., Song, Y., Gros-Louis, F., Pasinelli, P., Goolsby, H., Fontaine, B.A., Lemay, N., McKenna-Yasek, D., et al. (2010). Wild-type and mutant SOD1 share an aberrant conformation and a common pathogenic pathway in ALS. Nat. Neurosci. *13*, 1396–1403.

Brailov, I., Bancila, M., Brisorgueil, M.-J., Miquel, M.-C., Hamon, M., and Vergé, D. (2000). Localization of 5-HT6 receptors at the plasma membrane of neuronal cilia in the rat brain. Brain Res. *872*, 271–275.

Briscoe, J., and Thérond, P.P. (2013). The mechanisms of Hedgehog signalling and its roles in development and disease. Nat. Rev. Mol. Cell Biol. *14*, 416–429.

Brown, J.P., Couillard-Després, S., Cooper-Kuhn, C.M., Winkler, J., Aigner, L., and Kuhn, H.G. (2003). Transient expression of doublecortin during adult neurogenesis. J. Comp. Neurol. *467*, 1–10.

Bruijn, L.I., Houseweart, M.K., Kato, S., Anderson, K.L., Anderson, S.D., Ohama, E., Reaume, A.G., Scott, R.W., and Cleveland, D.W. (1998). Aggregation and Motor Neuron Toxicity of an ALS-Linked SOD1 Mutant Independent from Wild-Type SOD1. Science *281*, 1851–1854.

Chacon-Heszele, M.F., Choi, S.Y., Zuo, X., Baek, J.-I., Ward, C., and Lipschutz, J.H. (2014). The exocyst and regulatory GTPases in urinary exosomes. Physiol. Rep. *2*, e12116–e12116.

Chakravarthy, B., Gaudet, C., Ménard, M., Brown, L., Atkinson, T., LaFerla, F.M., Ito, S., Armato, U., Dal Prà, I., and Whitfield, J. (2012). Reduction of the immunostainable length of the hippocampal dentate granule cells' primary cilia in 3xAD-transgenic mice producing human Aβ1-42 and tau. Biochem. Biophys. Res. Commun. *427*, 218–222.

Chang, L.Y., Slot, J.W., Geuze, H.J., and Crapo, J.D. (1988). Molecular immunocytochemistry of the CuZn superoxide dismutase in rat hepatocytes. J. Cell Biol. *107*, 2169–2179.

Chia, R., Tattum, M.H., Jones, S., Collinge, J., Fisher, E.M.C., and Jackson, G.S. (2010). Superoxide dismutase 1 and tgSOD1 mouse spinal cord seed fibrils, suggesting a propagative cell death mechanism in amyotrophic lateral sclerosis. PloS One *5*, e10627.

Choudhary, C., Kumar, C., Gnad, F., Nielsen, M.L., Rehman, M., Walther, T.C., Olsen, J.V., and Mann, M. (2009). Lysine Acetylation Targets Protein Complexes and Co-Regulates Major Cellular Functions. Science *325*, 834–840.

Choudhary, C., Weinert, B.T., Nishida, Y., Verdin, E., and Mann, M. (2014). The growing landscape of lysine acetylation links metabolism and cell signalling. Nat. Rev. Mol. Cell Biol. *15*, 536–550.

Clement, C.A., Ajbro, K.D., Koefoed, K., Vestergaard, M.L., Veland, I.R., Henriques de Jesus, M.P.R., Pedersen, L.B., Benmerah, A., Andersen, C.Y., Larsen, L.A., et al. (2013). TGF-β Signaling Is Associated with Endocytosis at the Pocket Region of the Primary Cilium. Cell Rep. *3*, 1806–1814.

Codeluppi, S., Gregory, E.N., Kjell, J., Wigerblad, G., Olson, L., and Svensson, C.I. (2011). Influence of rat substrain and growth conditions on the characteristics of primary cultures of adult rat spinal cord astrocytes. J. Neurosci. Methods *197*, 118–127.

Cohen, T.J., Guo, J.L., Hurtado, D.E., Kwong, L.K., Mills, I.P., Trojanowski, J.Q., and Lee, V.M.Y. (2011). The acetylation of tau inhibits its function and promotes pathological tau aggregation. Nat. Commun. *2*, 252.

Corbit, K.C., Aanstad, P., Singla, V., Norman, A.R., Stainier, D.Y.R., and Reiter, J.F. (2005). Vertebrate Smoothened functions at the primary cilium. Nature *437*, 1018–1021.

Corbit, K.C., Shyer, A.E., Dowdle, W.E., Gaulden, J., Singla, V., and Reiter, J.F. (2008). Kif3a constrains β-catenin-dependent Wnt signalling through dual ciliary and non-ciliary mechanisms. Nat. Cell Biol. *10*, 70–76.

Corson, L.B., Strain, J.J., Culotta, V.C., and Cleveland, D.W. (1998). Chaperone-facilitated copper binding is a property common to several classes of familial amyotrophic lateral sclerosis-linked superoxide dismutase mutants. Proc. Natl. Acad. Sci. *95*, 6361–6366.

Cova, E., Ghiroldi, A., Guareschi, S., Mazzini, G., Gagliardi, S., Davin, A., Bianchi, M., Ceroni, M., and Cereda, C. (2010). G93A SOD1 alters cell cycle in a cellular model of Amyotrophic Lateral Sclerosis. Cell. Signal. *22*, 1477–1484.

Crapo, J.D., Oury, T., Rabouille, C., Slot, J.W., and Chang, L.Y. (1992). Copper,zinc superoxide dismutase is primarily a cytosolic protein in human cells. Proc. Natl. Acad. Sci. *89*, 10405–10409.

Crisp, M.J., Mawuenyega, K.G., Patterson, B.W., Reddy, N.C., Chott, R., Self, W.K., Weihl, C.C., Jockel-Balsarotti, J., Varadhachary, A.S., Bucelli, R.C., et al. (2015). In vivo kinetic approach reveals slow SOD1 turnover in the CNS. J. Clin. Invest. *125*, 2772–2780.

Culotta, V.C., Klomp, L.W.J., Strain, J., Casareno, R.L.B., Krems, B., and Gitlin, J.D. (1997). The Copper Chaperone for Superoxide Dismutase. J. Biol. Chem. *272*, 23469–23472.

Dal Canto, M.C., and Gurney, M.E. (1995). Neuropathological changes in two lines of mice carrying a transgene for mutant human Cu,Zn SOD, and in mice overexpressing wild type human SOD: a model of familial amyotrophic lateral sclerosis (FALS). Brain Res. *676*, 25–40.

Damiano, M., Starkov, A.A., Petri, S., Kipiani, K., Kiaei, M., Mattiazzi, M., Flint Beal, M., and Manfredi, G. (2006). Neural mitochondrial Ca2+ capacity impairment precedes the onset of motor symptoms in G93A Cu/Zn-superoxide dismutase mutant mice. J. Neurochem. *96*, 1349–1361.

Das, R.M., and Storey, K.G. (2014). Apical Abscission Alters Cell Polarity and Dismantles the Primary Cilium During Neurogenesis. Science *343*, 200–204.

De Vos, K.J.D., Chapman, A.L., Tennant, M.E., Manser, C., Tudor, E.L., Lau, K.-F., Brownlees, J., Ackerley, S., Shaw, P.J., McLoughlin, D.M., et al. (2007). Familial amyotrophic lateral sclerosis-linked SOD1 mutants perturb fast axonal transport to reduce axonal mitochondria content. Hum. Mol. Genet. *16*, 2720–2728.

DeJesus-Hernandez, M., Mackenzie, I.R., Boeve, B.F., Boxer, A.L., Baker, M., Rutherford, N.J., Nicholson, A.M., Finch, N.A., Flynn, H., Adamson, J., et al. (2011). Expanded GGGGCC Hexanucleotide Repeat in Noncoding Region of C9ORF72 Causes Chromosome 9p-Linked FTD and ALS. Neuron *72*, 245–256.

Deng, H.-X., Chen, W., Hong, S.-T., Boycott, K.M., Gorrie, G.H., Siddique, N., Yang, Y., Fecto, F., Shi, Y., Zhai, H., et al. (2011). Mutations in UBQLN2 cause dominant X-linked juvenile and adult-onset ALS and ALS/dementia. Nature *477*, 211–215.

Ding, G., Liu, H.-D., Huang, Q., Liang, H.-X., Ding, Z.-H., Liao, Z.-J., and Huang, G. (2013). HDAC6 promotes hepatocellular carcinoma progression by inhibiting P53 transcriptional activity. FEBS Lett. *587*, 880–886.

Domire, J.S., Green, J.A., Lee, K.G., Johnson, A.D., Askwith, C.C., and Mykytyn, K. (2011). Dopamine receptor 1 localizes to neuronal cilia in a dynamic process that requires the Bardet-Biedl syndrome proteins. Cell. Mol. Life Sci. *68*, 2951–2960.

Drazic, A., Myklebust, L.M., Ree, R., and Arnesen, T. (2016). The world of protein acetylation. Biochim. Biophys. Acta *1864*, 1372–1401.

Dubreuil, V., Marzesco, A.-M., Corbeil, D., Huttner, W.B., and Wilsch-Bräuninger, M. (2007). Midbody and primary cilium of neural progenitors release extracellular membrane particles enriched in the stem cell marker prominin-1. J. Cell Biol. *176*, 483–495.

Elam, J.S., Taylor, A.B., Strange, R., Antonyuk, S., Doucette, P.A., Rodriguez, J.A., Hasnain, S.S., Hayward, L.J., Valentine, J.S., Yeates, T.O., et al. (2003). Amyloid-like filaments and water-filled nanotubes formed by SOD1 mutant proteins linked to familial ALS. Nat. Struct. Mol. Biol. *10*, 461–467.

Elchuri, S., Oberley, T.D., Qi, W., Eisenstein, R.S., Jackson Roberts, L., Van Remmen, H., Epstein, C.J., and Huang, T.-T. (2004). CuZnSOD deficiency leads to persistent and widespread oxidative damage and hepatocarcinogenesis later in life. Oncogene *24*, 367–380.

Elian, M. (1991). Olfactory impairment in motor neuron disease: a pilot study. J. Neurol. Neurosurg. Psychiatry *54*, 927–928.

Endo, F., Komine, O., Fujimori-Tonou, N., Katsuno, M., Jin, S., Watanabe, S., Sobue, G., Dezawa, M., Wyss-Coray, T., and Yamanaka, K. (2015). Astrocyte-Derived TGF-β1 Accelerates Disease Progression in ALS Mice by Interfering with the Neuroprotective Functions of Microglia and T Cells. Cell Rep. *11*, 592–604.

Engelhardt, J.I., Tajti, J., and Appel, S.H. (1993). Lymphocytic infiltrates in the spinal cord in amyotrophic lateral sclerosis. Arch. Neurol. *50*, 30–36.

Estévez, A.G., Crow, J.P., Sampson, J.B., Reiter, C., Zhuang, Y., Richardson, G.J., Tarpey, M.M., Barbeito, L., and Beckman, J.S. (1999). Induction of Nitric Oxide -- Dependent Apoptosis in Motor Neurons by Zinc-Deficient Superoxide Dismutase. Science *286*, 2498–2500.

Ezzi, S.A., Urushitani, M., and Julien, J.-P. (2007). Wild-type superoxide dismutase acquires binding and toxic properties of ALS-linked mutant forms through oxidation. J. Neurochem. *102*, 170–178.

Fischer, L.R., Li, Y., Asress, S.A., Jones, D.P., and Glass, J.D. (2012). Absence of SOD1 leads to oxidative stress in peripheral nerve and causes a progressive distal motor axonopathy. Exp. Neurol. *233*, 163–171.

Flood, D.G., Reaume, A.G., Gruner, J.A., Hoffman, E.K., Hirsch, J.D., Lin, Y.-G., Dorfman, K.S., and Scott, R.W. (1999). Hindlimb Motor Neurons Require Cu/Zn Superoxide Dismutase for Maintenance of Neuromuscular Junctions. Am. J. Pathol. *155*, 663–672.

Forman, H.J., and Fridovich, I. (1973). On the Stability of Bovine Superoxide Dismutase: the effects of metals. J. Biol. Chem. *248*, 2645–2649.

Fridovich, I. (1995). Superoxide Radical and Superoxide Dismutases. Annu. Rev. Biochem. *64*, 97–112.

Frost, B., and Diamond, M.I. (2010). Prion-like mechanisms in neurodegenerative diseases. Nat. Rev. Neurosci. *11*, 155–159.

Gal, J., Chen, J., Barnett, K.R., Yang, L., Brumley, E., and Zhu, H. (2013). HDAC6 Regulates Mutant SOD1 Aggregation through Two SMIR Motifs and Tubulin Acetylation. J. Biol. Chem. *288*, 15035–15045.

Garcia-Gonzalo, F.R., Corbit, K.C., Sirerol-Piquer, M.S., Ramaswami, G., Otto, E.A., Noriega, T.R., Seol, A.D., Robinson, J.F., Bennett, C.L., Josifova, D.J., et al. (2011). A transition zone complex regulates mammalian ciliogenesis and ciliary membrane composition. Nat. Genet. *43*, 776–784.

Gertz, B., Wong, M., and Martin, L.J. (2012). Nuclear Localization of Human SOD1 and Mutant SOD1-Specific Disruption of Survival Motor Neuron Protein Complex in Transgenic Amyotrophic Lateral Sclerosis Mice. J. Neuropathol. Exp. Neurol. *71*, 162–177.

Getzoff, E.D., Tainer, J.A., Stempien, M.M., Bell, G.I., and Hallewell, R.A. (1989). Evolution of CuZn superoxide dismutase and the Greek key beta-barrel structural motif. Proteins *5*, 322–336.

Glozak, M.A., Sengupta, N., Zhang, X., and Seto, E. (2005). Acetylation and deacetylation of non-histone proteins. Gene *363*, 15–23.

Gnad, F., Gunawardena, J., and Mann, M. (2011). PHOSIDA 2011: the posttranslational modification database. Nucleic Acids Res. *39*, D253–D260.

Goedert, M., Clavaguera, F., and Tolnay, M. (2010). The propagation of prion-like protein inclusions in neurodegenerative diseases. Trends Neurosci. *33*, 317–325.

Goodsell, D.S., and Olson, and A.J. (2000). Structural Symmetry and Protein Function. Annu. Rev. Biophys. Biomol. Struct. *29*, 105–153.

Grad, L.I., Yerbury, J.J., Turner, B.J., Guest, W.C., Pokrishevsky, E., O'Neill, M.A., Yanai, A., Silverman, J.M., Zeineddine, R., Corcoran, L., et al. (2014). Intercellular propagated misfolding of wild-type Cu/Zn superoxide dismutase occurs via exosome-dependent and -independent mechanisms. Proc. Natl. Acad. Sci. U. S. A. *111*, 3620–3625.

Guareschi, S., Cova, E., Cereda, C., Ceroni, M., Donetti, E., Bosco, D.A., Trotti, D., and Pasinelli, P. (2012). An over-oxidized form of superoxide dismutase found in sporadic amyotrophic lateral sclerosis with bulbar onset shares a toxic mechanism with mutant SOD1. Proc. Natl. Acad. Sci. *109*, 5074–5079.

Guemez-Gamboa, A., Coufal, N.G., and Gleeson, J.G. (2014). Primary Cilia in the Developing and Mature Brain. Neuron *82*, 511–521.

Gurney, M.E., Pu, H., Chiu, A.Y., Canto, M.D., Polchow, C.Y., Alexander, D.D., Caliendo, J., Hentati, A., Kwon, Y.W., Deng, H.X., et al. (1994). Motor neuron degeneration in mice that express a human Cu,Zn superoxide dismutase mutation. Science *264*, 1772–1775.

Haberland, M., Montgomery, R.L., and Olson, E.N. (2009). The many roles of histone deacetylases in development and physiology: implications for disease and therapy. Nat. Rev. Genet. *10*, 32–42.

Han, E.-S., Muller, F.L., Pérez, V.I., Qi, W., Liang, H., Xi, L., Fu, C., Doyle, E., Hickey, M., Cornell, J., et al. (2008a). The in vivo gene expression signature of oxidative stress. Physiol. Genomics *34*, 112–126.

Han, Y.-G., Spassky, N., Romaguera-Ros, M., Garcia-Verdugo, J.-M., Aguilar, A., Schneider-Maunoury, S., and Alvarez-Buylla, A. (2008b). Hedgehog signaling and primary cilia are required for the formation of adult neural stem cells. Nat. Neurosci. *11*, 277–284.

Han, Y.M., Kang, G.M., Byun, K., Ko, H.W., Kim, J., Shin, M.-S., Kim, H.-K., Gil, S.Y., Yu, J.H., Lee, B., et al. (2014). Leptin-promoted cilia assembly is critical for normal energy balance. J. Clin. Invest. *124*, 2193–2197.

Händel, M., Schulz, S., Stanarius, A., Schreff, M., Erdtmann-Vourliotis, M., Schmidt, H., Wolf, G., and Höllt, V. (1999). Selective targeting of somatostatin receptor 3 to neuronal cilia. Neuroscience *89*, 909–926.

Hardiman, O., van den Berg, L.H., and Kiernan, M.C. (2011). Clinical diagnosis and management of amyotrophic lateral sclerosis. Nat. Rev. Neurol. *7*, 639–649.

Hashizume, K., Hirasawa, M., Imamura, Y., Noda, S., Shimizu, T., Shinoda, K., Kurihara, T., Noda, K., Ozawa, Y., Ishida, S., et al. (2008). Retinal Dysfunction and Progressive Retinal Cell Death in SOD1-Deficient Mice. Am. J. Pathol. *172*, 1325–1331.

Hawkes, C.H., Shephard, B.C., Geddes, J.F., Body, G.D., and Martin, J.E. (1998). Olfactory Disorder in Motor Neuron Disease. Exp. Neurol. *150*, 248–253.

He, Q., Wang, G., Wakade, S., Dasgupta, S., Dinkins, M., Kong, J.N., Spassieva, S.D., and Bieberich, E. (2014). Primary cilia in stem cells and neural progenitors are regulated by neutral sphingomyelinase 2 and ceramide. Mol. Biol. Cell *25*, 1715–1729.

Howland, D.S., Liu, J., She, Y., Goad, B., Maragakis, N.J., Kim, B., Erickson, J., Kulik, J., DeVito, L., Psaltis, G., et al. (2002). Focal loss of the glutamate transporter EAAT2 in a transgenic rat model of SOD1 mutant-mediated amyotrophic lateral sclerosis (ALS). Proc. Natl. Acad. Sci. *99*, 1604–1609.

Hu, C.-K., Coughlin, M., and Mitchison, T.J. (2012). Midbody assembly and its regulation during cytokinesis. Mol. Biol. Cell *23*, 1024–1034.

Hu, Q., Milenkovic, L., Jin, H., Scott, M.P., Nachury, M.V., Spiliotis, E.T., and Nelson, W.J. (2010). A Septin Diffusion Barrier at the Base of the Primary Cilium Maintains Ciliary Membrane Protein Distribution. Science *329*, 436–439.

Hubbert, C., Guardiola, A., Shao, R., Kawaguchi, Y., Ito, A., Nixon, A., Yoshida, M., Wang, X.-F., and Yao, T.-P. (2002). HDAC6 is a microtubule-associated deacetylase. Nature *417*, 455–458.

Imamura, Y., Noda, S., Hashizume, K., Shinoda, K., Yamaguchi, M., Uchiyama, S., Shimizu, T., Mizushima, Y., Shirasawa, T., and Tsubota, K. (2006). Drusen, choroidal neovascularization, and retinal pigment epithelium dysfunction in SOD1-deficient mice: A model of age-related macular degeneration. Proc. Natl. Acad. Sci. *103*, 11282–11287.

Ishikawa, H., Thompson, J., Yates, J.R., and Marshall, W.F. (2012). Proteomic Analysis of Mammalian Primary Cilia. Curr. Biol. *22*, 414–419.

Israelson, A., Arbel, N., Da Cruz, S., Ilieva, H., Yamanaka, K., Shoshan-Barmatz, V., and Cleveland, D.W. (2010). Misfolded Mutant SOD1 Directly Inhibits VDAC1 Conductance in a Mouse Model of Inherited ALS. Neuron *67*, 575–587.

Jenkins, P.M., McEwen, D.P., and Martens, J.R. (2009). Olfactory Cilia: Linking Sensory Cilia Function and Human Disease. Chem. Senses *34*, 451–464.

Kanekura, K., Suzuki, H., Aiso, S., and Matsuoka, M. (2009). ER Stress and Unfolded Protein Response in Amyotrophic Lateral Sclerosis. Mol. Neurobiol. *39*, 81–89.

Kato, S. (2007). Amyotrophic lateral sclerosis models and human neuropathology: similarities and differences. Acta Neuropathol. (Berl.) *115*, 97–114.

Kawaguchi, Y., Kovacs, J.J., McLaurin, A., Vance, J.M., Ito, A., and Yao, T.-P. (2003). The Deacetylase HDAC6 Regulates Aggresome Formation and Cell Viability in Response to Misfolded Protein Stress. Cell *115*, 727–738.

Kawamata, H., and Manfredi, G. (2010). Import, Maturation, and Function of SOD1 and Its Copper Chaperone CCS in the Mitochondrial Intermembrane Space. Antioxid. Redox Signal. *13*, 1375–1384.

Ke, Y.-N., and Yang, W.-X. (2014). Primary cilium: an elaborate structure that blocks cell division? Gene *547*, 175–185.

Keithley, E.M., Canto, C., Zheng, Q.Y., Wang, X., Fischel-Ghodsian, N., and Johnson, K.R. (2005). Cu/Zn superoxide dismutase and age-related hearing loss. Hear. Res. *209*, 76–85.

Keller, G.A., Warner, T.G., Steimer, K.S., and Hallewell, R.A. (1991). Cu,Zn superoxide dismutase is a peroxisomal enzyme in human fibroblasts and hepatoma cells. Proc. Natl. Acad. Sci. *88*, 7381–7385.

Kenna, K.P., van Doormaal, P.T.C., Dekker, A.M., Ticozzi, N., Kenna, B.J., Diekstra, F.P., van Rheenen, W., van Eijk, K.R., Jones, A.R., Keagle, P., et al. (2016). NEK1 variants confer susceptibility to amyotrophic lateral sclerosis. Nat. Genet. *48*, 1037–1042.

Keryer, G., Pineda, J.R., Liot, G., Kim, J., Dietrich, P., Benstaali, C., Smith, K., Cordelières, F.P., Spassky, N., Ferrante, R.J., et al. (2011). Ciliogenesis is regulated by a huntingtin-HAP1-PCM1 pathway and is altered in Huntington disease. J. Clin. Invest. *121*, 4372–4382.

Khare, S.D., Caplow, M., and Dokholyan, N.V. (2004). The rate and equilibrium constants for a multistep reaction sequence for the aggregation of superoxide dismutase in amyotrophic lateral sclerosis. Proc. Natl. Acad. Sci. U. S. A. *101*, 15094–15099.

Kim, G.W., Gasche, Y., Grzeschik, S., Copin, J.-C., Maier, C.M., and Chan, P.H. (2003). Neurodegeneration in Striatum Induced by the Mitochondrial Toxin 3-Nitropropionic Acid: Role of Matrix Metalloproteinase-9 in Early Blood-Brain Barrier Disruption? J. Neurosci. *23*, 8733–8742.

Kim, S., Zaghloul, N.A., Bubenshchikova, E., Oh, E.C., Rankin, S., Katsanis, N., Obara, T., and Tsiokas, L. (2011). Nde1-mediated inhibition of ciliogenesis affects cell cycle re-entry. Nat. Cell Biol. *13*, 351–360.

Kinoshita, Y., Ito, H., Hirano, A., Fujita, K., Wate, R., Nakamura, M., Kaneko, S., Nakano, S., and Kusaka, H. (2009). Nuclear Contour Irregularity and Abnormal Transporter Protein Distribution in Anterior Horn Cells in Amyotrophic Lateral Sclerosis. J. Neuropathol. Exp. Neurol. *68*, 1184–1192.

Kiprilov, E.N., Awan, A., Desprat, R., Velho, M., Clement, C.A., Byskov, A.G., Andersen, C.Y., Satir, P., Bouhassira, E.E., Christensen, S.T., et al. (2008). Human embryonic stem cells in culture possess primary cilia with hedgehog signaling machinery. J. Cell Biol. *180*, 897–904.

Kirkinezos, I.G., Bacman, S.R., Hernandez, D., Oca-Cossio, J., Arias, L.J., Perez-Pinzon, M.A., Bradley, W.G., and Moraes, C.T. (2005). Cytochrome c Association with the Inner Mitochondrial Membrane Is Impaired in the CNS of G93A-SOD1 Mice. J. Neurosci. *25*, 164–172.

Knapp, L.T., and Klann, E. (2002). Potentiation of Hippocampal Synaptic Transmission by Superoxide Requires the Oxidative Activation of Protein Kinase C. J. Neurosci. *22*, 674–683.

Kojima, T., Wakamatsu, T.H., Dogru, M., Ogawa, Y., Igarashi, A., Ibrahim, O.M.A., Inaba, T., Shimizu, T., Noda, S., Obata, H., et al. (2012). Age-Related Dysfunction of the Lacrimal Gland and Oxidative Stress: Evidence from the Cu,Zn-Superoxide Dismutase-1 (Sod1) Knockout Mice. Am. J. Pathol. *180*, 1879–1896.

Kondo, T., Reaume, A.G., Huang, T.-T., Carlson, E., Murakami, K., Chen, S.F., Hoffman, E.K., Scott, R.W., Epstein, C.J., and Chan, P.H. (1997). Reduction of CuZn-Superoxide Dismutase Activity Exacerbates Neuronal Cell Injury and Edema Formation after Transient Focal Cerebral Ischemia. J. Neurosci. *17*, 4180–4189.

Kong, J., and Xu, Z. (1998). Massive Mitochondrial Degeneration in Motor Neurons Triggers the Onset of Amyotrophic Lateral Sclerosis in Mice Expressing a Mutant SOD1. J. Neurosci. *18*, 3241–3250.

Kouzarides, T. (2000). Acetylation: a regulatory modification to rival phosphorylation? EMBO J. *19*, 1176–1179.

Kulaga, H.M., Leitch, C.C., Eichers, E.R., Badano, J.L., Lesemann, A., Hoskins, B.E., Lupski, J.R., Beales, P.L., Reed, R.R., and Katsanis, N. (2004). Loss of BBS proteins causes anosmia in humans and defects in olfactory cilia structure and function in the mouse. Nat. Genet. *36*, 994–998.

Kwiatkowski, T.J., Bosco, D.A., LeClerc, A.L., Tamrazian, E., Vanderburg, C.R., Russ, C., Davis, A., Gilchrist, J., Kasarskis, E.J., Munsat, T., et al. (2009). Mutations in the FUS/TLS Gene on Chromosome 16 Cause Familial Amyotrophic Lateral Sclerosis. Science *323*, 1205–1208.

Larkin, L.M., Davis, C.S., Sims-Robinson, C., Kostrominova, T.Y., Remmen, H.V., Richardson, A., Feldman, E.L., and Brooks, S.V. (2011). Skeletal muscle weakness due to deficiency of CuZn-superoxide dismutase is associated with loss of functional innervation. Am. J. Physiol. - Regul. Integr. Comp. Physiol. *301*, R1400–R1407.

Lee, K.K., and Workman, J.L. (2007). Histone acetyltransferase complexes: one size doesn't fit all. Nat. Rev. Mol. Cell Biol. *8*, 284–295.

Lee, D.-Y., Jeon, G.S., Shim, Y., Seong, S.-Y., Lee, K.-W., and Sung, J.-J. (2015). Modulation of SOD1 Subcellular Localization by Transfection with Wild- or Mutant-type SOD1 in Primary Neuron and Astrocyte Cultures from ALS Mice. Exp. Neurobiol. *24*, 226–234.

Lee, J.-Y., Koga, H., Kawaguchi, Y., Tang, W., Wong, E., Gao, Y.-S., Pandey, U.B., Kaushik, S., Tresse, E., Lu, J., et al. (2010). HDAC6 controls autophagosome maturation essential for ubiquitin-selective quality-control autophagy. EMBO J. *29*, 969–980.

Lepock, J.R., Arnold, L.D., Torrie, B.H., Andrews, B., and Kruuv, J. (1985). Structural analyses of various Cu2+, Zn2+-superoxide dismutases by differential scanning calorimetry and Raman spectroscopy. Arch. Biochem. Biophys. *241*, 243–251.

Lewén, A., Matz, P., and Chan, P.H. (2000). Free radical pathways in CNS injury. J. Neurotrauma *17*, 871–890.

Li, Q., Velde, C.V., Israelson, A., Xie, J., Bailey, A.O., Dong, M.-Q., Chun, S.-J., Roy, T., Winer, L., Yates, J.R., et al. (2010). ALS-linked mutant superoxide dismutase 1 (SOD1) alters mitochondrial protein composition and decreases protein import. Proc. Natl. Acad. Sci. *107*, 21146–21151.

Liem, K.F., Ashe, A., He, M., Satir, P., Moran, J., Beier, D., Wicking, C., and Anderson, K.V. (2012). The IFT-A complex regulates Shh signaling through cilia structure and membrane protein trafficking. J Cell Biol *197*, 789–800.

Lin, Z.-F., Xu, H.-B., Wang, J.-Y., Lin, Q., Ruan, Z., Liu, F.-B., Jin, W., Huang, H.-H., and Chen, X. (2013). SIRT5 desuccinylates and activates SOD1 to eliminate ROS. Biochem. Biophys. Res. Commun. *441*, 191–195.

Liu, J.-P., and Zeitlin, S.O. (2011). The long and the short of aberrant ciliogenesis in Huntington disease. J. Clin. Invest. *121*, 4237–4241.

Lundby, A., Lage, K., Weinert, B.T., Bekker-Jensen, D.B., Secher, A., Skovgaard, T., Kelstrup, C.D., Dmytriyev, A., Choudhary, C., Lundby, C., et al. (2012). Proteomic Analysis of Lysine Acetylation Sites in Rat Tissues Reveals Organ Specificity and Subcellular Patterns. Cell Rep. *2*, 419–431.

Ma, X., Peterson, R., and Turnbull, J. (2011). Adenylyl Cyclase type 3, a marker of primary cilia, is reduced in primary cell culture and in lumbar spinal cord in situ in G93A SOD1 mice. BMC Neurosci. *12*, 71.

Magrané, J., Hervias, I., Henning, M.S., Damiano, M., Kawamata, H., and Manfredi, G. (2009). Mutant SOD1 in neuronal mitochondria causes toxicity and mitochondrial dynamics abnormalities. Hum. Mol. Genet. *18*, 4552–4564.

Magrané, J., Cortez, C., Gan, W.-B., and Manfredi, G. (2014). Abnormal mitochondrial transport and morphology are common pathological denominators in SOD1 and TDP43 ALS mouse models. Hum. Mol. Genet. *23*, 1413–1424.

Maruyama, H., Morino, H., Ito, H., Izumi, Y., Kato, H., Watanabe, Y., Kinoshita, Y., Kamada, M., Nodera, H., Suzuki, H., et al. (2010). Mutations of optineurin in amyotrophic lateral sclerosis. Nature *465*, 223–226.

Matsumoto, S., Kusaka, H., Ito, H., Shibata, N., Asayama, T., and Imai, T. (1996). Sporadic amyotrophic lateral sclerosis with dementia and Cu/Zn superoxide dismutase-positive Lewy body-like inclusions. Clin. Neuropathol. *15*, 41–46.

Matsuyama, A., Shimazu, T., Sumida, Y., Saito, A., Yoshimatsu, Y., Seigneurin-Berny, D., Osada, H., Komatsu, Y., Nishino, N., Khochbin, S., et al. (2002). In vivo destabilization of dynamic microtubules by HDAC6-mediated deacetylation. EMBO J. *21*, 6820–6831.

Mattiazzi, M., D'Aurelio, M., Gajewski, C.D., Martushova, K., Kiaei, M., Beal, M.F., and Manfredi, G. (2002). Mutated human SOD1 causes dysfunction of oxidative phosphorylation in mitochondria of transgenic mice. J. Biol. Chem.

McCord, J.M., and Fridovich, I. (1969). Superoxide Dismutase. An Enzymic Function For Erythrocuprein (Hemocuprein). J. Biol. Chem. *244*, 6049–6055.

Ming, G., and Song, H. (2011). Adult Neurogenesis in the Mammalian Brain: Significant Answers and Significant Questions. Neuron *70*, 687–702.

Mizzen, C.A., Yang, X.-J., Kokubo, T., Brownell, J.E., Bannister, A.J., Owen-Hughes, T., Workman, J., Wang, L., Berger, S.L., Kouzarides, T., et al. (1996). The TAFII250 Subunit of TFIID Has Histone Acetyltransferase Activity. Cell *87*, 1261–1270.

Molnar, K.S., Karabacak, N.M., Johnson, J.L., Wang, Q., Tiwari, A., Hayward, L.J., Coales, S.J., Hamuro, Y., and Agar, J.N. (2009). A Common Property of Amyotrophic Lateral Sclerosis-associated Variants DESTABILIZATION OF THE COPPER/ZINC SUPEROXIDE DISMUTASE ELECTROSTATIC LOOP. J. Biol. Chem. *284*, 30965–30973.

Muller, F.L., Liu, Y., and Remmen, H.V. (2004). Complex III Releases Superoxide to Both Sides of the Inner Mitochondrial Membrane. J. Biol. Chem. *279*, 49064–49073.

Münch, C., Sedlmeier, R., Meyer, T., Homberg, V., Sperfeld, A.D., Kurt, A., Prudlo, J., Peraus, G., Hanemann, C.O., Stumm, G., et al. (2004). Point mutations of the p150 subunit of dynactin (DCTN1) gene in ALS. Neurology *63*, 724–726.

Münch, C., O'Brien, J., and Bertolotti, A. (2011). Prion-like propagation of mutant superoxide dismutase-1 misfolding in neuronal cells. Proc. Natl. Acad. Sci. *108*, 3548–3553.

Murakami, K., Murata, N., Noda, Y., Tahara, S., Kaneko, T., Kinoshita, N., Hatsuta, H., Murayama, S., Barnham, K.J., Irie, K., et al. (2011). SOD1 (copper/zinc superoxide dismutase)

deficiency drives amyloid β protein oligomerization and memory loss in mouse model of Alzheimer disease. J. Biol. Chem. *286*, 44557–44568.

Murakami, K., Murata, N., Noda, Y., Irie, K., Shirasawa, T., and Shimizu, T. (2012). Stimulation of the amyloidogenic pathway by cytoplasmic superoxide radicals in an Alzheimer's disease mouse model. Biosci. Biotechnol. Biochem. *76*, 1098–1103.

Nauli, S.M., Alenghat, F.J., Luo, Y., Williams, E., Vassilev, P., Li, X., Elia, A.E.H., Lu, W., Brown, E.M., Quinn, S.J., et al. (2003). Polycystins 1 and 2 mediate mechanosensation in the primary cilium of kidney cells. Nat. Genet. *33*, 129–137.

Neumann, M., Sampathu, D.M., Kwong, L.K., Truax, A.C., Micsenyi, M.C., Chou, T.T., Bruce, J., Schuck, T., Grossman, M., Clark, C.M., et al. (2006). Ubiquitinated TDP-43 in Frontotemporal Lobar Degeneration and Amyotrophic Lateral Sclerosis. Science *314*, 130–133.

Nguyen, M.D., Boudreau, M., Kriz, J., Couillard-Després, S., Kaplan, D.R., and Julien, J.-P. (2003). Cell Cycle Regulators in the Neuronal Death Pathway of Amyotrophic Lateral Sclerosis Caused by Mutant Superoxide Dismutase 1. J. Neurosci. *23*, 2131–2140.

Ogryzko, V.V., Schiltz, R.L., Russanova, V., Howard, B.H., and Nakatani, Y. (1996). The Transcriptional Coactivators p300 and CBP Are Histone Acetyltransferases. Cell *87*, 953–959.

Okado-Matsumoto, A., and Fridovich, I. (2001). Subcellular Distribution of Superoxide Dismutases (SOD) in Rat Liver Cu,Zn-SOD IN MITOCHONDRIA. J. Biol. Chem. *276*, 38388–38393.

Ott, C., Elia, N., Jeong, S.Y., Insinna, C., Sengupta, P., and Lippincott-Schwartz, J. (2012). Primary cilia utilize glycoprotein-dependent adhesion mechanisms to stabilize long-lasting cilia-cilia contacts. Cilia *1*, 3.

Pampliega, O., Orhon, I., Patel, B., Sridhar, S., Díaz-Carretero, A., Beau, I., Codogno, P., Satir, B.H., Satir, P., and Cuervo, A.M. (2013). Functional interaction between autophagy and ciliogenesis. Nature *502*, 194–200.

Pandey, U.B., Nie, Z., Batlevi, Y., McCray, B.A., Ritson, G.P., Nedelsky, N.B., Schwartz, S.L., DiProspero, N.A., Knight, M.A., Schuldiner, O., et al. (2007). HDAC6 rescues neurodegeneration and provides an essential link between autophagy and the UPS. Nature *447*, 860–864.

Pardo, C.A., Xu, Z., Borchelt, D.R., Price, D.L., Sisodia, S.S., and Cleveland, D.W. (1995). Superoxide dismutase is an abundant component in cell bodies, dendrites, and axons of motor neurons and in a subset of other neurons. Proc. Natl. Acad. Sci. *92*, 954–958.

Parthun, M.R., Widom, J., and Gottschling, D.E. (1996). The Major Cytoplasmic Histone Acetyltransferase in Yeast: Links to Chromatin Replication and Histone Metabolism. Cell *87*, 85–94.

Pazour, G.J., San Agustin, J.T., Follit, J.A., Rosenbaum, J.L., and Witman, G.B. (2002). Polycystin-2 localizes to kidney cilia and the ciliary level is elevated in orpk mice with polycystic kidney disease. Curr. Biol. *12*, R378–R380.

Pedrini, S., Sau, D., Guareschi, S., Bogush, M., Brown, R.H., Naniche, N., Kia, A., Trotti, D., and Pasinelli, P. (2010). ALS-linked mutant SOD1 damages mitochondria by promoting conformational changes in Bcl-2. Hum. Mol. Genet. *19*, 2974–2986.

Peterson, R., and Turnbull, J. (2011). Sonic Hedgehog is Cytoprotective against Oxidative Challenge in a Cellular Model of Amyotrophic Lateral Sclerosis. J. Mol. Neurosci. *47*, 31–41.

Pirkmajer, S., and Chibalin, A.V. (2011). Serum starvation: caveat emptor. Am. J. Physiol. - Cell Physiol. *301*, C272–C279.

Prudencio, M., and Borchelt, D.R. (2011). Superoxide dismutase 1 encoding mutations linked to ALS adopts a spectrum of misfolded states. Mol. Neurodegener. *6*, 77.

Prudencio, M., Durazo, A., Whitelegge, J.P., and Borchelt, D.R. (2009a). Modulation of mutant superoxide dismutase 1 aggregation by co-expression of wild-type enzyme. J. Neurochem. *108*, 1009–1018.

Prudencio, M., Hart, P.J., Borchelt, D.R., and Andersen, P.M. (2009b). Variation in aggregation propensities among ALS-associated variants of SOD1: Correlation to human disease. Hum. Mol. Genet. *18*, 3217–3226.

Pugacheva, E.N., Jablonski, S.A., Hartman, T.R., Henske, E.P., and Golemis, E.A. (2007). HEF1-Dependent Aurora A Activation Induces Disassembly of the Primary Cilium. Cell *129*, 1351–1363.

Rakhit, R., Cunningham, P., Furtos-Matei, A., Dahan, S., Qi, X.-F., Crow, J.P., Cashman, N.R., Kondejewski, L.H., and Chakrabartty, A. (2002). Oxidation-induced Misfolding and Aggregation of Superoxide Dismutase and Its Implications for Amyotrophic Lateral Sclerosis. J. Biol. Chem. *277*, 47551–47556.

Ravits, J. (2014). Focality, stochasticity and neuroanatomic propagation in ALS pathogenesis. Exp. Neurol. *262*, *Part B*, 121–126.

Reaume, A.G., Elliott, J.L., Hoffman, E.K., Kowall, N.W., Ferrante, R.J., Siwek, D.R., Wilcox, H.M., Flood, D.G., Beal, M.F., Brown, R.H., et al. (1996). Motor neurons in Cu/Zn superoxide

dismutase-deficient mice develop normally but exhibit enhanced cell death after axonal injury. Nat. Genet. *13*, 43–47.

Reddi, A.R., and Culotta, V.C. (2013). SOD1 Integrates Signals from Oxygen and Glucose to Repress Respiration. Cell *152*, 224–235.

Redler, R.L., Wilcox, K.C., Proctor, E.A., Fee, L., Caplow, M., and Dokholyan, N.V. (2011). Glutathionylation at Cys-111 Induces Dissociation of Wild Type and FALS Mutant SOD1 Dimers. Biochemistry (Mosc.) *50*, 7057–7066.

Rohatgi, R., Milenkovic, L., and Scott, M.P. (2007). Patched1 Regulates Hedgehog Signaling at the Primary Cilium. Science *317*, 372–376.

Rosen, D.R., Siddique, T., Patterson, D., Figlewicz, D.A., Sapp, P., Hentati, A., Donaldson, D., Goto, J., O'Regan, J.P., and Deng, H.X. (1993). Mutations in Cu/Zn superoxide dismutase gene are associated with familial amyotrophic lateral sclerosis. Nature *362*, 59–62.

Rosenbaum, J.L., and Witman, G.B. (2002). Intraflagellar transport. Nat. Rev. Mol. Cell Biol. *3*, 813–825.

Rotunno, M.S., and Bosco, D.A. (2013). An emerging role for misfolded wild-type SOD1 in sporadic ALS pathogenesis. Front. Cell. Neurosci. *7*, 253.

Saccon, R.A., Bunton-Stasyshyn, R.K.A., Fisher, E.M.C., and Fratta, P. (2013). Is SOD1 loss of function involved in amyotrophic lateral sclerosis? Brain *136*, 2342–2358.

Sahawneh, M.A., Ricart, K.C., Roberts, B.R., Bomben, V.C., Basso, M., Ye, Y., Sahawneh, J., Franco, M.C., Beckman, J.S., and Estévez, A.G. (2010). Cu,Zn-Superoxide Dismutase Increases Toxicity of Mutant and Zinc-deficient Superoxide Dismutase by Enhancing Protein Stability. J. Biol. Chem. *285*, 33885–33897.

Sasaki, S., and Iwata, M. (1996). Impairment of fast axonal transport in the proximal axons of anterior horn neurons in amyotrophic lateral sclerosis. Neurology *47*, 535–540.

Sasaki, S., Warita, H., Abe, K., and Iwata, M. (2005). Impairment of axonal transport in the axon hillock and the initial segment of anterior horn neurons in transgenic mice with a G93A mutant SOD1 gene. Acta Neuropathol. (Berl.) *110*, 48–56.

Schneider, L., Clement, C.A., Teilmann, S.C., Pazour, G.J., Hoffmann, E.K., Satir, P., and Christensen, S.T. (2005). PDGFRαα Signaling Is Regulated through the Primary Cilium in Fibroblasts. Curr. Biol. *15*, 1861–1866.

Schwer, B., Eckersdorff, M., Li, Y., Silva, J.C., Fermin, D., Kurtev, M.V., Giallourakis, C., Comb, M.J., Alt, F.W., and Lombard, D.B. (2009). Calorie restriction alters mitochondrial protein acetylation. Aging Cell *8*, 604–606.

Schwob, J.E., and Price, J.L. (1984). The development of axonal connections in the central olfactory system of rats. J. Comp. Neurol. *223*, 177–202.

Seeley, E.S., and Nachury, M.V. (2010). The perennial organelle: assembly and disassembly of the primary cilium. J. Cell Sci. *123*, 511–518.

Shackelford, R.E., Kaufmann, W.K., and Paules, R.S. (2000). Oxidative stress and cell cycle checkpoint function. Free Radic. Biol. Med. *28*, 1387–1404.

Shi, P., Ström, A.-L., Gal, J., and Zhu, H. (2010). Effects of ALS-related SOD1 mutants on dynein- and KIF5-mediated retrograde and anterograde axonal transport. Biochim. Biophys. Acta BBA - Mol. Basis Dis. *1802*, 707–716.

Shibata, N., Hirano, A., Kobayashi, M., Sasaki, S., Kato, T., Matsumoto, S., Shiozawa, Z., Komori, T., Ikemoto, A., and Umahara, T. (1994). Cu/Zn superoxide dismutase-like immunoreactivity in Lewy body-like inclusions of sporadic amyotrophic lateral sclerosis. Neurosci. Lett. *179*, 149–152.

Shida, T., Cueva, J.G., Xu, Z., Goodman, M.B., and Nachury, M.V. (2010). The major α-tubulin K40 acetyltransferase αTAT1 promotes rapid ciliogenesis and efficient mechanosensation. Proc. Natl. Acad. Sci. *107*, 21517–21522.

Silverman, J.M., Fernando, S.M., Grad, L.I., Hill, A.F., Turner, B.J., Yerbury, J.J., and Cashman, N.R. (2016). Disease Mechanisms in ALS: Misfolded SOD1 Transferred Through Exosome-Dependent and Exosome-Independent Pathways. Cell. Mol. Neurobiol. *36*, 377–381.

Singla, V., and Reiter, J.F. (2006). The Primary Cilium as the Cell's Antenna: Signaling at a Sensory Organelle. Science *313*, 629–633.

Slivka, A., Spina, M.B., and Cohen, G. (1987). Reduced and oxidized glutathione in human and monkey brain. Neurosci. Lett. *74*, 112–118.

Smith, B.N., Ticozzi, N., Fallini, C., Gkazi, A.S., Topp, S., Kenna, K.P., Scotter, E.L., Kost, J., Keagle, P., Miller, J.W., et al. (2014). Exome-wide Rare Variant Analysis Identifies TUBA4A Mutations Associated with Familial ALS. Neuron *84*, 324–331.

Smith, R., Myers, K., Ravits, J., and Bowser, R. (2015). Amyotrophic lateral sclerosis: Is the spinal fluid pathway involved in seeding and spread? Med. Hypotheses *85*, 576–583.

Song, W., Song, Y., Kincaid, B., Bossy, B., and Bossy-Wetzel, E. (2013). Mutant SOD1G93A triggers mitochondrial fragmentation in spinal cord motor neurons: neuroprotection by SIRT3 and PGC-1α. Neurobiol. Dis. *51*, 72–81.

Sotthibundhu, A., Li, Q.-X., Thangnipon, W., and Coulson, E.J. (2009). Aβ1–42 stimulates adult SVZ neurogenesis through the p75 neurotrophin receptor. Neurobiol. Aging *30*, 1975–1985.

Spalloni, A., Albo, F., Ferrari, F., Mercuri, N., Bernardi, G., Zona, C., and Longone, P. (2004). Cu/Zn-superoxide dismutase (GLY93→ALA) mutation alters AMPA receptor subunit expression and function and potentiates kainate-mediated toxicity in motor neurons in culture. Neurobiol. Dis. *15*, 340–350.

Speake, T., Whitwell, C., Kajita, H., Majid, A., and Brown, P.D. (2001). Mechanisms of CSF secretion by the choroid plexus. Microsc. Res. Tech. *52*, 49–59.

Ström, A.-L., Shi, P., Zhang, F., Gal, J., Kilty, R., Hayward, L.J., and Zhu, H. (2008). Interaction of Amyotrophic Lateral Sclerosis (ALS)-related Mutant Copper-Zinc Superoxide Dismutase with the Dynein-Dynactin Complex Contributes to Inclusion Formation. J. Biol. Chem. *283*, 22795–22805.

Sturtz, L.A., Diekert, K., Jensen, L.T., Lill, R., and Culotta, V.C. (2001). A Fraction of Yeast Cu,Zn-Superoxide Dismutase and Its Metallochaperone, CCS, Localize to the Intermembrane Space of Mitochondria A PHYSIOLOGICAL ROLE FOR SOD1 IN GUARDING AGAINST MITOCHONDRIAL OXIDATIVE DAMAGE. J. Biol. Chem. *276*, 38084–38089.

Sun, X., Haley, J., Bulgakov, O.V., Cai, X., McGinnis, J., and Li, T. (2012). Tubby is required for trafficking G protein-coupled receptors to neuronal. Cilia *1*, 21.

Taes, I., Timmers, M., Hersmus, N., Bento-Abreu, A., Bosch, L.V.D., Damme, P.V., Auwerx, J., and Robberecht, W. (2013). Hdac6 deletion delays disease progression in the SOD1G93A mouse model of ALS. Hum. Mol. Genet. *22*, 1783–1790.

Tainer, J.A., Getzoff, E.D., Beem, K.M., Richardson, J.S., and Richardson, D.C. (1982). Determination and analysis of the 2 Å structure of copper, zinc superoxide dismutase. J. Mol. Biol. *160*, 181–217.

Tang, Z., Lin, M.G., Stowe, T.R., Chen, S., Zhu, M., Stearns, T., Franco, B., and Zhong, Q. (2013). Autophagy promotes primary ciliogenesis by removing OFD1 from centriolar satellites. Nature *502*, 254–257.

Taunton, J., Hassig, C.A., and Schreiber, S.L. (1996). A Mammalian Histone Deacetylase Related to the Yeast Transcriptional Regulator Rpd3p. Science *272*, 408–411.

Tsang, C.K., Liu, Y., Thomas, J., Zhang, Y., and Zheng, X.F.S. (2014). Superoxide dismutase 1 acts as a nuclear transcription factor to regulate oxidative stress resistance. Nat. Commun. *5*, 3446.

Urushitani, M., Kurisu, J., Tsukita, K., and Takahashi, R. (2002). Proteasomal inhibition by misfolded mutant superoxide dismutase 1 induces selective motor neuron death in familial amyotrophic lateral sclerosis. J. Neurochem. *83*, 1030–1042.

Urushitani, M., Ezzi, S.A., and Julien, J.-P. (2007). Therapeutic effects of immunization with mutant superoxide dismutase in mice models of amyotrophic lateral sclerosis. Proc. Natl. Acad. Sci. *104*, 2495–2500.

Usui, S., Oveson, B.C., Iwase, T., Lu, L., Lee, S.Y., Jo, Y.-J., Wu, Z., Choi, E.-Y., Samulski, R.J., and Campochiaro, P.A. (2011). Overexpression of SOD in retina: Need for increase in H2O2-detoxifying enzyme in same cellular compartment. Free Radic. Biol. Med. *51*, 1347–1354.

Vance, C., Rogelj, B., Hortobágyi, T., Vos, K.J.D., Nishimura, A.L., Sreedharan, J., Hu, X., Smith, B., Ruddy, D., Wright, P., et al. (2009). Mutations in FUS, an RNA Processing Protein, Cause Familial Amyotrophic Lateral Sclerosis Type 6. Science *323*, 1208–1211.

Ventura, M., Mateo, F., Serratosa, J., Salaet, I., Carujo, S., Bachs, O., and Pujol, M.J. (2010). Nuclear translocation of glyceraldehyde-3-phosphate dehydrogenase is regulated by acetylation. Int. J. Biochem. Cell Biol. *42*, 1672–1680.

Verdin, E., Hirschey, M.D., Finley, L.W.S., and Haigis, M.C. (2010). Sirtuin regulation of mitochondria: energy production, apoptosis, and signaling. Trends Biochem. Sci. *35*, 669–675.

Viggiano, A., Serù, R., Damiano, S., De Luca, B., Santillo, M., and Mondola, P. (2012). Inhibition of long-term potentiation by CuZn superoxide dismutase injection in rat dentate gyrus: Involvement of muscarinic M1 receptor. J. Cell. Physiol. *227*, 3111–3115.

Volkening, K., Leystra-Lantz, C., Yang, W., Jaffee, H., and Strong, M.J. (2009). Tar DNA binding protein of 43 kDa (TDP-43), 14-3-3 proteins and copper/zinc superoxide dismutase (SOD1) interact to modulate NFL mRNA stability. Implications for altered RNA processing in amyotrophic lateral sclerosis (ALS). Brain Res. *1305*, 168–182.

Wagner, S.A., Beli, P., Weinert, B.T., Nielsen, M.L., Cox, J., Mann, M., and Choudhary, C. (2011). A Proteome-wide, Quantitative Survey of In Vivo Ubiquitylation Sites Reveals Widespread Regulatory Roles. Mol. Cell. Proteomics *10*, M111.013284.

Wang, J., Silva, M., Haas, L.A., Morsci, N.S., Nguyen, K.C.Q., Hall, D.H., and Barr, M.M. (2014). C. elegans Ciliated Sensory Neurons Release Extracellular Vesicles that Function in Animal Communication. Curr. Biol. *24*, 519–525.

Wang, L., Deng, H.-X., Grisotti, G., Zhai, H., Siddique, T., and Roos, R.P. (2009). Wild-type SOD1 overexpression accelerates disease onset of a G85R SOD1 mouse. Hum. Mol. Genet. *18*, 1642–1651.

Wang, L., Popko, B., and Roos, R.P. (2011a). The unfolded protein response in familial amyotrophic lateral sclerosis. Hum. Mol. Genet. *20*, 1008–1015.

Wang, L., Gutmann, D.H., and Roos, R.P. (2011b). Astrocyte loss of mutant SOD1 delays ALS disease onset and progression in G85R transgenic mice. Hum. Mol. Genet. *20*, 286–293.

Wang, X., Culotta, V.C., and Klee, C.B. (1996). Superoxide dismutase protects calcineurin from inactivation. Nature *383*, 434–437.

Warita, H., Itoyama, Y., and Abe, K. (1999). Selective impairment of fast anterograde axonal transport in the peripheral nerves of asymptomatic transgenic mice with a G93A mutant SOD1 gene. Brain Res. *819*, 120–131.

Watanabe, K., Shibuya, S., Koyama, H., Ozawa, Y., Toda, T., Yokote, K., and Shimizu, T. (2013). Sod1 Loss Induces Intrinsic Superoxide Accumulation Leading to p53-Mediated Growth Arrest and Apoptosis. Int. J. Mol. Sci. *14*, 10998–11010.

Watanabe, K., Shibuya, S., Ozawa, Y., Nojiri, H., Izuo, N., Yokote, K., and Shimizu, T. (2014). Superoxide Dismutase 1 Loss Disturbs Intracellular Redox Signaling, Resulting in Global Age-Related Pathological Changes. BioMed Res. Int. *2014*, e140165.

Wei, J.-P.J., Srinivasan, C., Han, H., Valentine, J.S., and Gralla, E.B. (2001). Evidence for a Novel Role of Copper-Zinc Superoxide Dismutase in Zinc Metabolism. J. Biol. Chem. *276*, 44798–44803.

Wei, Q., Zhang, Y., Li, Y., Zhang, Q., Ling, K., and Hu, J. (2012). The BBSome controls IFT assembly and turnaround in cilia. Nat. Cell Biol. *14*, 950–957.

Weinert, B.T., Schölz, C., Wagner, S.A., Iesmantavicius, V., Su, D., Daniel, J.A., and Choudhary, C. (2013). Lysine Succinylation Is a Frequently Occurring Modification in Prokaryotes and Eukaryotes and Extensively Overlaps with Acetylation. Cell Rep. *4*, 842–851.

Wheatley, D.N., Wang, A.M., and Strugnell, G.E. (1996). Expression of primary cilia in mammalian cells. Cell Biol. Int. *20*, 73–81.

Wheway, G., Parry, D.A., and Johnson, C.A. (2013). The role of primary cilia in the development and disease of the retina. Organogenesis *10*, 69–85.

Wiedau-Pazos, M., Goto, J.J., Rabizadeh, S., Gralla, E.B., Roe, J.A., Lee, M.K., Valentine, J.S., and Bredesen, D.E. (1996). Altered Reactivity of Superoxide Dismutase in Familial Amyotrophic Lateral Sclerosis. Science *271*, 515–518.

Wilcox, K.C., Zhou, L., Jordon, J.K., Huang, Y., Yu, Y., Redler, R.L., Chen, X., Caplow, M., and Dokholyan, N.V. (2009). Modifications of Superoxide Dismutase (SOD1) in Human Erythrocytes. J. Biol. Chem. *284*, 13940–13947.

Williamson, T.L., and Cleveland, D.W. (1999). Slowing of axonal transport is a very early event in the toxicity of ALS–linked SOD1 mutants to motor neurons. Nat. Neurosci. *2*, 50–56.

Winer L, Srinivasan D, Chun S, and et al (2013). SOd1 in cerebral spinal fluid as a pharmacodynamic marker for antisense oligonucleotide therapy. JAMA Neurol. *70*, 201–207.

Wong, P.C., Pardo, C.A., Borchelt, D.R., Lee, M.K., Copeland, N.G., Jenkins, N.A., Sisodia, S.S., Cleveland, D.W., and Price, D.L. (1995). An adverse property of a familial ALS-linked SOD1 mutation causes motor neuron disease characterized by vacuolar degeneration of mitochondria. Neuron *14*, 1105–1116.

Wood, C.R., Huang, K., Diener, D.R., and Rosenbaum, J.L. (2013). The Cilium Secretes Bioactive Ectosomes. Curr. Biol. *23*, 906–911.

Wu, C.-H., Fallini, C., Ticozzi, N., Keagle, P.J., Sapp, P.C., Piotrowska, K., Lowe, P., Koppers, M., McKenna-Yasek, D., Baron, D.M., et al. (2012). Mutations in the profilin 1 gene cause familial amyotrophic lateral sclerosis. Nature *488*, 499–503.

Wu, Q., Cheng, Z., Zhu, J., Xu, W., Peng, X., Chen, C., Li, W., Wang, F., Cao, L., Yi, X., et al. (2015). Suberoylanilide Hydroxamic Acid Treatment Reveals Crosstalks among Proteome, Ubiquitylome and Acetylome in Non-Small Cell Lung Cancer A549 Cell Line. Sci. Rep. *5*, 9520.

Yamanaka, K., Chun, S.J., Boillee, S., Fujimori-Tonou, N., Yamashita, H., Gutmann, D.H., Takahashi, R., Misawa, H., and Cleveland, D.W. (2008). Astrocytes as determinants of disease progression in inherited amyotrophic lateral sclerosis. Nat. Neurosci. *11*, 251–253.

Yang, L., Vaitheesvaran, B., Hartil, K., Robinson, A.J., Hoopmann, M.R., Eng, J.K., Kurland, I.J., and Bruce, J.E. (2011). The Fasted/Fed Mouse Metabolic Acetylome: N6-Acetylation Differences Suggest Acetylation Coordinates Organ-Specific Fuel Switching. J. Proteome Res. *10*, 4134–4149.

Yokoyama, A., Ohno, K., Hirano, A., Shintaku, M., Kato, M., Hayashi, K., and Kato, S. (2014). Cerebellar Expression of Copper Chaperone for Superoxide, Cytosolic Cu/Zn-Superoxide Dismutase, 4-Hydroxy-2-Nonenal, Acrolein and Heat Shock Protein 32 in Patients with Menkes Kinky Hair Disease: Immunohistochemical Study. Yonago Acta Med. *57*, 23–35.

Yon, J.-M., Baek, I.-J., Lee, S.-R., Kim, M.-R., Lee, B.J., Yun, Y.W., and Nam, S.-Y. (2008). Immunohistochemical identification and quantitative analysis of cytoplasmic Cu/Zn superoxide dismutase in mouse organogenesis. J. Vet. Sci. *9*, 233–240.

Yuki, K., Ozawa, Y., Yoshida, T., Kurihara, T., Hirasawa, M., Ozeki, N., Shiba, D., Noda, K., Ishida, S., and Tsubota, K. (2011). Retinal Ganglion Cell Loss in Superoxide Dismutase 1 Deficiency. Investig. Opthalmology Vis. Sci. *52*, 4143.

Yuki, K., Yoshida, T., Miyake, S., Tsubota, K., and Ozawa, Y. (2013). Neuroprotective role of superoxide dismutase 1 in retinal ganglion cells and inner nuclear layer cells against N-methyl-d-aspartate-induced cytotoxicity. Exp. Eye Res. *115*, 230–238.

Zhang, J., Ito, H., Wate, R., Ohnishi, S., Nakano, S., and Kusaka, H. (2006). Altered distributions of nucleocytoplasmic transport-related proteins in the spinal cord of a mouse model of amyotrophic lateral sclerosis. Acta Neuropathol. (Berl.) *112*, 673–680.

Zhang, Q., Nishimura, D., Vogel, T., Shao, J., Swiderski, R., Yin, T., Searby, C., Carter, C.S., Kim, G., Bugge, K., et al. (2013). BBS7 is required for BBSome formation and its absence in mice results in Bardet-Biedl syndrome phenotypes and selective abnormalities in membrane protein trafficking. J. Cell Sci. *126*, 2372–2380.

Zhao, S., Xu, W., Jiang, W., Yu, W., Lin, Y., Zhang, T., Yao, J., Zhou, L., Zeng, Y., Li, H., et al. (2010). Regulation of Cellular Metabolism by Protein Lysine Acetylation. Science *327*, 1000–1004.